THE UNIVERSITY OF MICHIGAN

INDUSTRY PROGRAM OF THE COLLEGE OF ENGINEERING

SOIL TRANSIENTS BY CHARACTERISTICS METHOD

by

Constantine Nicholas Papadakis

A dissertation submitted in partial fulfillment
of the requirements for the degree of
Doctor of Philosophy
in The University of Michigan
Department of Civil Engineering
1973

October 1973

IP-854

Ἀφιεροῦται εἰς τήν

Σπουδάζουσαν Νεολαίαν

τῆς Πατρίδος μου

ACKNOWLEDGMENTS

The author extends his profound gratitude to Professor Victor L. Streeter, Co-chairman of his doctoral committee, for the inspiration, advice, continuous guidance and patience throughout the course of this study. The critical judgment, the keen interest and the numerous suggestions offered by Professor E. Benjamin Wylie, Co-chairman of the doctoral committee, are deeply appreciated. The suggestions and continuous cooperation of Professor Frank E. Richart, Jr., have been extremely valuable. The counsel, interest and encouragement tendered by Professors Robert C. Bartels and Ernest F. Brater are gratefully acknowledged.

The use of the excellent facilities of the Computing Center of the University of Michigan, including the IBM 360/67 computer and the CALCOMP 780/763 digital plotter, and the generous donation of computer time which made this study possible, are greatly appreciated.

This study was supported in part by the National Science Foundation, initially through project GK-14213 "Transient Flow Through Open and Closed Conduits" but mainly through project GI-34771 "Earthquake Induced Transient Pore Pressures in Earth Dams" directed by Professors Victor L. Streeter and E. Benjamin Wylie, under whom the author had the privilege to work. The author is indebted to the

University of Michigan for granting him a teaching fellowship and to the Horace W. King Grant for providing him with tuition scholarship throughout his graduate study.

The author affectionately thanks his wife Eliana for her encouragement, understanding and exceptional patience during his two years of graduate work at the University of Michigan.

Appreciation is extended to the staff of the Industry Program of the College of Engineering of the University of Michigan for the final typing of the manuscript and the publication of this study.

TABLE OF CONTENTS

TABLE OF CONTENTS (CONT'D)

LIST OF FIGURES

LIST OF FIGURES (CONT'D)

LIST OF FIGURES (CONT'D)

LIST OF FIGURES (CONT'D)

LIST OF FIGURES (CONT'D)

LIST OF APPENDICES

NOMENCLATURE

Symbol	Units	Meaning
A_0	(ft^2)	horizontal cross-sectional area of earth dam
A, A_1, A_2, A_1', A_2'		constants determined from boundary conditions
a_g	(ft/sec^2)	horizontal acceleration
a_m, a_m', a_s	(ft)	Fourier coefficients
B, B_1, B_2, B_1', B_2'		constants determined from boundary conditions
$\bar{B}$	(psf)	bulk modulus of compressibility
b	($lb \cdot sec/ft^4$)	parameter depending on soil permeability and fluid viscosity
b_m		Fourier coefficient
C_1, C_2, C_3		parameters defining elastic properties
C_b	(psf^{-1})	bulk compressibility of soil skeleton
C_ℓ	(psf^{-1})	fluid compressibility
C_p	(psf^{-1})	pore compressibility
C_s	(psf^{-1})	compressibility of soil particles
C^+, C^-		refer to characteristics equations
c		viscous damping coefficient
D		critical damping ratio
d		constant
E	(psf)	modulus of elasticity

Symbol	Units	Meaning
E_j	(ft)	displacement amplitudes of incident shear wave
e	(2.71828...)	base of natural (Napierian) logarithms
F_1, F_2, F_3		parameters defining dynamic properties
F_j	(ft)	displacement amplitudes of reflected shear waves
F(z)	(ft)	amplitude function
f		constant
G	(psf)	shear modulus
G_0	(psf)	shear modulus at zero shearing strain amplitude
G*	(psf)	complex shear modulus
g	(ft/sec^2)	acceleration of gravity
H	(ft)	thickness of soil deposit; height of an earth dam
$H_q^{(1)}, H_q^{(2)}$		Hankel functions of order q
h	(ft)	amount of dam crest truncation
h_j	(ft)	thickness of soil sublayers
i		unit of complex number, equal to $\sqrt{-1}$
J_q		Bessel functions of the first kind, of order q
j		integer used for indexing
K	(ft^2)	intrinsic permeability
k	(ft/sec)	coefficient of permeability
ℓ		constant exponent (integer)
M	(psf)	constrained modulus of elasticity

Symbol	Units	Meaning
m		integer used for indexing
n		porosity
p	(psf)	porewater pressure
Q	(psf)	Biot's coupling coefficient
q		order of Bessel functions
R	(psf)	Biot's coupling coefficient
R_0		exponent in Ramber-Osgood relation
r		ratio of wave velocities
s	(psf)	stress on fluid per unit area
T_f	(sec)	forcing period
T_n	(sec)	natural period
t	(sec)	time
U	(ft/sec)	vertical velocity of fluid filling pores
u	(ft)	horizontal soil particle displacement (for unsaturated soil)
V	(ft/sec)	horizontal soil particle velocity (for unsaturated soil) or vertical (for saturated)
V	(ft/sec)	velocities perpendicular to 4 faces of transfer element
V´	(ft/sec)	velocities parallel to 4 faces of transfer element
v*	(ft/sec)	complex shear wave velocity
v_c	(ft/sec)	characteristic wave velocity

Symbol	Units	Meaning
v_d, v_{d_1}, v_{d_2}	(ft/sec)	p-wave transmission velocities in saturated soil
v_L	(ft/sec)	pressure wave velocity through liquid part
v_M	(ft/sec)	pressure wave velocity through soil skeleton
v_p	(ft/sec)	pressure wave velocity in unsaturated soil
v_s	(ft/sec)	shear wave velocity in unsaturated soil
W	(ft)	amplitude of a given harmonic displacement
w	(ft)	vertical soil particle displacement (for saturated soil)
$\bar{w}$	(ft)	vertical displacement of liquid particles (saturated soil)
X		complex parameter
x	(ft)	horizontal distance
x_0		ratio of wave velocities
x_1, x_2, x_1', x_2'		roots of biquadratic equations
Y_q		Bessel functions of the second kind, of order q
z	(ft)	vertical distance
α		slope of earth dam sides
α_j		complex impedance ratios
$\beta', \beta_1, \beta_2, \beta_{11}, \beta_{22}$		auxiliary variables (saturated soil analysis)
γ		shearing strain
γ_1		particular shearing strain at stress reversal

Symbol	Units	Meaning
γ_E	(0.577215...)	Euler's constant
γ_s	(lb/ft^3)	unit weight of soil
Δt	(sec)	time interval
$\Delta x, \Delta z, \Delta z'$	(ft)	distance intervals
η_j		phase angles
$\theta, \theta_1, \theta_2$		multipliers in characteristics method
λ	(psf)	Lame's constant
μ	(lb·sec/ft^2)	soil viscosity
μ_L	(lb·sec/ft^2)	dynamic viscosity of fluid filling pores
ν		Poisson ratio
ξ		weighting factor
π	(3.141592...)	constant
ρ	(slugs/ft^3)	mass density of soil
ρ_{11}	(slugs/ft^3)	mass of solid per unit volume of aggregate
ρ_{22}	(slugs/ft^3)	mass of liquid per unit volume of aggregate
ρ_{12}	(slugs/ft^3)	apparent mass per unit volume of aggregate
ρ_a	(slugs/ft^3)	apparent mass density
ρ_L	(slugs/ft^3)	mass density of liquid
ρ_S	(slugs/ft^3)	mass density of solid
σ	(psf)	stress on the solid part per unit area
τ	(psf)	shearing stress
τ_1	(psf)	particular shearing stress at stress reversal

Symbol	Units	Meaning
τ_y	(psf)	yield shearing stress
ϕ, ϕ_m		phase angles
ϕ_0		angle of internal friction
ϕ_1, ϕ_2		auxiliary variables (saturated soil analysis)
$\psi_1, \psi_2, \psi_3, \psi_4$		auxiliary variables (saturated soil analysis)
ω	(rad/sec)	angular frequency
ω_m, ω_s	(rad/sec)	angular frequencies in Fourier analysis
ω_n	(rad/sec)	fundamental frequency

CHAPTER I

INTRODUCTION

Analytical methods have been developed in recent years to evaluate the ground motions induced in soil deposits during earthquakes. A knowledge of these motions is essential to the understanding of the earthquake behavior of structures.

The characteristics method opens a new approach to the solution of problems of earthquake generated transient disturbances traveling through soil deposits. One of the first attempts to compute soil motions using the method of characteristics was made by Streeter, Wylie and Richart [71]*. The method has not been thoroughly exploited and tested as in the case of hydraulic transient problems [69]. Therefore, the research reported herein was not restricted to a narrow objective but a modest contribution was attempted to a wider range of problems often encountered in soil vibrations induced by earthquakes.

In this study the characteristics method is applied to problems involving the computation of bedrock motions from recorded ground surface motions, the propagation of shear waves through tapered cross sections (earth dams), the propagation of pressure waves through saturated soil deposits, and two dimensional simulations.

---

*Numbers in brackets indicate references listed at the end of the thesis; numbers in parentheses denote equations.

A review of methods for the one-dimensional shear wave propagation through horizontal layers of unsaturated soil is presented in Chapter II. The rather extensive review is broad in scope to provide an overall background of the subject and to facilitate the presentation of the subsequent investigations. The accuracy of results obtained by the method of characteristics compared to closed form solutions is briefly examined in Chapter III.

For the computation of bedrock motions from recorded ground surface motions the Base Motion Synthesis method based on the method of characteristics and on a centered implicit method is developed in Chapter IV. Shear waves traveling vertically through horizontal unsaturated soil deposits are considered. Assuming that the soil reacts as a linear viscoelastic material, the aforementioned method is compared with an analytical method developed by Schnabel et al [58]. The Base Motion Synthesis method is extended to situations where the soil reacts as a "strain-softening" material. Ramberg-Osgood type shearing stress-shearing strain curves are employed in this case to model the non-linear behavior of the soil.

One-dimensional shear wave propagation through tapered cross-sections of earth dams with truncated crests is examined in Chapter V. A closed form solution is obtained involving Hankel functions with complex arguments in the case in which the earth dam material is unsaturated and linear viscoelastic. The characteristics method is

used to provide a solution to the same problem. The two methods compare favorably. An additional confirmation emanates from a comparison between the method of characteristics and the shear slice theory [63].

The vertical propagation of pressure waves through saturated horizontal elastic soil deposits is treated in Chapter VI. Biot's field equations [9] are reduced to one-dimension. An analytical solution is obtained which accounts for wave reflections at the boundaries (free surface and bedrock). The method of characteristics is also used to solve the four partial differential equations involved, and to calculate pore pressures and stresses under seismic loading.

Two-dimensional transmission of shear and pressure waves through unsaturated viscoelastic layered systems is studied in Chapter VII. A latticework of one-dimensional elements is used to simulate two-dimensional earth structures, i.e. earth dams, earth embankments or valleys. Sixteen linear equations are solved simultaneously at each interior node of the latticework. Eight of these equations are the characteristics equations from the linear elements surrounding the node and they represent the relation between pressure or shear and the corresponding velocities. Investment in computer time for solving two-dimensional problems by the latticework method is small in contrast with other widely used two-dimensional analyses.

A number of examples are included in each Chapter to illustrate the applicability of the characteristics method

and to provide comparisons of the solutions obtained from the method of characteristics and from other methods of analysis.

CHAPTER II

REVIEW OF ONE-DIMENSIONAL SHEAR WAVE PROPAGATION METHODS THROUGH HORIZONTAL SOIL LAYERS

Ground motions near the surface of a horizontal unsaturated soil deposit may be attributed mainly to the vertical propagation of shear waves from an underlying rock formation. In such cases the soil deposit can be considered as a one-dimensional shear beam, since the ground motions induced by a seismic excitation at the base are only the result of shear deformations in the soil.

One of the first attempts to calculate the motion of a soil layer subjected to a base vibration was made by Jacobsen [40] in 1930. Jacobsen assumed that the soil behaves as a linear viscoelastic material, that the rigidity of the soil deposit is constant with depth and that the motion of the base of the layer is horizontal and simple harmonic. His objective was to find the amplification of the base motion in alluvial deposits. Kanai [43,44], Herrera and Rosenblueth [29], and others studied more thoroughly the same problem. The equation of motion used by those investigators to model the response of a soil deposit of finite depth to a horizontal seismic motion at its base is:

$$\rho \frac{\partial^2 u}{\partial t^2} + c \frac{\partial u}{\partial t} - \frac{\partial}{\partial z}[G(z)\frac{\partial u}{\partial z}] = - \rho a_g \qquad (1)$$

in which ρ = mass density of soil; c = viscous damping coefficient; u = relative displacement at a depth z from

the surface of the deposit at time t; a_g = horizontal seismic acceleration at the base of the deposit; and G(z) = shear modulus at a depth z. If G(z) is constant with depth, Equation (1) reduces to a linear hyperbolic partial differential equation. If a_g is taken as zero, u in Equation (1) is the absolute displacement at a depth z.

Ambraseys [1] considered that the rigidity of a soil deposit increases linearly with depth, i.e., G(z) = fz, where f is a constant. The amplification of the base motion and the natural period of the deposit were then found analytically.

Since experimental investigations [21,26] have shown that the modulus of a cohesionless soil varies with the confining pressure to powers of 1/3 to 1/2, Idriss and Seed [35,36] used a shear modulus variation prescribed by $G(z) = fz^d$, where f and d are constants and d = 1/3. Thus, Equation (1) becomes a second order hyperbolic partial differential equation, a closed-form solution of which was obtained by the method of separation of variables.

In order to analyze the response of a soil deposit having linearly elastic but irregularly varying soil properties, Idriss and Seed [35,36] used a lumped mass analysis. The lumped mass solution was essentially a finite difference method for the solution of Equation (1).

A generalized viscoelastic solid is specified by the existence of a functional equation of state connecting stress, strain and time. A linear viscoelastic solid is

further restricted to the requirement that its mechanical properties conform to the Boltzmann superposition principle. The simplest examples of linear viscoelastic solids are: a Voigt solid (a spring connected in parallel with a dashpot); a Maxwell solid (a spring connected in series with a dashpot); and a Newtonian fluid.

In Equation (1), the dissipative force was assumed to be proportional to the velocity. However, internal friction depends also on frequency. In 1927, Sezawa [65] assumed that soil behaves as a Voigt solid for small vibration amplitudes. Adopting this assumption, Kanai [42] approximated a solution to the problem of vertical propagation of plane shear waves through a viscoelastic soil layer. The equation of motion for this distributed system is:

$$\rho \frac{\partial^2 u}{\partial t^2} - G \frac{\partial^2 u}{\partial z^2} - \mu \frac{\partial^3 u}{\partial z^2 \partial t} = 0 \qquad (2)$$

where ρ = soil mass density; G = shear modulus, constant or function of depth z; μ = soil viscosity; and u = absolute displacement at a depth z from the ground surface at time t.

Equation (2) was used by Schnabel, Lysmer and Seed [58] to compute the responses of a soil deposit for a design motion given anywhere in the system.

In the simple case where the base of a soil formation is subjected to a harmonic displacement of frequency ω and amplitude W, the solution to the wave equation (2) is:

$$u(z,t) = We^{i\omega t} \frac{e^{i\omega z/v^*} + e^{-i\omega z/v^*}}{e^{i\omega H/v^*} + e^{-i\omega H/v^*}} \qquad (3)$$

then

$$V(z,t) = i\omega u(z,t) \tag{4}$$

where H = total thickness of soil deposit; V = absolute particle velocity at depth z at time t; and v* = complex shear wave velocity equal to

$$v^* = \sqrt{(G + i\mu\omega)/\rho} = \sqrt{G^*/\rho} \tag{5}$$

where G* is the complex shear modulus.

The method of characteristics in the form of a graphical solution was first used by Westergaard [72] in 1933 to find horizontal shear in buildings idealized as shear beams. However, the method could be used only if the ground excitation was of a very simple form.

During the past decade, solutions of hyperbolic partial differential equations by the method of characteristics have been applied to a variety of hydraulic transient problems [69,67,68]. In 1973, Streeter, Wylie and Richart [71], applied the method of characteristics to wave propagation through soils. Shear waves induced by earthquake motions in linear viscoelastic and "strain-softening" materials were considered. Voigt's assumption that the stress components in a solid can be expressed as the sum of two terms, the first term being proportional to the strains and the second term being proportional to the rate of change of the strains, was adopted. Under this assumption

the dynamic stress-strain relationship for the soil considered to behave as a viscoelastic material was written:

$$\tau = G \frac{\partial u}{\partial z} + \mu \frac{\partial^2 u}{\partial z \partial t} \tag{6}$$

where τ = shearing stress; μ = soil viscosity; and u = absolute horizontal displacement at a depth z at time t.

Under dynamic conditions the equation of motion was written as:

$$\rho \frac{\partial^2 u}{\partial t^2} - \frac{\partial \tau}{\partial z} = 0 \tag{7}$$

It should be noted that if Equation (6) is differentiated with respect to z and substituted into Equation (7), Equation (2) is developed. Since the particle velocity is $V = \partial u/\partial t$, Equation (7) was written as:

$$\rho \frac{\partial V}{\partial t} - \frac{\partial \tau}{\partial z} = 0 \tag{8}$$

Differentiating the equation of state (6) with respect to time and using the particle velocities instead of the particle displacements, Streeter, Wylie and Richart obtained the equation:

$$\frac{\partial \tau}{\partial t} - G \frac{\partial V}{\partial z} - \mu \frac{\partial^2 V}{\partial z \partial t} = 0 \tag{9}$$

The third term of Equation (9) was approximated as:

$$\frac{\partial^2 V}{\partial z \partial t} = \frac{\partial}{\partial t}\left(\frac{\partial V}{\partial z}\right) = \frac{1}{\Delta t}\left[\frac{\partial V}{\partial z} - \left(\frac{\partial V}{\partial z}\right)_C\right] \tag{10}$$

where the subscript C denotes the value determined at point C on the z-t diagram (Fig. 2). With this finite difference

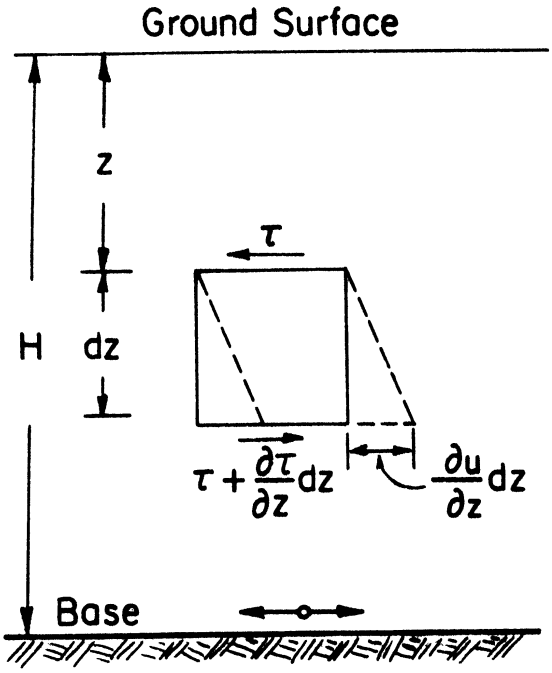

Figure 1. One-dimensional soil element.

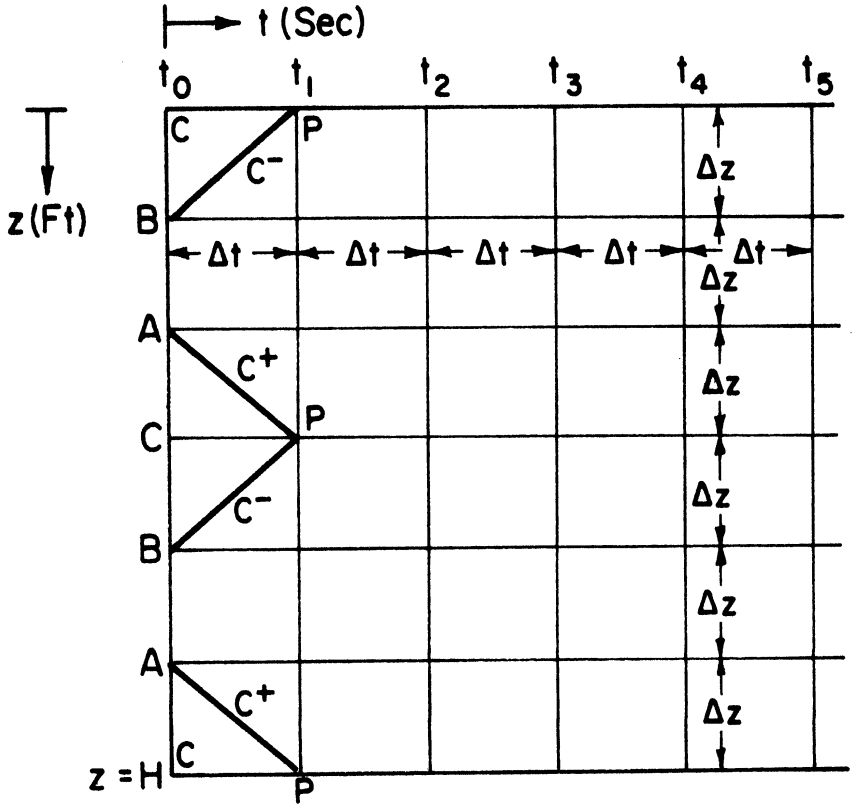

Figure 2. Characteristics in z-t plane for six soil reaches.

approximation, Equation (9) becomes:

$$\frac{\partial \tau}{\partial t} - \left(G + \frac{\mu}{\Delta t}\right) \frac{\partial V}{\partial z} + \frac{\mu}{\Delta t} \left(\frac{\partial V}{\partial z}\right)_C = 0 \qquad (11)$$

Equations (8) and (11) are two linear hyperbolic partial differential equations in terms of two dependent variables, shear stress and particle velocity, and two independent variables, depth along the soil layer and time. The method of characteristics is a mathematical technique used to transform these two partial differential equations into four ordinary differential equations which are then solved by a suitable finite-difference technique.

In reference [71], Equation (8) multiplied by an unknown multiplier θ was added to Equation (11) to obtain:

$$\left[\frac{\partial \tau}{\partial t} + \theta \frac{\partial \tau}{\partial z}\right] - \rho\theta \left[\frac{\partial V}{\partial t} + \frac{1}{\rho\theta} \left(G + \frac{\mu}{\Delta t}\right) \frac{\partial V}{\partial z}\right] + \frac{\mu}{\Delta t} \left(\frac{\partial V}{\partial z}\right)_C = 0 \qquad (12)$$

From the definition of an Eulerian derivative, i.e., $\frac{d}{dt} = \frac{\partial}{\partial t} + \frac{dz}{dt} \frac{\partial}{\partial z}$, it is apparent that the bracketed terms in Equation (12) become total derivatives if

$$\frac{dz}{dt} = \theta = \frac{1}{\theta\rho} \left(G + \frac{\mu}{\Delta t}\right) \qquad (13)$$

from which

$$\theta = \pm \sqrt{\frac{G}{\rho} + \frac{\mu}{\rho \Delta t}} = \pm v_s \qquad (14)$$

in which v_s is the apparent shear wave velocity in the soil, equal to the slope of the characteristic lines in the z-t

diagram of Figure 2. Equations (12) and (13) are designated as C^+ when the plus sign is used for θ and C^- when the negative sign is used:

$$C^+ \begin{cases} \frac{d\tau}{dt} - \rho v_s \frac{dV}{dt} + \frac{\mu}{\Delta t} \left(\frac{\partial V}{\partial z}\right)_C = 0 & (15) \\ \frac{dz}{dt} = v_s & (16) \end{cases}$$

$$C^- \begin{cases} \frac{d\tau}{dt} + \rho v_s \frac{dV}{dt} + \frac{\mu}{\Delta t} \left(\frac{\partial V}{\partial z}\right)_C = 0 & (17) \\ \frac{dz}{dt} = -v_s & (18) \end{cases}$$

The quantity $(\partial V/\partial z)_C$ was expressed in terms of central finite differences for the interior points of the z-t diagram. A forward and backward finite difference scheme was used at the boundaries. After specifying a convenient time interval Δt, to be kept constant throughout the calculations, Equations (15) and (17) in finite-difference form become:

$$C^+: \quad \tau_P - \tau_A - \rho v_s (V_P - V_A) + \frac{\mu}{2\Delta z} (V_B - V_A) = 0 \qquad (19)$$

$$C^-: \quad \tau_P - \tau_B + \rho v_s (V_P - V_B) + \frac{\mu}{2\Delta z} (V_B - V_A) = 0 \qquad (20)$$

By solving Equations (19) and (20) the unknown quantities τ_P and V_P can be found. The distance interval Δz in Equations (19) and (20) is equal to:

$$\Delta z = \Delta t \sqrt{\frac{G}{\rho} + \frac{\mu}{\rho \Delta t}} \qquad (21)$$

In the simplest case, Δz could be found to be a sub-multiple of the soil deposit's total thickness. However, in reference [71], more sophisticated cases, such as G changing in a prescribed way with depth, were treated by using interpolations.

At the ground surface the boundary condition is $\tau_P = 0$. Then V_P can be found from the C^- characteristic, as:

$$V_P = V_B + \frac{\tau_B}{\rho v_s} - \frac{\mu}{\Delta z} (V_C - V_B) \frac{1}{\rho v_s} \qquad (22)$$

At the base, the boundary condition consists of a known V_P as a function of time from the seismic excitation under consideration. Then, τ_P can be found from the C^+ characteristic as:

$$\tau_P = \tau_A + \rho v_s (V_P - V_A) - \frac{\mu}{\Delta z} (V_C - V_A) \qquad (23)$$

The z-t diagram (Fig. 2) facilitates the understanding of the step by step solution. At time t_0 the shearing stresses τ and particle velocities V are assumed to be known (initial conditions). If the earthquake starts at time t_0, since the soil deposit is horizontal, τ and V are zero throughout (static conditions). These values permit calculation of τ and V at points P (one time step later) by using Equations (19), (20), (22) and (23). The same procedure is used for the next time step.

To this point all methods mentioned considered the soil to behave as a linear viscoelastic material which could be the case for small strains. However, shearing stress-shearing strain curves for most soils are nonlinear and Hardin and Drnevich [25] have experimentally demonstrated that this relationship may be approximated by a hyperbola.

Heierli [28] theoretically and experimentally studied the problem of one-dimensional pressure wave propagation in inelastic media such as soils. "Locking-up" dynamic stress-strain curves were determined experimentally for the material. The theory developed using a step-by-step procedure, closely resembles the method of characteristics.

Parmelee, et al. [52], and Seed and Idriss [61,35,36] used a lumped-mass solution to evaluate the seismic response of soil layers with shearing stress-strain characteristics approximated by a bilinear hysteretic model (Fig. A-1). The lumped masses were connected with a Voigt model attached in series to a dashpot, the latter to represent creep characteristics of the soil. The equations of motion were then solved using a step-by-step procedure [74].

Constantopoulos [15] modeled the soil as a series of lumped masses, springs and dashpots. The springs were defined by a nonlinear shearing stress-shearing strain relationship frequently adopted by structural engineers, known as the Ramberg-Osgood curve (Appendix 1). The solution was then carried out by direct numerical integration in the time domain.

Streeter, Wylie and Richart [71] used the Ramberg-Osgood nonlinear stress-strain relationship in conjunction with the appropriate equations of state and motion. They used a distributed parameter model and they solved the problem of one-dimensional shear wave propagation by employing the method of characteristics with specified time intervals and interpolations.

CHAPTER III

THE ACCURACY OF THE METHOD OF CHARACTERISTICS

In order to examine the accuracy obtained by using the method of characteristics and the sensitivity of the method to varying time increments as well as to varying degrees of viscous damping, the author conducted a series of simple case studies, three of which are presented in the following:

A homogeneous dry elastic soil deposit having constant mass density $\rho = 4.0$ slugs/ft^3, constant shear modulus $G = 10^6$ psf and a thickness of 50 feet was subjected at its base to a horizontal harmonic excitation of the form $V=0.2\sin 4\pi t$ feet/second. The shear wave velocity was equal to $\sqrt{G/\rho} = 500$ ft/sec, therefore the natural period of the system was $T_n = 4 \times 50/500 = 0.4$ sec and the forcing period was $T_f = 0.5$ sec. Since $T_n < T_f$ and no viscous damping was present, the excitation and the response were in phase [57]. Equation (4) was used to find analytically the particle velocities at the surface and at mid-height of the layer (Fig.3). The shearing forces at any depth were obtained from Equation (6) after substituting u from Equation (3). A time interval of 0.01 sec and reaches of length $\Delta z = 5.0$ feet were used in the method of characteristics. The use of $\tau = 0$ and $V = 0$ throughout the soil layer as initial conditions for the method of characteristics would cause the generation of an initial transient which would not vanish since no dissipating mechanism is available ($\mu = 0$). By using as initial

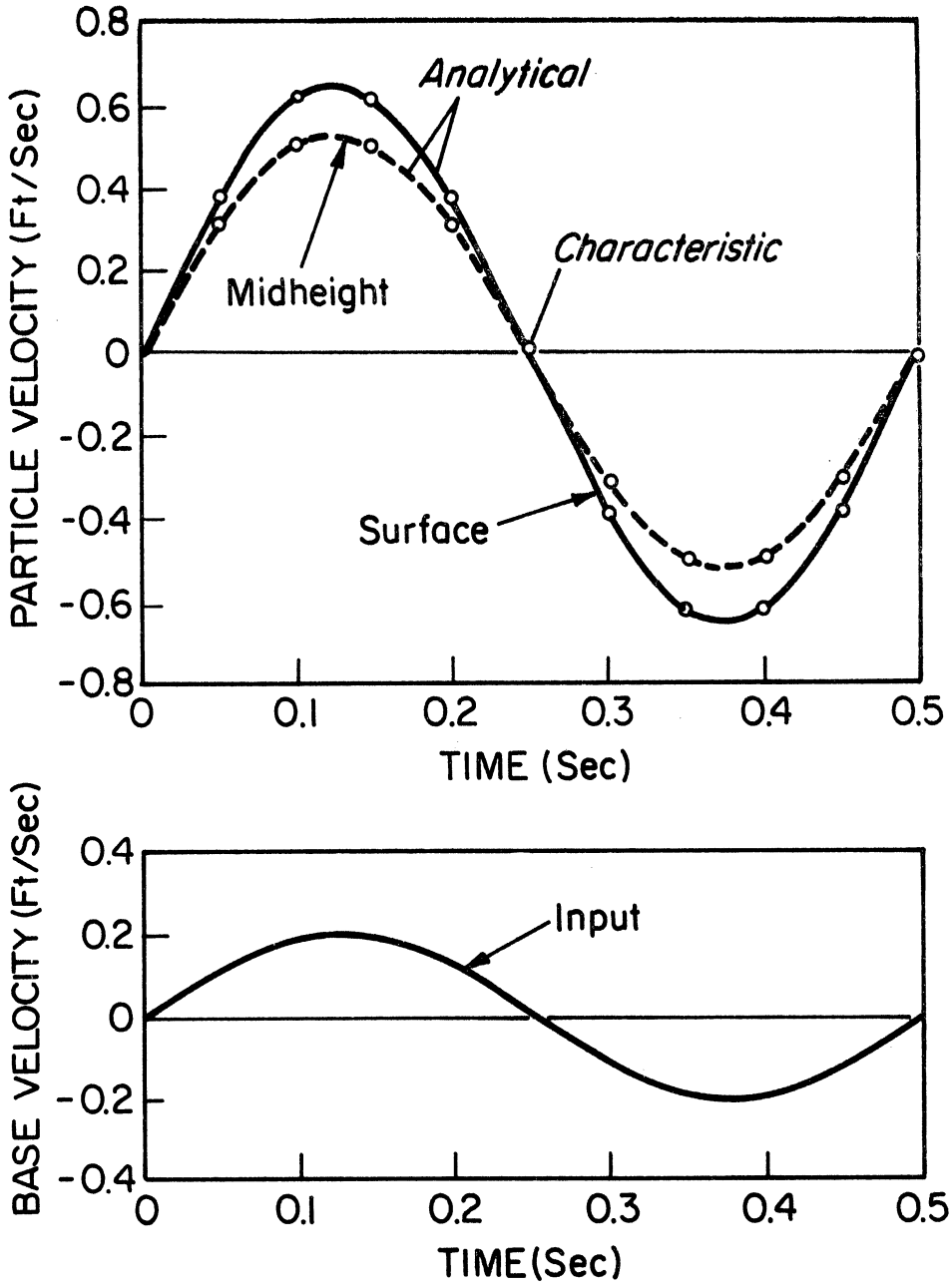

Figure 3. Comparison of method of characteristics vs. analytical for a 50 ft elastic soil layer (μ = 0).

conditions the shearing stresses and the particle velocities found from the analytical solution at time t = 0, at equal distances of 5 feet throughout the soil layer, the method of characteristics immediately converged on the exact solution as shown in Figure 3.

A homogeneous dry viscoelastic soil deposit 141.4 feet thick resting on a horizontal rock base was next considered. The mass density ρ = 4 slugs/ft^3, the shear modulus G = 8 x 10^5 psf and the viscosity μ = 12000 lb·sec/ft^2 were assumed constant throughout the soil layer. A horizontal sinusoidal velocity having an amplitude of 1.0 ft/sec and a frequency of 4π rad/sec was exerted on the base rock. The shear wave velocity was 447.2 ft/sec. Two time intervals were used. For Δt = 0.010 sec the soil deposit was divided into 20 reaches with Δz = 7.07 feet. For Δt = 0.025 sec the soil deposit was divided into 10 reaches with Δz = 14.14 feet. Shearing stresses and velocities both equal to zero were used as initial conditions to the method of characteristics. After 18 cycles, the initial transient vanished completely due to the presence of viscous damping. The particle velocities at the surface of the formation computed by the method of characteristics after 9.0 seconds were found to be in agreement with the velocities obtained from the analytical solution (Fig. 4). Slight differences of less than 1% when using Δt = 0.025 sec were attributed to the coarser discretization used. Since discretization depends on both Δt and Δz, the case with Δt = 0.010 sec and Δz = 7.07 ft was five

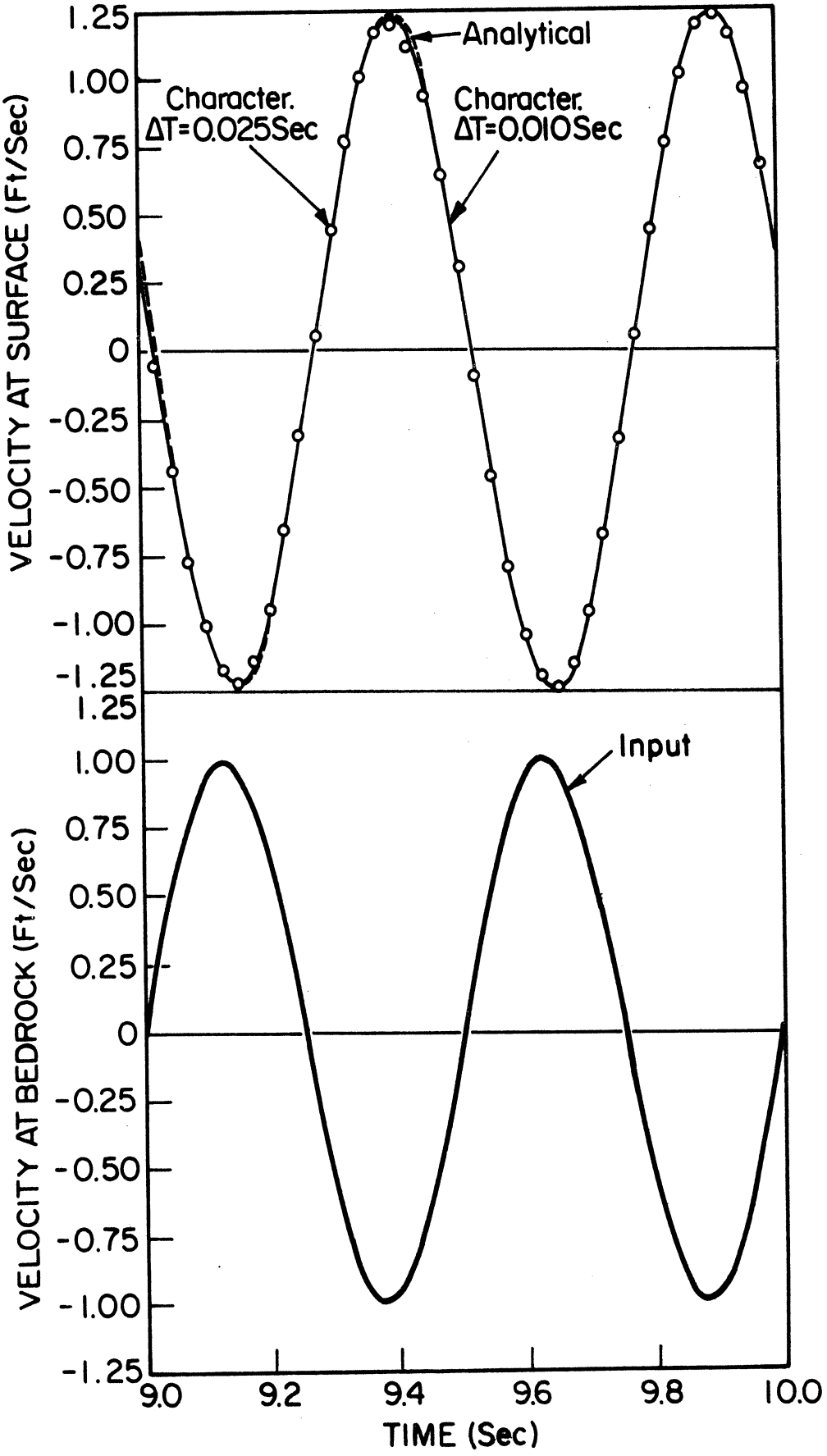

Figure 4. Velocity at surface of a 141.4 ft viscoelastic soil deposit, computed analytically and by method of characteristics (two dif. time incr.).

times more densely discretized than the case with $\Delta t = 0.025$ sec and $\Delta z = 14.14$ ft. However, even such a difference in discretization did not influence the results obtained. In Figure 5 the shearing stresses computed at the rock base were plotted for comparison. The small differences observed between the closed form solution and the method of characteristics should be mainly attributed to the numerical approximations which accompany the latter. The differences between the two characteristics solutions were more pronounced due to numerical approximation errors in addition to discretization.

In order to demonstrate the influence of the viscosity term in the response of a soil layer to a periodic excitation, a soil layer 100 feet thick resting on horizontal bedrock was considered. The soil was assumed to have a mass density $\rho = 4$ slugs/ft^3 and a shear modulus $G = 8 \times 10^5$ psf constant throughout the depth of the deposit. The base rock developed a horizontal periodic excitation $V=0.2\sin 4\pi t$ in feet per second. The period of the forced vibration was $T_f = 0.5$ sec and since the shear wave velocity was 447.2 ft/sec the natural period of the system was $T_n = 0.894$ sec. Since $T_n > T_f$, for the case of $\mu = 0$, as it was expected the forcing function and the response were 180° out of phase (Fig. 6). Increase of the viscosity to values of 20,000 lb·sec/ft^2 and 40,000 lb·sec/ft^2 resulted in a decrease of the corresponding amplitudes of the particle velocities at the surface of the formation and to an additional change in

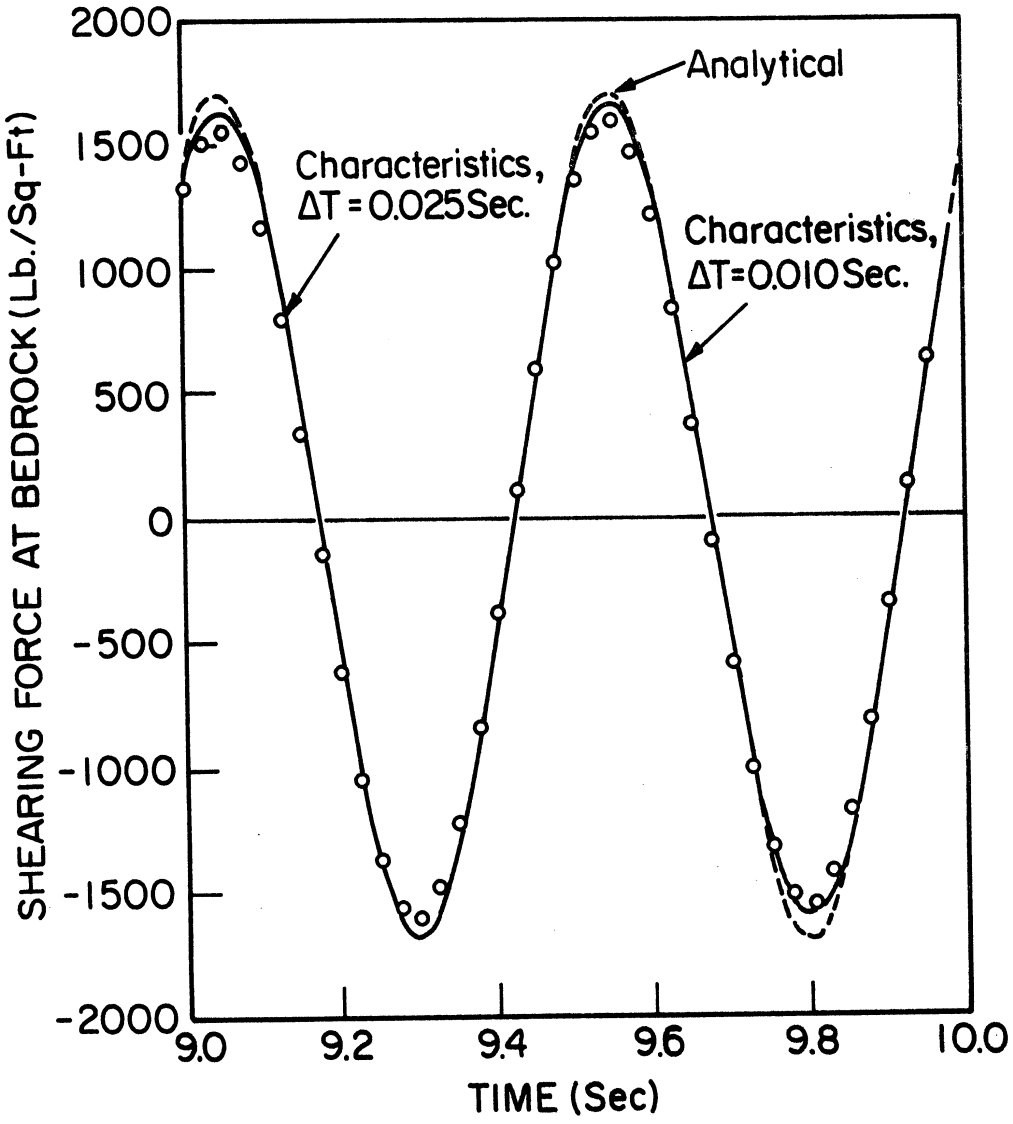

Figure 5. Shear at the base of a 141.4 ft viscoelastic soil deposit, computed analytically and by method of characteristics (two dif. time incr.).

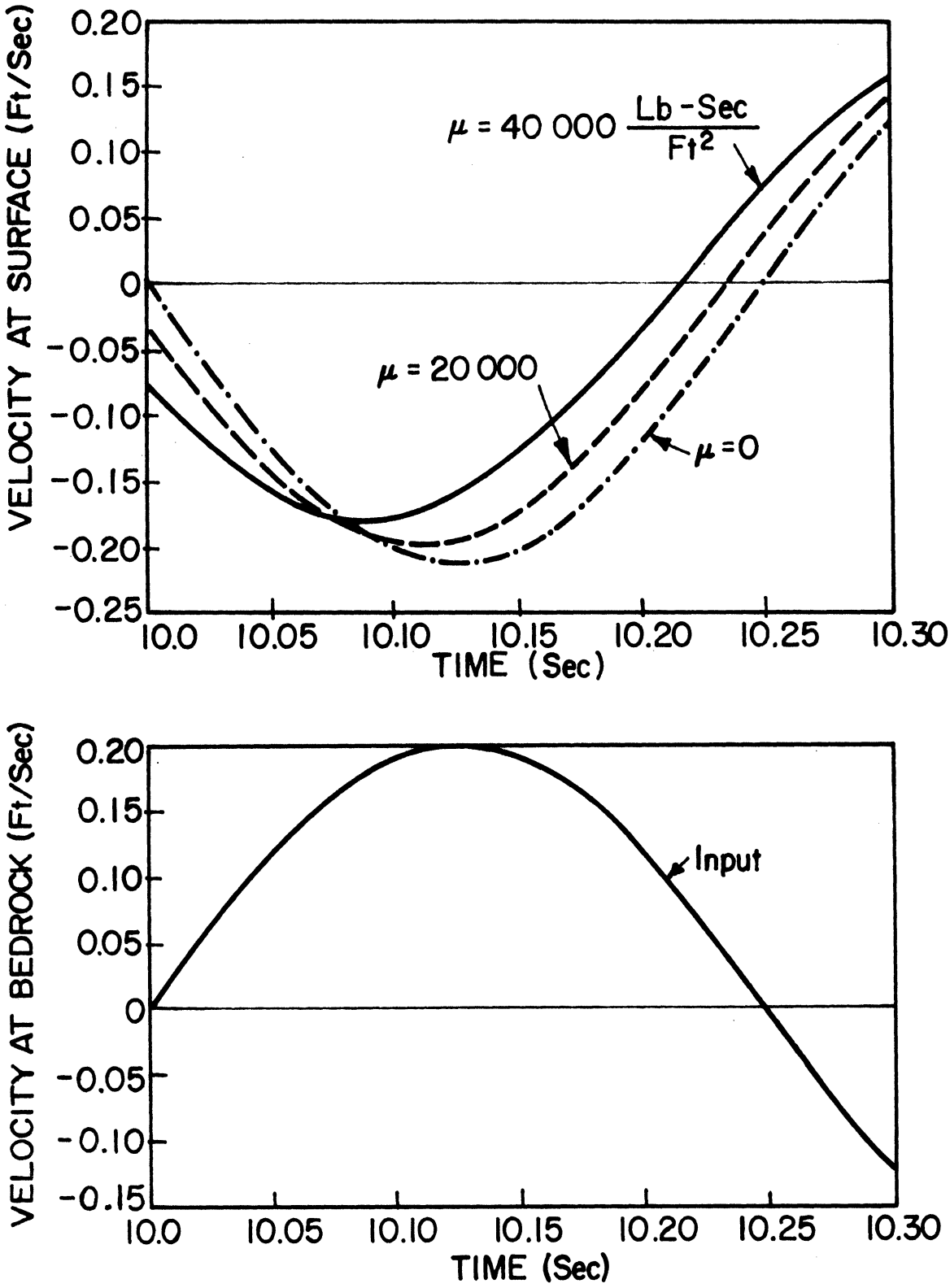

Figure 6. Influence of viscosity on phase angle and amplitude amplification of the response of a 100 ft soil layer.

phase. The analytical solution and that obtained by the method of characteristics were in perfect agreement after 20 cycles (Fig. 6).

These examples were presented mainly to demonstrate that solutions obtained by the method of characteristics are only slightly influenced by the degree of discretization employed and that numerical approximation errors are negligible. In spite of the fact that the method of characteristics is a numerical method developed to solve transient problems, it can also successfully handle steady oscillatory problems when the viscous damping is enough to gradually dissipate the initial transient generated.

CHAPTER IV

COMPUTATION OF BEDROCK MOTION FROM A RECORDED GROUND SURFACE MOTION

Review of Literature

In the United States, most seismographs that recorded strong earthquake motions were located on alluvial soil deposits. Therefore, data on rock motions are very limited. Prior to the San Fernando earthquake of February 9, 1971, the only strong rock motion recordings on sedimentary rock were those of Helena, Montana, 1935; Taft, California, 1952; and Golden Gate Park, San Francisco, 1957 [31].

Assuming that upward shear wave propagation from the underlying rock is the main cause of horizontal ground motions during earthquakes [54], various procedures have been developed (Chapter II) to compute the response of a soil deposit to a known bedrock motion. Since ground surface records of earthquake motions are more numerous, it is of importance to use these records to determine the rock motions from which they were generated. This is desirable because the computed bedrock motions could be used to find ground responses of adjacent but different soil formations overlying the same bedrock.

Schnabel, Seed and Lysmer [59] developed a computational method to model shear wave transmission through layers of viscoelastic soil overlying bedrock. All displacements were assumed to be horizontal caused by shear waves propagating vertically through the soil. The damped wave

equation (Eq. 2) was used to model the system's response. A soil deposit was subdivided into n layers each of thickness h_j (j=1,...n), with a local coordinate system z for each layer. The soil properties at each layer were considered to be constant. The boundary conditions used at the ground surface were zero shearing stresses and a harmonic displacement with frequency ω and known amplitude W of the form:

$$u_1(z=0,t) = We^{i\omega t} \tag{24}$$

The solution to the wave equation for a harmonic motion of frequency ω, for the jth layer was:

$$u_j(z,t) = E_{j+1}\, e^{i\omega(z/v_j^*+t)} + F_{j+1}\, e^{-i\omega(z/v_j^*-t)} \tag{25}$$

where $h_j > z > 0$, and $v_j^* = \sqrt{(G_j + i\omega\mu_j)/\rho_j} = \sqrt{G_j^*/\rho_j}$
The first term of Equation (25) represents the incident wave traveling upwards and the second term the reflected wave traveling downwards (in the positive z direction). The amplitudes E_{j+1} and F_{j+1} of these two waves were computed by a recursion formula developed from the condition that stresses and displacements should be continuous at all layer interfaces. These amplitudes are functions of the complex impedance ratio α_j:

$$E_{j+1} = 0.5E_j\,(1+\alpha_j)\,\exp(K_j) + 0.5F_j\,(1-\alpha_j)\,\exp(-K_j) \tag{26}$$

$$F_{j+1} = 0.5E_j(1-\alpha_j)\ \exp(K_j) + 0.5F_j(1+\alpha_j)\ \exp(-K_j) \quad (27)$$

where

$$K_j = i\omega h_j/v_j^* \quad (28)$$

$$\alpha_j = \rho_j\ v_j^*\ /\ \rho_{j+1}\ v_{j+1}^* \quad (29)$$

and $\exp(K_j)$ is equal to the base of the natural logarithms e raised to the K_j power.

The above expressions developed by Schnabel, et al. [58,59] are valid only for steady state harmonic motions. If the surface of a soil deposit develops a harmonic displacement of the form of Equation (24), then the rock motion $u_{n+1}(z=h_n,t)$ which caused this displacement may be computed from Equation (25).

Schnabel, Lysmer and Seed [58] extended the theory to transient motions through the use of Fourier transformation by employing the Fast Fourier Transform algorithm developed by Cooley and Tukey [16] (Appendix 2). In the case of transient motions the assumption was made that the complex shear modulus is independent of frequency and equal to:

$$G^* = G(1+2iD) \quad (30)$$

where D is the critical damping ratio assumed constant for any value of ω. Generally, D and ω are related through the expression [57]:

$$D = \omega\mu/(2G) \tag{31}$$

The above analytical method is used later in this chapter to compare with the method of characteristics in a case study.

Base Motion Synthesis. Viscoelastic Soil.

The methods reviewed in Chapter II, to calculate the ground surface motion of a soil deposit for a known bedrock motion are methods of analysis (feed-back process). The method of characteristics is used in the following to solve the reverse problem, i.e., to compute the bedrock motion which caused a known transient motion at the ground surface. This method resembles the valve stroking concept as used in hydraulic transients [66] and may be characterized as a method of synthesis (feed-forward process). It is termed herein, "Base Motion Synthesis" method.

Propagation of shear waves vertically through horizontal layers of dry soil is treated as a one-dimensional problem described by the partial differential equations of state and motion (Equations 6 and 7). By using the method of characteristics, Equations (6) and (7) are transformed into four ordinary differential equations (Equations 15, 16, 17 and 18). After a time interval Δt is selected, the soil deposit is divided into reaches of length:

$$\Delta z_j = \Delta t \sqrt{\frac{G_j}{\rho_j} + \frac{\mu_j}{\rho_j \Delta t}} \tag{32}$$

The soil properties G, ρ, μ, although they can be considered to change with depth in a prescribed manner, are assumed to be constant within each reach (j) and their values at mid-thickness of the reach are used.

Referring to the z-t diagram in Figure 7, shearing stresses and velocities are zero at all the nodes of the diagram to the left of line FA. At the surface points A, C, B and E, shear is zero and velocity is known. By using the method of Base Motion Synthesis, the shearing stresses and particle velocities at the base ($\overline{FG}$) that produced the surface motion are sought. In terms of forward and backward finite differences, the compatibility equations which are valid along the C^+ and C^- characteristic lines (Equations 15 and 17) reduce to:

$$C^+: \quad \tau_P - \tau_A - \rho v_s (V_P - V_A) + \frac{\mu}{\Delta z} (V_D - V_A) = 0 \tag{33}$$

$$C^-: \quad \tau_B - \tau_P + \rho v_s (V_B - V_P) + \frac{\mu}{\Delta z} (V_P - V_C) = 0 \tag{34}$$

The distance intervals Δz are given by Equation (32) and v_s is equal to $\Delta z/\Delta t$. The simultaneous solution of Equations (33) and (34) is facilitated if all the known quantities of each of these two equations are gathered together and called CP (for the C^+) and CM (for the C^-):

$$CP = \tau_A - \rho v_s V_A - \frac{\mu}{\Delta z}(V_D - V_A) \tag{35}$$

$$CM = \tau_B + \rho v_s V_B - \frac{\mu}{\Delta z} V_C \tag{36}$$

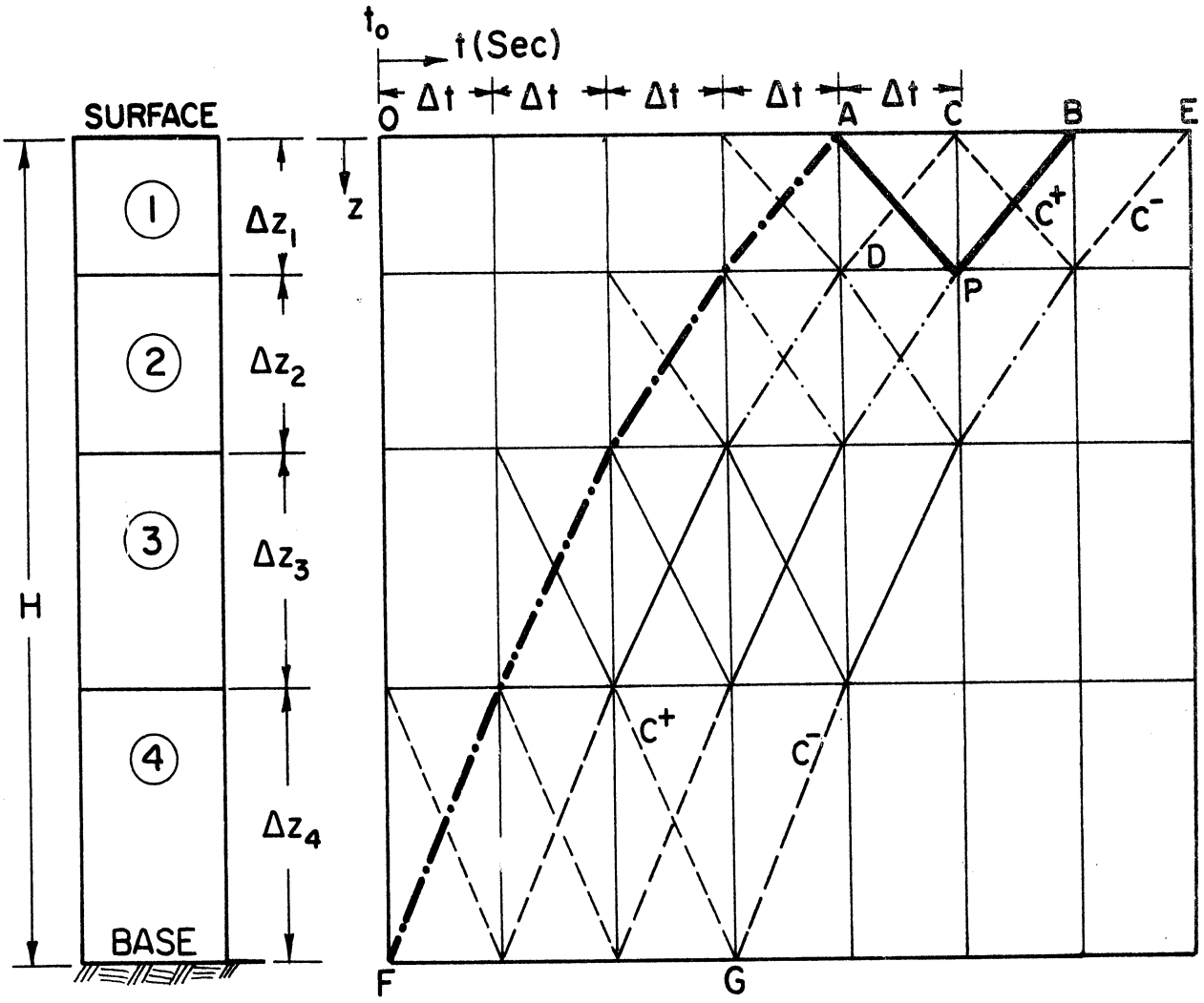

Figure 7. Layer designation and z-t diagram.

Then, the unknown shearing stress and particle velocity at point P are obtained as:

$$V_P = \frac{CM - CP}{2\rho v_s - \mu/\Delta z} \tag{37}$$

$$\tau_P = CP + \rho v_s \frac{CM - CP}{2\rho v_s - \mu/\Delta z} \tag{38}$$

Considering that an "action" at the bedrock causes a "reaction" at the surface of a soil deposit, the Base Motion Synthesis method can generate the "action" if the "reaction" is known. This ability of the method becomes evident by studying the z-t diagram in Figure 7. Shearing stress and velocity at P are influenced by conditions existing one time step later at a distance Δz away from P (point B), because the incident shear wave travels the distance Δz_1 in time Δt. Following the C^- characteristics from point E downwards, it is observed that "reaction" conditions at E ($z=0$, $t=7\Delta t$) are related to "action" conditions at G ($z=H$, $t=3\Delta t$).

A step-by-step procedure greatly facilitates the computations. Based on known conditions at the surface, Equations (37) and (38) yield the shearing stresses and particle velocities at a depth $z = \Delta z_1$ in the time domain. Based on known conditions at depth $z = \Delta z_1$, Equations (37) and (38) yield the shearing stresses and particle velocities at a depth $z = \Delta z_1 + \Delta z_2$ in the time domain. The same procedure is repeated until the bedrock is reached. Thus, the method also provides the user with intermediate results, calculating

shearing stresses and particle velocities at all reach interfaces.

Example An unsaturated soil deposit 218.82 feet thick was selected for study. The soil deposit consists of four layers: 36.38 feet of fill with ρ = 3.73 slugs/ft^3, G = 1.375 x 10^6 psf, μ = 30,000 lb·sec/ft^2; 46.34 feet of soft clay with ρ = 3.26 slugs/ft^3, G = 0.5 x 10^6 psf, μ = 10,000 lb·sec/ft^2; 64.0 feet of medium clay with ρ = 3.42 slugs/ft^3, G = 10^6 psf, μ = 20,000 lb·sec/ft^2; and 72.1 feet of sand and gravel with ρ = 4.04 slugs/ft^3, G = 6 x 10^6 psf, μ = 120,000 lb·sec/ft^2 resting on a horizontal rock base (Figure 8). The first 8 seconds of the North-South component of the 1940 El Centro earthquake accelerogram (Figure 9) were considered to be the hypothetical reaction of the ground surface. Two methods were used to find the bedrock excitation, the analytical method [58] reviewed previously, and the Base Motion Synthesis method. The analytical method uses as input the displacement record of the North-South component of the 1940 El Centro earthquake obtained by twice integrating numerically the earthquake accelerogram [8]. The Base Motion Synthesis method uses as input the velocity record of the North-South component of the 1940 El Centro earthquake obtained by integrating numerically the earthquake accelerogram.

A value of D = 0.01 was used in the analytical method. This assumption of a constant ratio $\mu\omega/G$, tends to underdamp the higher frequency harmonics of the Fourier transform and

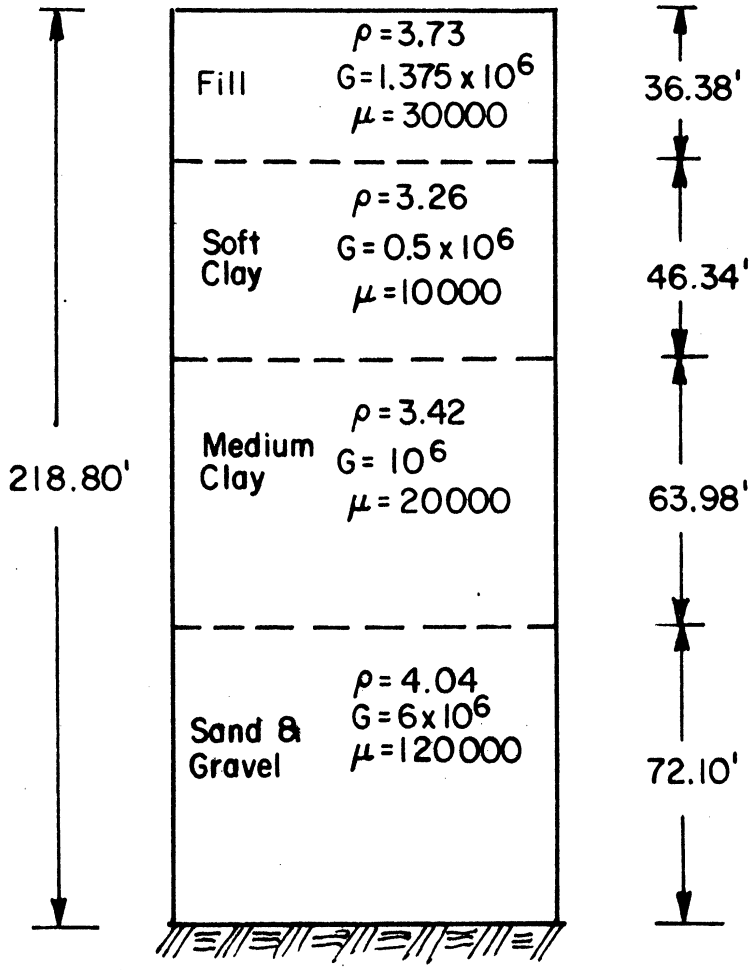

Figure 8. Profile of soil deposit.

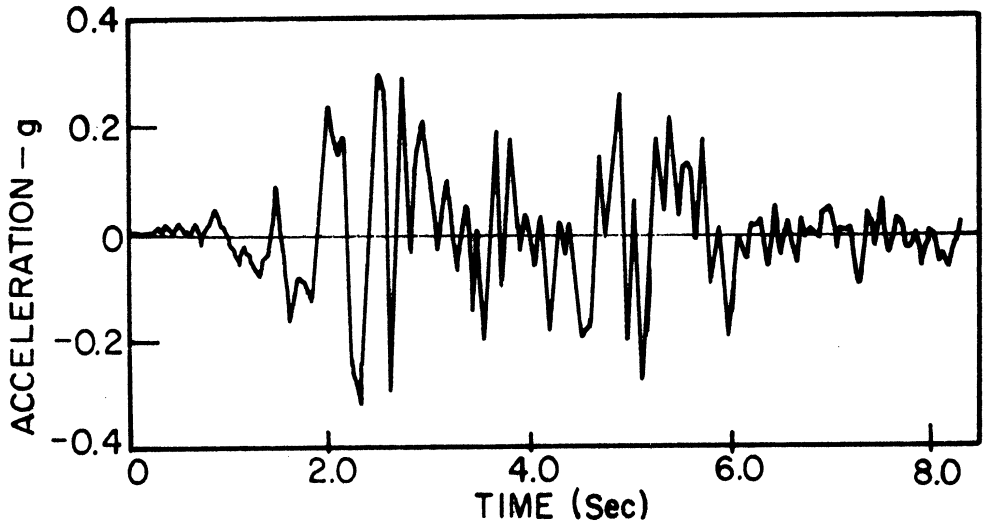

Figure 9. Accelerogram of El Centro earthquake, 1940, North-South component.

overdamp the lower frequency harmonics. A time interval of 0.05 seconds was used in the Base Motion Synthesis method. A computer program written in FORTRAN IV Language, presented in Appendix 5, performed all the necessary computations for the Base Motion Synthesis method. For this specific example, the computer time required by the Base Motion Synthesis method was approximately half the time required by the analytical method. The base rock displacements and velocities calculated by both methods are plotted in Figures 10 and 11 for comparison. Small differences observed are mainly due to the fact that the analytical method does not use the whole range of frequencies of the Fourier transform in the evaluation of the complex shear modulus G*.

An additional confirmation of the Base Motion Synthesis method is obtained by the method of characteristics (method of analysis) reviewed in Chapter II. The base rock velocity resulting from the Base Motion Synthesis method was used as input to the method of analysis. The velocity response at the surface of the soil deposit computed by using the method of analysis was found to be substantially the same as that used as input to the Base Motion Synthesis method (Figure 11).

In Figure 12, the shearing stress at the base rock computed by the Base Motion Synthesis method is plotted versus time.

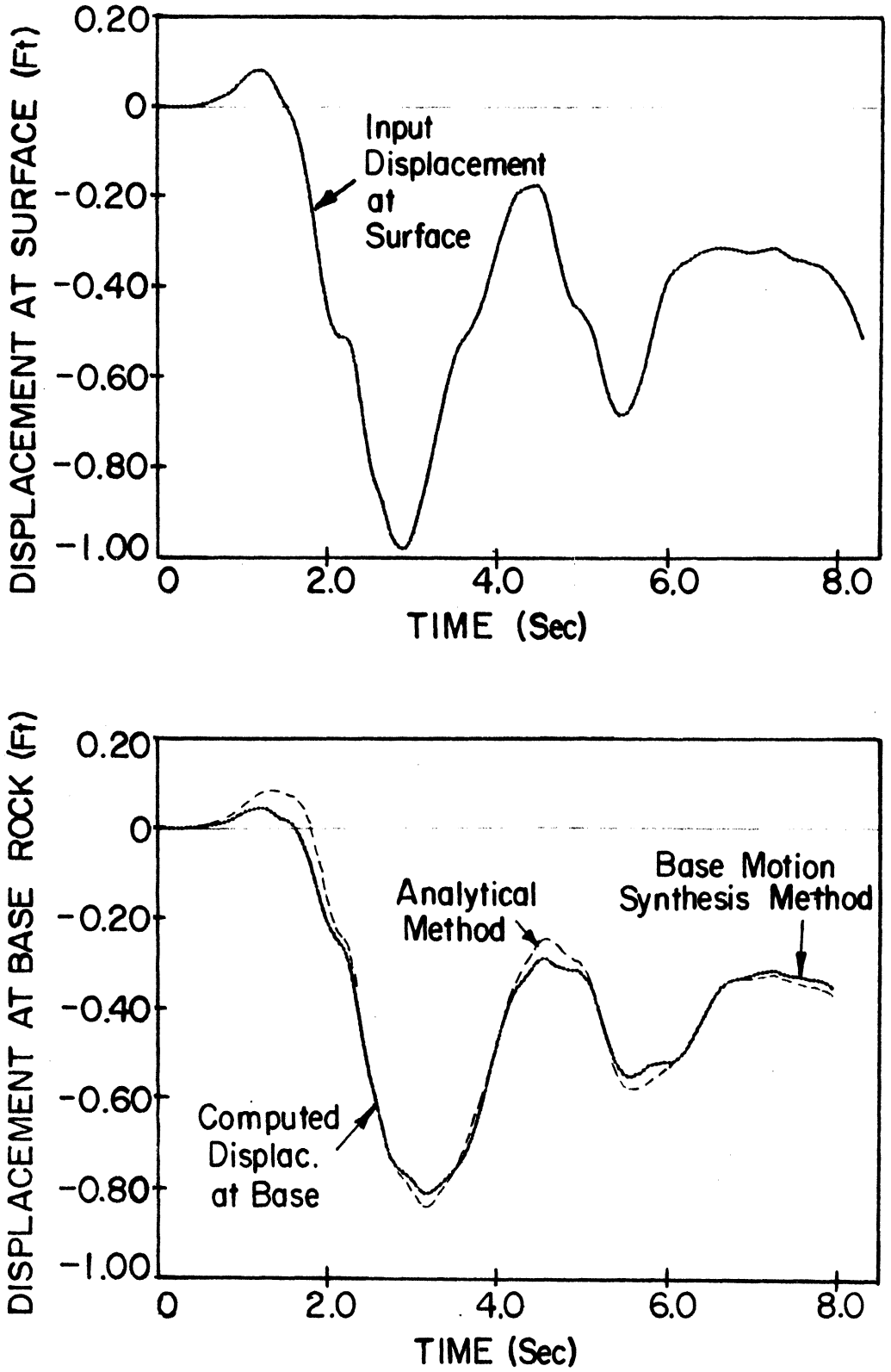

Figure 10. Displacement applied at surface (El Centro, 1940, N-S) and computed base rock displacement.

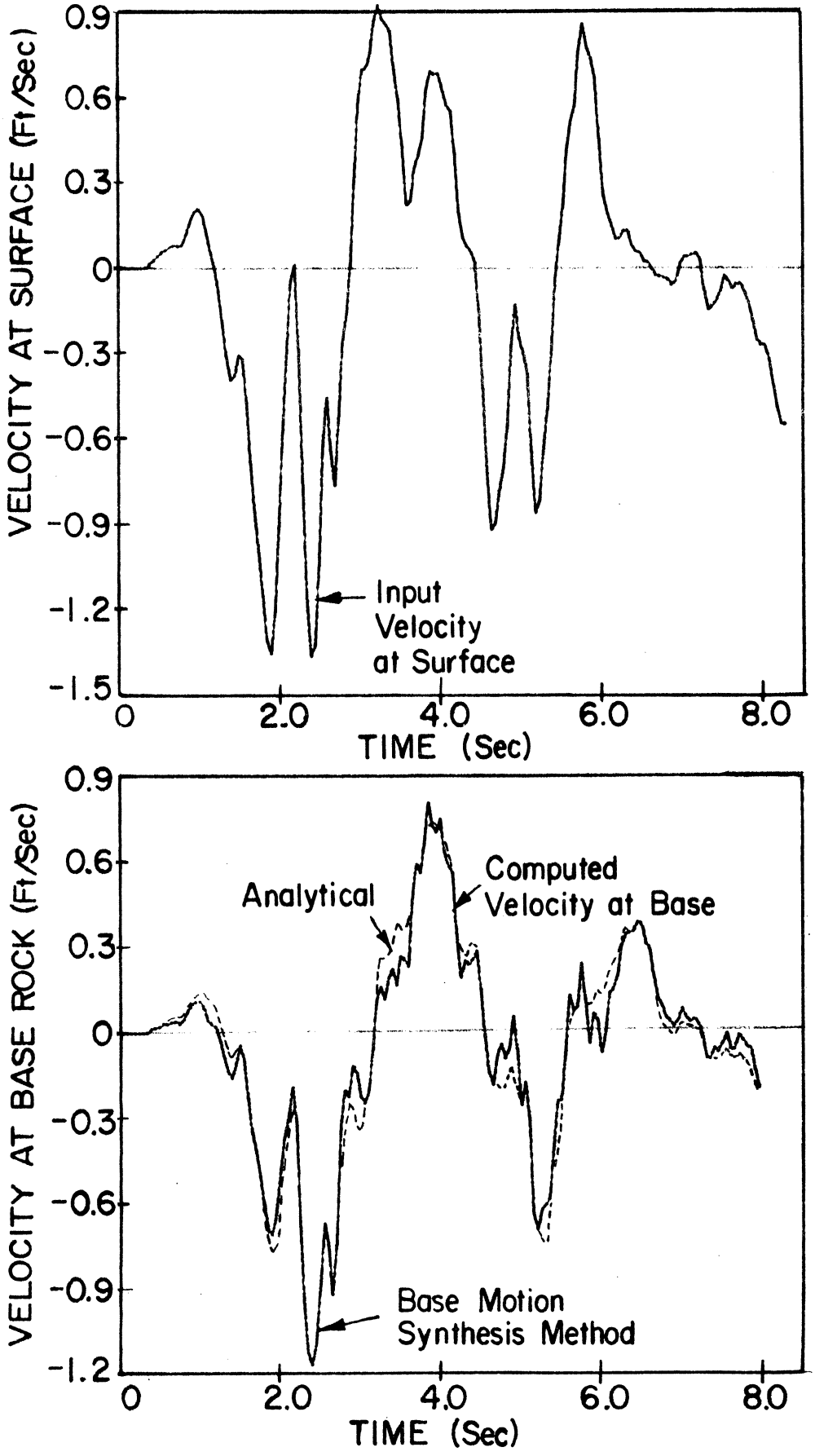

Figure 11. Velocity applied at surface (El Centro, 1940, N-S) and computed velocity at base rock.

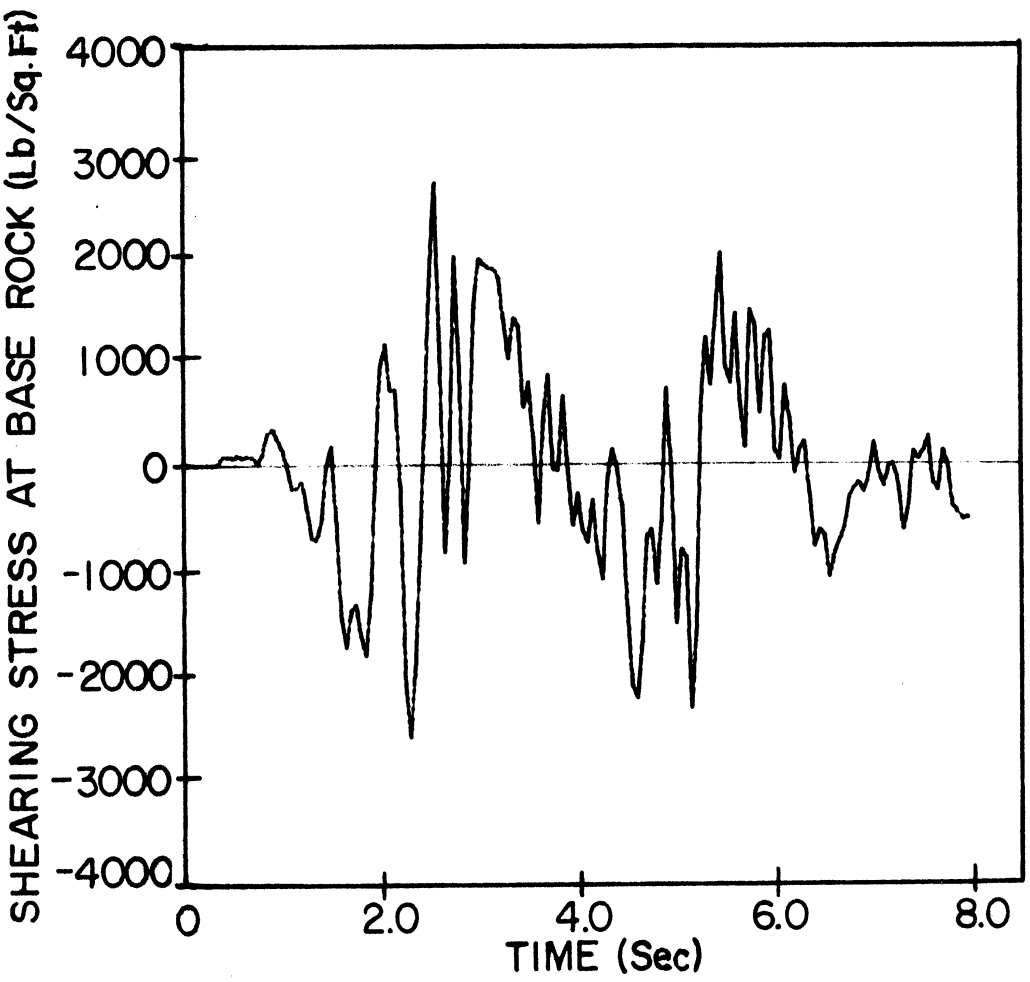

Figure 12. Computed shearing stress at base rock by base motion synthesis method.

Base Motion Synthesis. Inelastic Soil.

The inelastic or "strain-softening" behavior of soil may be modeled by shearing stress-shearing strain curves of the Ramberg-Osgood type (Appendix 1). The method of characteristics in conjunction with a Ramberg-Osgood hysteretic model was used by Streeter, Wylie and Richart [71] to solve problems of one-dimensional shear wave transmission through horizontal layers of dry soil. A seismic disturbance was applied to the base rock and the response of the soil layer overlying the bedrock was computed. This forward type of solution is a method of analysis. In the following development, the Base Motion Synthesis method is modified so inelastic soil behavior can be modeled. Thus, the solution is obtained to the reverse problem which is to find the seismic disturbance at the base rock that caused a known response at the surface of the overlying soil layer. The method of characteristics in conjunction with a centered implicit method are used in this development.

The damping effect of a Ramberg-Osgood hysteresis model is more pronounced than that obtained by a viscoelastic hysteresis loop. Therefore, since the presentation gains also in simplicity, the viscous term is omitted from the governing differential equations. However, viscous damping can also be considered if necessary.

Under dynamic conditions the equation of motion is:

$$\frac{\partial \tau}{\partial z} - \rho \frac{\partial V}{\partial t} = 0 \qquad (39)$$

where τ is the shearing stress and V is the particle velocity at a depth z; ρ is the mass density of the soil. The dynamic stress-strain relationship is:

$$d\tau = G\, d\gamma \tag{40}$$

in which γ is the shearing strain equal to $\partial u/\partial z$, G is the shear modulus and u is displacement at a depth z. From Equation (40) the following differential equation may be derived:

$$\frac{\partial \tau}{\partial t} - G \frac{\partial V}{\partial z} = 0 \tag{41}$$

In Equation (41) the tangent shear modulus G, for static and low frequency deformations is given by

$$G = d\tau/d\gamma \tag{42}$$

Multiplying Equation (39) by an unknown multiplier θ, and adding to it Equation (41) gives:

$$\left(\theta \frac{\partial \tau}{\partial z} + \frac{\partial \tau}{\partial t}\right) - \theta\rho\left(G \frac{1}{\theta\rho} \frac{\partial V}{\partial z} + \frac{\partial V}{\partial t}\right) = 0 \tag{43}$$

The terms in parenthesis become total derivatives if:

$$\frac{dz}{dt} = \theta = \frac{1}{\theta\rho} G \tag{44}$$

from which

$$\theta = \pm\sqrt{G/\rho} = \pm v_s \tag{45}$$

where v_s is the shear wave velocity in the soil. Two pairs of total differential equations emanate from Equation (43), designated C^+ when the plus sign is used for θ and C^- when the negative sign is used:

$$C^+ \begin{cases} \frac{d\tau}{dt} - \rho v_s \frac{dV}{dt} = 0 & (46) \\ \frac{dz}{dt} = v_s & (47) \end{cases}$$

$$C^- \begin{cases} \frac{d\tau}{dt} + \rho v_s \frac{dV}{dt} = 0 & (48) \\ \frac{dz}{dt} = -v_s & (49) \end{cases}$$

To solve numerically Equations (46) to (49), a convenient time interval Δt is selected to be kept constant throughout the calculations and the soil layer is divided into distance intervals equal to

$$(\Delta z)_j = \Delta t \sqrt{(G_0)_j/\rho_j} \qquad (50)$$

where G_0 is the shear modulus for $\gamma = 0$, usually changing as the square or cubic root of depth. However, the value of G_0 calculated at mid-thickness of a layer (j) is used as constant throughout that layer.

A shearing stress-shearing strain curve of the Ramberg-Osgood type requires that $G \leqslant G_0$ in each layer (the equal sign holds at the turning points of the curves). This means that $(\overline{CP})$ in Figure 13 is always less than the corresponding $(\Delta z)_j$, i.e. $v_s \cdot \Delta t \leqslant (\Delta z)_j$ at all times, a necessary condition for the method of characteristics to be stable.

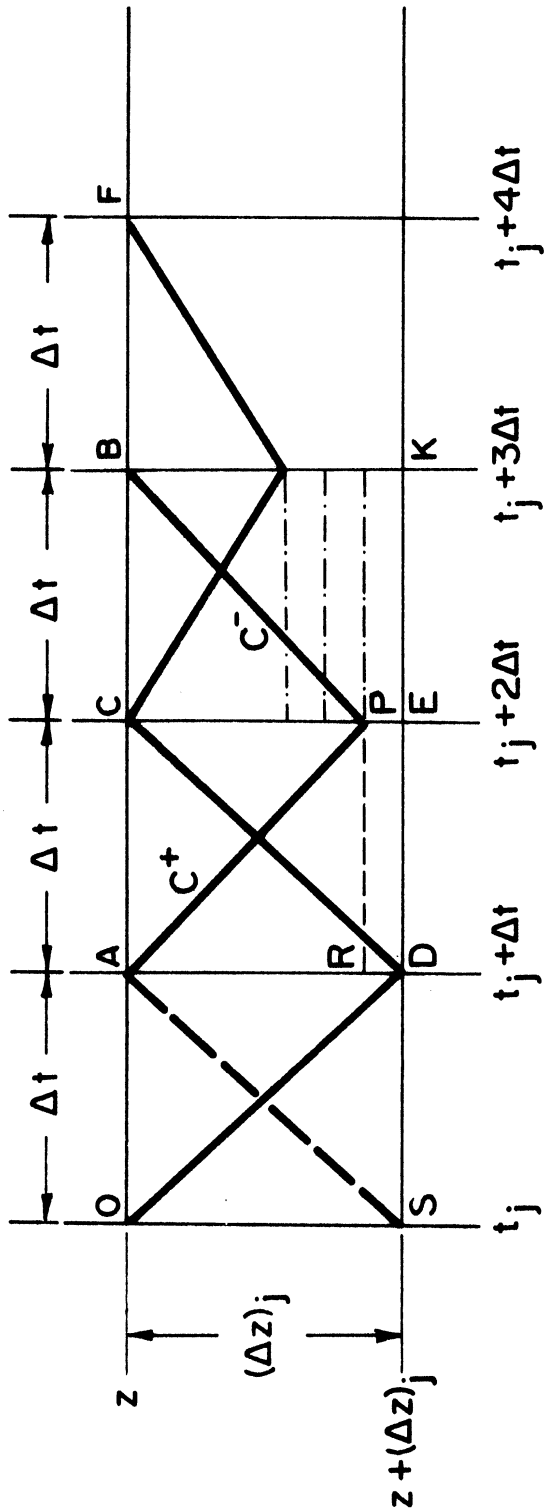

Figure 13. Part of the z-t diagram for a layer of inelastic soil. Method of base motion synthesis.

In Figure 13, the part of the z-t diagram corresponding to a layer (j) is drawn. Assuming that t_j is the time required for the shear wave to reach the bottom of layer (j) from the base rock, conditions to the left of line ($\overline{AS}$) are static. Also, conditions (i.e. shearing stresses and particle velocities) at points A, C, B, and F are known from the overlying layer $(\Delta z)_{j-1}$. The objective is to find the conditions at points D, E and K of the z-t diagram. The procedure is then repeated for the underlying layer $(\Delta z)_{j+1}$ until the base rock is reached.

Equations (46) and (48) can be expressed in a finite difference form:

$$C^+: \qquad \tau_P - \tau_A - \rho v_s (V_P - V_A) = 0 \tag{51}$$

$$C^-: \qquad \tau_B - \tau_P + \rho v_s (V_B - V_P) = 0 \tag{52}$$

where $v_s = \sqrt{G/\rho}$ is the shear wave velocity for the layer under consideration. Equations (51) and (52) solved simultaneously yield the values of τ and V at point P:

$$\tau_P = \frac{\tau_A + \tau_B}{2} + \frac{V_B - V_A}{2} \rho v_s \tag{53}$$

$$V_P = \frac{V_A + V_B}{2} + \frac{\tau_B - \tau_A}{2 \rho v_s} \tag{54}$$

At time $t_j + \Delta t$, the shear modulus G is still equal to G_0, therefore points P and D coincide and Equations (53) and (54) are sufficient to find τ_D and V_D. A time interval

later $G < G_0$ and $(\overline{CP}) < (\Delta z)_j$. In this case, shear and velocity at point E can be found by employing a generalized centered implicit method [67].

The terms in Equations (39) and (41) in finite difference notation become:

$$\frac{\partial V}{\partial z} = \frac{\xi(V_E - V_P) + (1-\xi)(V_D - V_R)}{(\Delta z)_j - v_s \Delta t} \tag{55}$$

$$\frac{\partial \tau}{\partial z} = \frac{\xi(\tau_E - \tau_P) + (1-\xi)(\tau_D - \tau_R)}{(\Delta z)_j - v_s \Delta t} \tag{56}$$

$$\frac{\partial V}{\partial t} = \frac{V_P + V_E - V_R - V_D}{2\ \Delta t} \tag{57}$$

$$\frac{\partial \tau}{\partial t} = \frac{\tau_P + \tau_E - \tau_R - \tau_D}{2\ \Delta t} \tag{58}$$

where ξ is a weighting factor. The quantities V_R and τ_R are found by linear interpolation between the known values of V_A, τ_A and V_D, τ_D, as follows:

$$\tau_R = \tau_A + \frac{v_s\ \Delta t}{(\Delta z)_j} (\tau_D - \tau_A) \tag{59}$$

$$V_R = V_A + \frac{v_s\ \Delta t}{(\Delta z)_j} (V_D - V_A) \tag{60}$$

Equations (55) to (58) are substituted back into Equations (39) and (41) which become:

$$\frac{\xi(\tau_E-\tau_P) + (1-\xi)(\tau_D-\tau_R)}{(\Delta z)_j - v_s \Delta t} - \rho \frac{V_P + V_E - V_R - V_D}{2\Delta t} = 0 \quad (61)$$

$$\frac{\tau_P + \tau_E - \tau_R - \tau_D}{2\Delta t} - G \frac{\xi(V_E-V_P) + (1-\xi)(V_D-V_R)}{(\Delta z)_j - v_s \Delta t} = 0 \quad (62)$$

The quantities τ_P and V_P are known from Equations (53) and (54), τ_R and V_R are known from Equations (59) and (60) and τ_D and V_D are known from the previous time step. Therefore, Equations (61) and (62) are solved simultaneously to find the only unknowns τ_E and V_E. In this case only one centered implicit cell (DRPE) was used. However, if $v_s \cdot \Delta t$ becomes small compared with $(\Delta z)_j$, more implicit cells should be used improving considerably the results obtained.

The implicit scheme has neutral stability if the weighting factor $\xi = 0.50$ and it is unconditionally stable for $0.5 < \xi \leq 1.0$. The stability of the implicit method does not depend on the ratio $(\overline{PE})/\Delta t$ as do the explicit and characteristic methods. Under certain conditions however, the implicit method has been observed to exhibit instabilities [6,46]. In the present analysis instabilities did not occur and improved results were obtained by using a weighting factor ξ of 0.9 or even 1.0.

The Base Motion Synthesis method as modified above for the case of inelastic soil behavior, is still based on

a feed-forward process since conditions at time t + Δt and depth z (i.e. point B) influence conditions at time t and depth z + $(\Delta z)_j$ (i.e. point P and subsequently point E, in Figure 13).

The same procedure is repeated for each time step. A new value of G is obtained from the proper Ramberg-Osgood curve (loading or unloading) based on the average value of the shearing stress over the layer one time interval earlier. The computational scheme moves forward in the time domain for each layer starting from the top layer and proceeding to the base rock. A solution by the Base Motion Synthesis method is thus made feasible.

Example. An unsaturated sand deposit 70.4 feet thick rests on horizontal bedrock. The sand has a unit weight γ_s = 100 lb/ft^3. The static shear modulus, G_0, is determined at the mid-point of each layer at a depth z from the expression:

$$G_0 = 50000 \sqrt{\gamma_s z} \qquad (lb/ft^2) \tag{63}$$

The time interval selected is Δt = 0.01 seconds. According to Equation (50) the soil deposit is subdivided into eight layers with thicknesses of 5.0, 6.8, 7.9, 8.8, 9.6, 10.2, 10.8, and 11.3 feet (Figure 14). Soil viscosity is assumed to be zero. The yield shearing stress, τ_y, is determined from the expression [57]:

$$\tau_y = 0.8\ \gamma_s\ z\ \tan\phi_0 \tag{64}$$

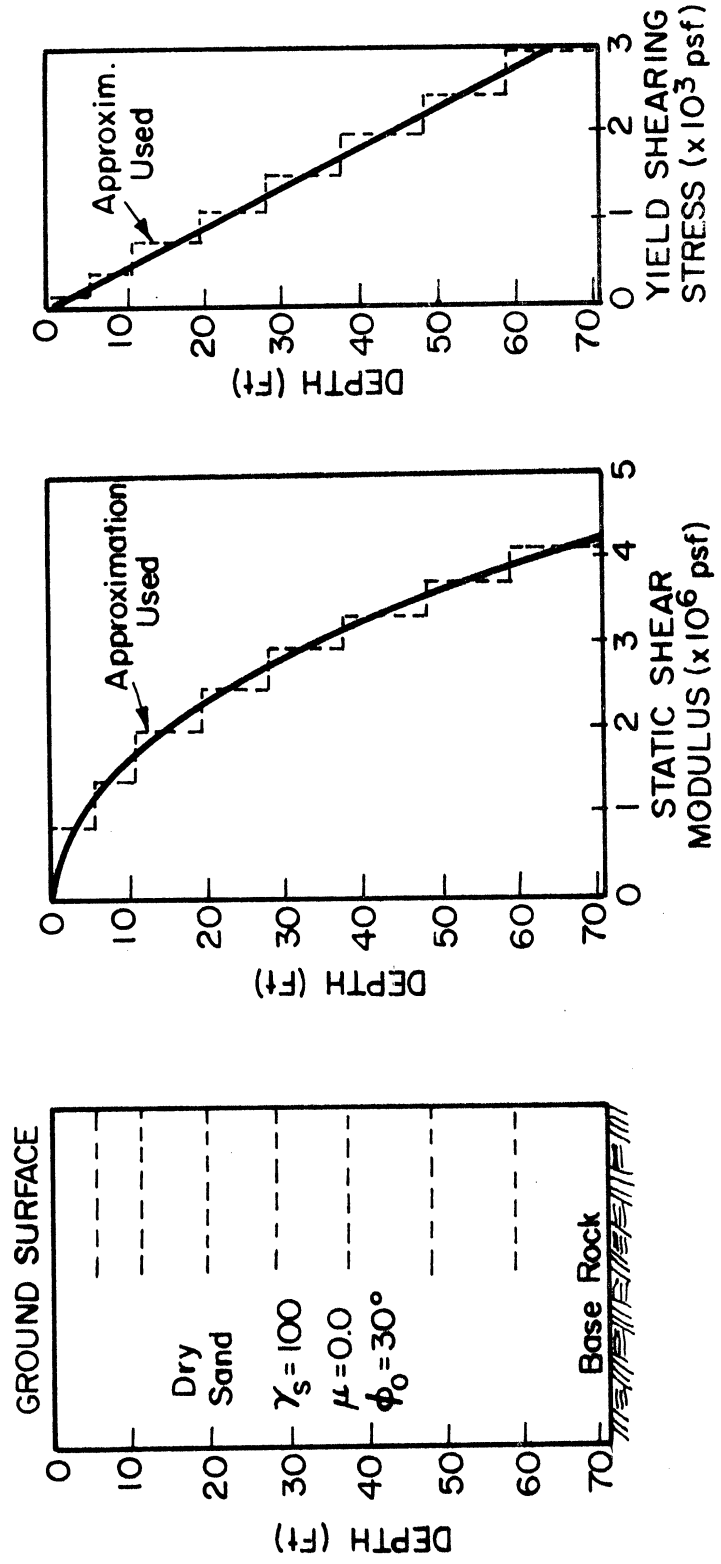

Figure 14. Soil layer with shear modulus proportional to square foot of depth.

where ϕ_0 is the angle of internal friction assumed equal to 30°. To describe the stress-strain relationship for the sand, an exponent $R_0 = 5$ is used in the Ramberg-Osgood Equations (Appendix 1).

Streeter, Wylie and Richart [71] applied a simulated seismic disturbance at the base of the deposit described above. Horizontal particle velocities at the base were calculated from a random acceleration function suggested by Bogdanoff, Goldberg and Bernard [12]:

$$a_g = t\, e^{-0.333t} \sum_{j=1}^{10} \cos(\omega_j t + \eta_j) \qquad (65)$$

where the frequencies ω_j and the phase angles η_j suggested by Parmelee et al. [53] were used. In reference [71], the velocity at the ground surface was computed from the velocity applied at the base of the deposit by using the method of characteristics (method of analysis).

The Base Motion Synthesis method used as input the ground surface velocity found from the method of analysis (Figure 15). The computed base rock velocities are in agreement with the velocities calculated from expression (65) that were originally used as input to the method of analysis (Figure 16).

The normalized Ramberg-Osgood stress-strain diagram computed at a depth of 8.4 feet by the method of analysis and the Base Motion Synthesis method is plotted in Figure 17. The sequential alphabetic characters at the turning points of the Ramberg-Osgood curves correspond to the time

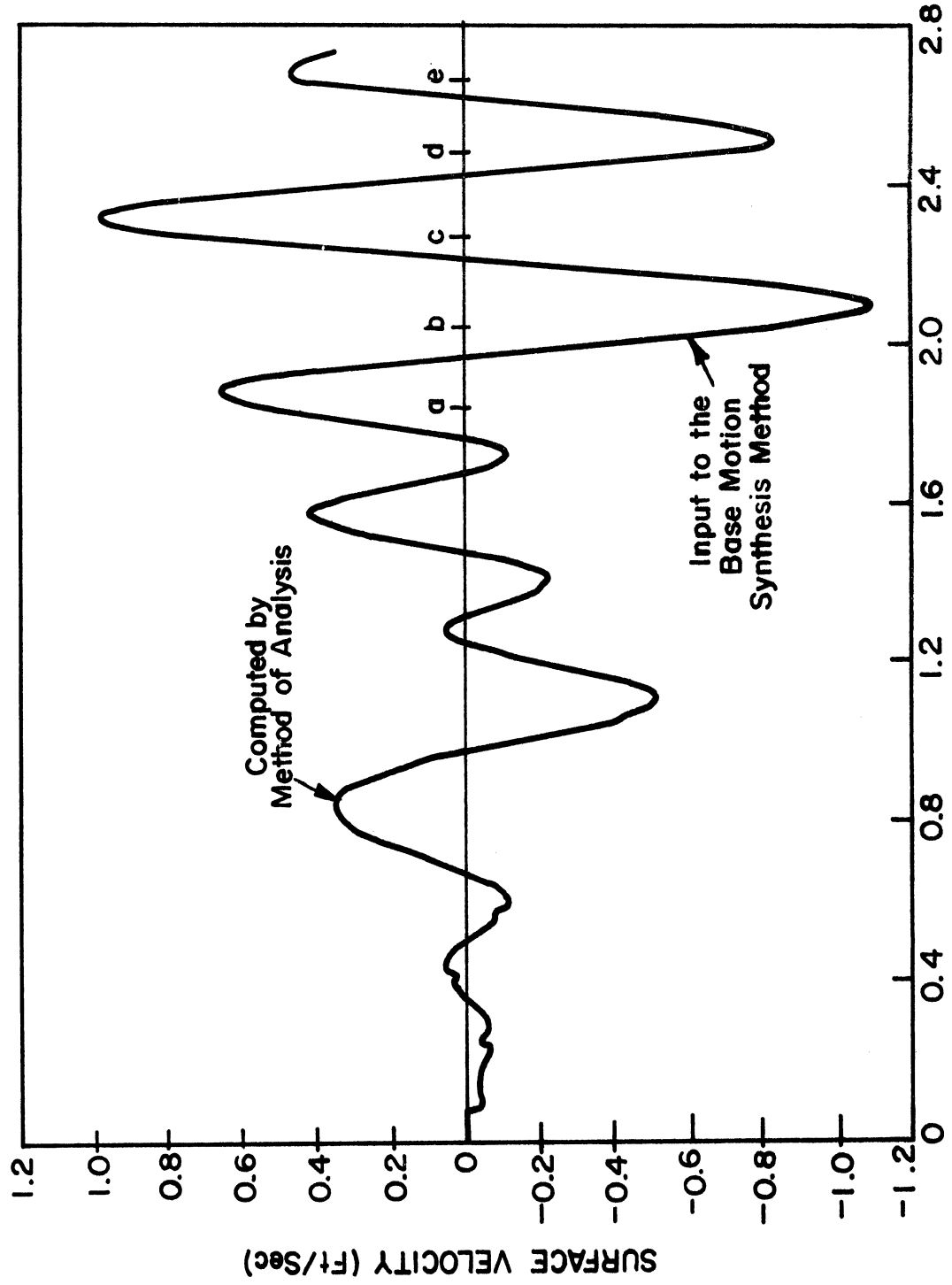

Figure 15. Seismic surface velocity.

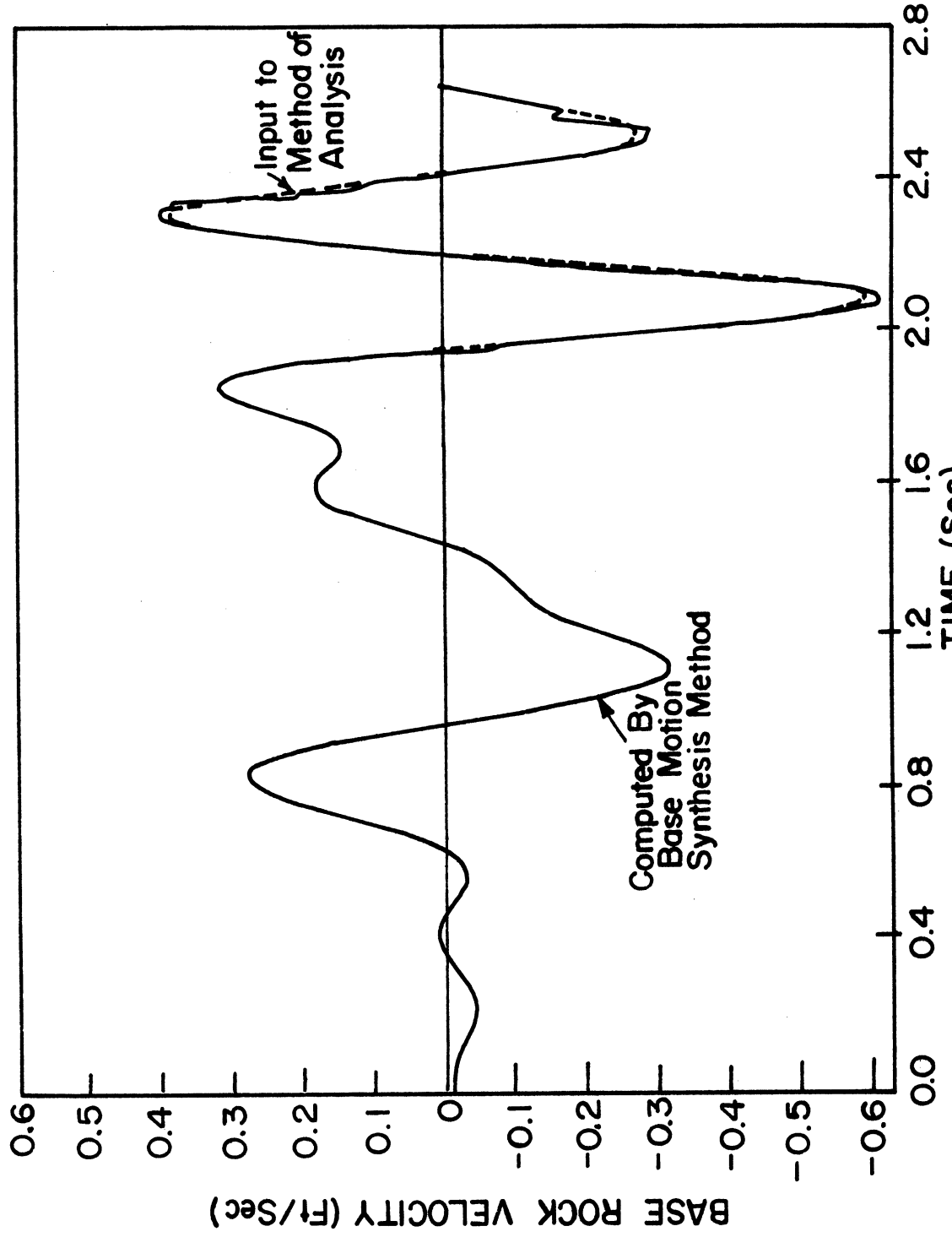

Figure 16. Simulated seismic velocity at base rock.

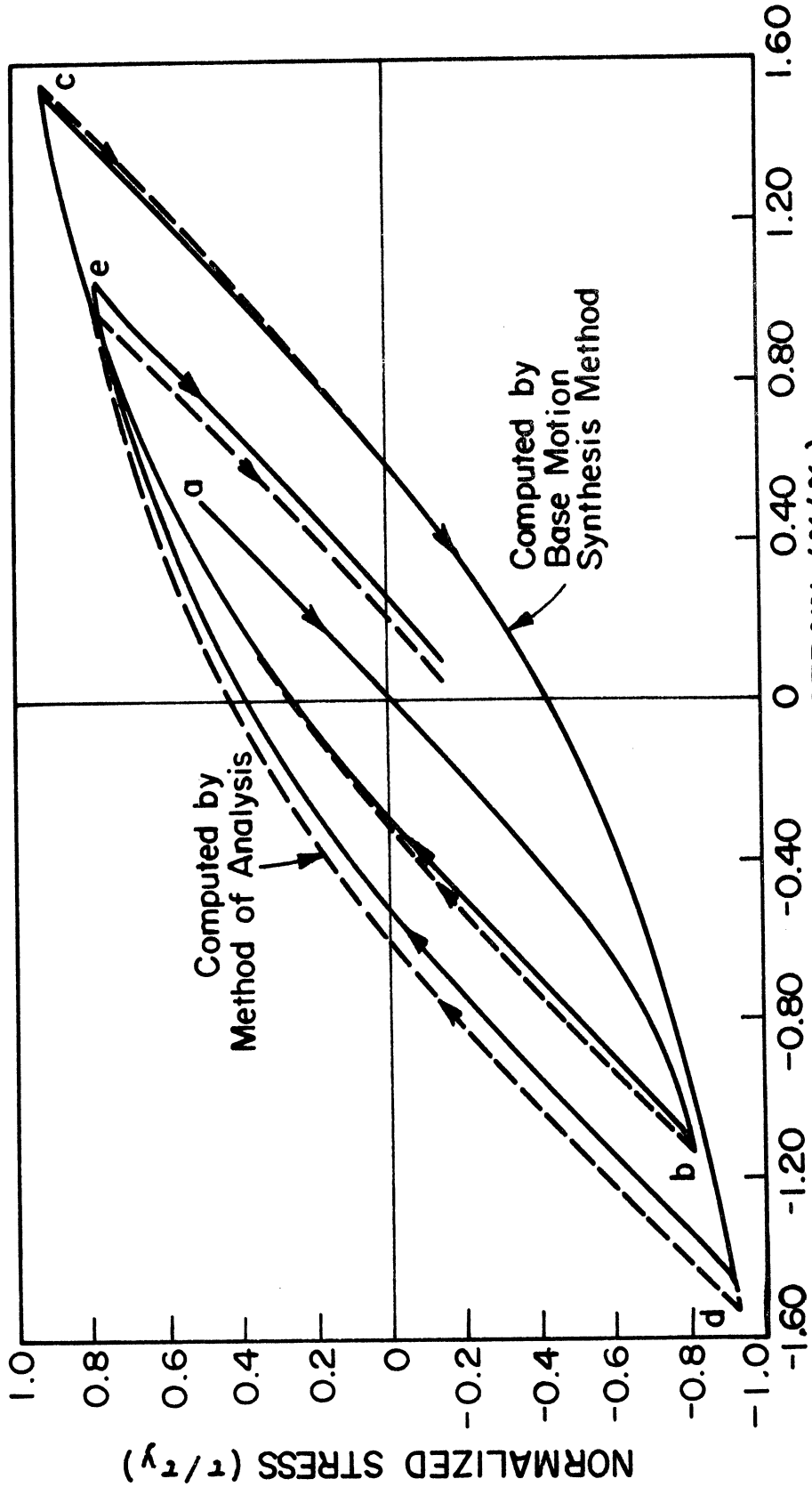

Figure 17. Ramberg-Osgood stress-strain diagram computed at a depth of 8.4 ft.

indicated by the same letters on Figure 15. The differences observed in Figure 17 are attributed mainly to the approximations introduced by the implicit scheme in the Base Motion Synthesis method. The larger differences occurred at the turning points of the Ramberg-Osgood curves (i.e. at point d in Figure 17 where unloading stops and loading starts), the reason being the abrupt change in the value of G from its minimum to its maximum value G_0 during one time interval.

The computations for the Base Motion Synthesis method were carried out by using the computer program appearing in Appendix 6. The computing time for compilation, execution and printout for this example was 57 seconds on the IBM 360/67 computer, while the solution by the method of analysis required 31 seconds of computing time.

CHAPTER V

ONE-DIMENSIONAL SHEAR WAVE PROPAGATION THROUGH EARTH DAMS

Review of Literature

Mononobe, Takata, and Matumura [48] in 1936, presented one of the first dynamic response analyses of earth dams. Their theoretical development was based on the following simplifying assumptions: the earth dam material was homogeneous and viscoelastic having uniform density and shear modulus; the earth dam cross section was wedge-shaped and the foundation was rigid; the dam was infinitely long and its base width was greater than its height so that bending deformations could be considered negligible compared with deformations due to shear; the water stored in the earth dam was not considered in the analysis; and shear stresses over any horizontal plane were assumed to be uniformly distributed.

Hatanaka [27] in 1955 studied the case of a triangular elastic cross section in a rectangular canyon and computed the horizontal response over the length and the height of the dam. Ambraseys [3,4,5] studied extensively the dynamic reaction of dams to earthquakes. In 1960, he investigated the shear response of a two dimensional symmetric wedge of finite length which had a truncated crest. The wedge was considered to be linearly elastic, bounded at its base and its two vertical sides by rigid planes. Internal or Coulomb friction was modeled by a viscous damping term proportional

to the particle velocities. The shear modulus was assumed to be constant since Ambraseys previous work showed that an error of less than 10% occurred in computing natural frequencies when the variable shear modulus was replaced with its mean value.

In 1966, Seed and Martin [63] summarized all the previous work done on the elastic response analysis of earth dams in what they called the one-dimensional shear slice theory. The derived differential equation of motion was solved analytically for a random horizontal base motion. Viscous damping forces were considered to be proportional to the particle velocities. Making use of the orthogonal properties of mode shapes and the principle of mode superposition, the general solution of the equation of motion was obtained as a summation of an infinite number of terms involving Duhammel (or Convolution) integrals. The dissipation mechanism was represented in the solution by the fraction of critical damping for each mode. Results obtained by the above analysis were of similar form with measurements of the response of the Cachuma Dam in California during a small earthquake in 1957 [4] and with measurements of the response of the 100 foot high Sannokai Dam in Japan to several small earthquakes [51].

During 1966 and 1967 Clough and Chopra [14] and Chopra [13] applied the finite element method in an attempt to develop an improved analysis to the problem of shear wave propagation through earth dams. The dam material was

considered to be isotropic and linear viscoelastic. The influence of stored water was ignored. The analysis was two dimensional. For the same dam height differences in geometry of the cross section lead to differences in the natural modes, a result not obtainable from the shear slice theory. During the last few years numerous applications of the finite element method appeared in the literature; a more detailed review is presented in Chapter VII, since the present chapter is dealing with the one-dimensional dam analysis.

Analytical Method

The basic assumption of the one-dimensional shear slice theory, that shearing stress is uniformly distributed over any horizontal plane is maintained through the following development. The earth dam material is assumed to be viscoelastic. The dam cross sections considered are wedge-shaped with bank slopes 1 vertical to $\alpha/2$ horizontal having truncated crests.

For the one-dimensional shear wave transmission through an earth dam under dynamic conditions, the equation of motion for a thin horizontal slice at depth z below the crest O (Figure 18), is:

$$-\tau A_0 + \left[\tau A_0 + \frac{\partial(\tau A_0)}{\partial z}\, dz\right] = \rho dz \left[A_0 + \frac{\partial A_0}{\partial z}\frac{dz}{2}\right]\frac{\partial^2 u}{\partial t^2} \quad (66)$$

where $A_0 = \alpha z$ is the area of the horizontal plane per unit length; τ = shearing stress uniformly distributed over the

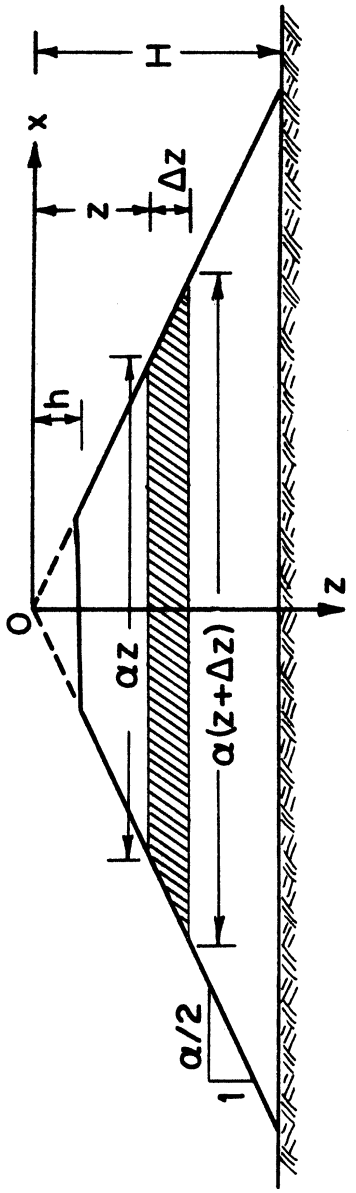

Figure 18. One-dimensional shear slice.

horizontal plane of area A_0; ρ = mass density of the soil; u = absolute horizontal displacement of the slice. Omitting second order differentials and considering that $A_0 = \alpha z$ and $\partial A_0/\partial z = \alpha$, Equation (66) reduces to:

$$\frac{\partial \tau}{\partial z} + \frac{\tau}{z} - \rho \frac{\partial^2 u}{\partial t^2} = 0 \qquad (67)$$

It should be noted that the slope α of the dam sides has cancelled out and does not appear in Equation (67). The effect of the tapered cross section is depicted by the term (τ/z) for any degree of taper. For $\alpha \to 0$ this term vanishes and Equation (67) reduces to the equation of motion for the shear wave propagation through a one-dimensional shear beam. Values of α often encountered in practice are $1.5 < \alpha < 3$. Such differences in the geometry of a dam cross section clearly affect the dam's response. Therefore, the advantage of using a two-dimensional analysis becomes apparent. However, the one-dimensional approach is a simple and inexpensive method to examine the reaction of dams to earthquakes. Results obtained by this approach are usually satisfactory along the dam's axis of symmetry.

The equation of state relating shear stress and stain for a viscoelastic material, with the viscous damping term proportional to the rate of change of strain, is:

$$\tau = G \frac{\partial u}{\partial z} + \mu \frac{\partial^2 u}{\partial z \partial t} \qquad (68)$$

where G = shear modulus or modulus of rigidity; $\partial u/\partial z$ is the strain; and μ = soil viscosity.

If Equation (68) is differentiated with respect to z and Equation (67) is substituted, the equation presented by Mononobe et al. [48] is obtained:

$$\rho \frac{\partial^2 u}{\partial t^2} - \frac{\partial}{\partial z}(G \frac{\partial u}{\partial z} + \mu \frac{\partial^2 u}{\partial z \partial t}) - \frac{1}{z} (G \frac{\partial u}{\partial z} + \mu \frac{\partial^2 u}{\partial z \partial t}) = 0 \quad (69)$$

Using the mean values of μ and G for the whole height of the dam and neglecting their possible variation with depth, Equation (69) reduces to:

$$\rho \frac{\partial^2 u}{\partial t^2} - G(\frac{\partial^2 u}{\partial z^2} + \frac{1}{z} \frac{\partial u}{\partial z}) - \mu (\frac{\partial^3 u}{\partial z^2 \partial t} + \frac{1}{z} \frac{\partial^2 u}{\partial z \partial t}) = 0 \quad (70)$$

The motion produced by a harmonic excitation applied at the base of a dam must also be harmonic with the same period as the excitation. Therefore, a steady state solution of Equation (70) is assumed in the form:

$$u(z,t) = F(z)e^{i\omega t} \quad (71)$$

where ω = circular frequency of the imposed excitation; F = a function of z to be found.

Substitution of Equation (71) into Equation (70) results to the equation:

$$\frac{d^2F}{dz^2} + \frac{1}{z} \frac{dF}{dz} + (\frac{\omega}{v^*})^2 F = 0 \quad (72)$$

where

$$v^* = \sqrt{\frac{G}{\rho} + i\frac{\mu\omega}{\rho}} \quad (73)$$

The quantity v^* is called herein complex velocity of shear wave propagation. If $\mu = 0$, then the soil is elastic,

$v^* = \sqrt{G/\rho}$ is the real shear wave velocity and Equation (72) reduces to an ordinary Bessel equation [30].

A general solution of Equation (72) in terms of Hankel functions, is:

$$F(z) = AH_0^{(1)}(\omega z/v^*) + BH_0^{(2)}(\omega z/v^*) \tag{74}$$

where A and B are constants to be determined from the boundary conditions. The Hankel functions of order q are:

$$H_q^{(1)}(\omega z/v^*) = J_q(\omega z/v^*) + iY_q(\omega z/v^*) \tag{75}$$

$$H_q^{(2)}(\omega z/v^*) = J_q(\omega z/v^*) - iY_q(\omega z/v^*) \tag{76}$$

where J_q are Bessel functions of the first kind of order q, and Y_q are Bessel functions of the second kind of order q. If the viscous term is not zero, it is evident that the arguments of the Hankel and Bessel functions are complex numbers. In this case, a special technique to evaluate these functions is presented in Appendix 3. A computer subprogram was written and used (Appendix 7) since existing tables [49,50] require cumbersome interpolations.

The solution of Equation (70) becomes

$$u(z,t) = e^{i\omega t}[AH_0^{(1)}(\omega z/v^*) + BH_0^{(2)}(\omega z/v^*)] \tag{77}$$

At the truncated crest, where z = h, the shearing stress τ should be zero. By substituting Equation (77)

into Equation (68) and considering that $\tau = 0$, the following expression is obtained:

$$\frac{\omega}{v^*} e^{i\omega t}(G+i\mu\omega)\left[AH_1^{(1)}(\omega h/v^*) + BH_1^{(2)}(\omega h/v^*)\right] = 0 \qquad (78)$$

from which

$$B = -AH_1^{(1)}(\omega h/v^*)/H_1^{(2)}(\omega h/v^*) \qquad (79)$$

At the base of the dam, where $z = H$, a harmonic excitation acts having a single amplitude W and a frequency ω, in the form:

$$u(H,t) = W\cos\omega t = \mathrm{Re}(We^{i\omega t}) \qquad (80)$$

where Re stands for "real part of." The letters Re are dropped in the following but it is understood that only the real parts of all complex expressions represent their numerical values. Equation (77) for $z = H$ yields the value of A when B is substituted from Equation (79):

$$A = W/\left[H_0^{(1)}(\omega H/v^*) - H_0^{(2)}(\omega H/v^*)H_1^{(1)}(\omega h/v^*)/H_1^{(2)}(\omega h/v^*)\right] \qquad (81)$$

The solution of the equation of motion (70) becomes:

$$u(z,t) = We^{i\omega t}\left(\frac{H_0^{(1)}(\omega z/v^*) - H_0^{(2)}(\omega z/v^*)H_1^{(1)}(\omega h/v^*)/H_1^{(2)}(\omega h/v^*)}{H_0^{(1)}(\omega H/v^*) - H_0^{(2)}(\omega H/v^*)H_1^{(1)}(\omega h/v^*)/H_1^{(2)}(\omega h/v^*)}\right) \qquad (82)$$

This solution is valid only for $h \neq 0$, since if $h = 0$, then $Y_1(0) \to -\infty$. Fortunately the case of a truncated crest is the rule and not the exception.

The horizontal velocity of displacement of a thin slice of the dam is:

$$V(z,t) = \partial u/\partial t = i\omega u(z,t) \tag{83}$$

The shearing stress uniformly distributed over a horizontal cross section at depth z can be found from the equation of state substituting u from Equation (82):

$$\tau(z,t)=\omega\rho v^* We^{i\omega t}\left(\frac{H_1^{(1)}(\omega z/v^*)-H_1^{(2)}(\omega z/v^*)H_1^{(1)}(\omega h/v^*)/H_1^{(2)}(\omega h/v^*)}{H_0^{(1)}(\omega H/v^*)-H_0^{(2)}(\omega H/v^*)H_1^{(1)}(\omega h/v^*)/H_1^{(2)}(\omega h/v^*)}\right) \tag{84}$$

The above formulas apply only to steady oscillatory motions. If n equidistant displacement values are obtained from a digitized seismogram, the transient motion of the dam base can be analyzed to a series of harmonics by applying Fourier techniques and a least squares criterion (Appendix 2). This procedure allows the user to select a number of harmonics less than the number of equidistant tabulated data points but sufficient to accurately represent the transient motion. The frequencies obtained from the harmonic analysis can be maintained without the need of introducing the critical damping ratio into Equation (73). Each one of the harmonic components of the Fourier transform generates a solution of the form of Equation (82). The superposition of these solutions by an Inverse Fourier Transform provides the transient response of the dam to

the applied excitation. A computer program written in FORTRAN IV Language to perform all the above calculations is presented in Appendix 7.

Natural Frequencies of Truncated Dams

Considering the undamped vibration of a wedge-shaped dam of height H, the natural frequencies of oscillation of the dam are obtained from the zero values of the frequency equation $J_0(\omega H\sqrt{\rho/G}) = 0$. Thus, for the first mode of vibration the fundamental frequency is:

$$\omega_n = \frac{2.4}{H}\sqrt{\frac{G}{\rho}} \tag{85}$$

The degree of truncation h of the crest of a wedge-shaped dam as well as the amount of damping influence its natural frequency. The bracketed term in Equation (82) is the amplification factor of the response. A plot of the modulus of the amplification factor for different frequencies versus these frequencies (Figure 19), for a given degree of damping, reveals the response characteristics of the system. Two dams with H = 100 ft, h = 25 ft, and H = 150 ft, h = 25 ft were studied. The mass density of the dam material was assumed to be ρ = 3.1 slugs/ft^3 and the shear modulus G = 650000 psf. Two values of viscosity were considered: μ = 0 and μ = 6250 lb·sec/ft^2. The natural frequency of the 75 ft high truncated dam for both viscosity values was about the same, equal to ω_n = 12.22 rad/sec. For higher damping, it would be expected that the corresponding

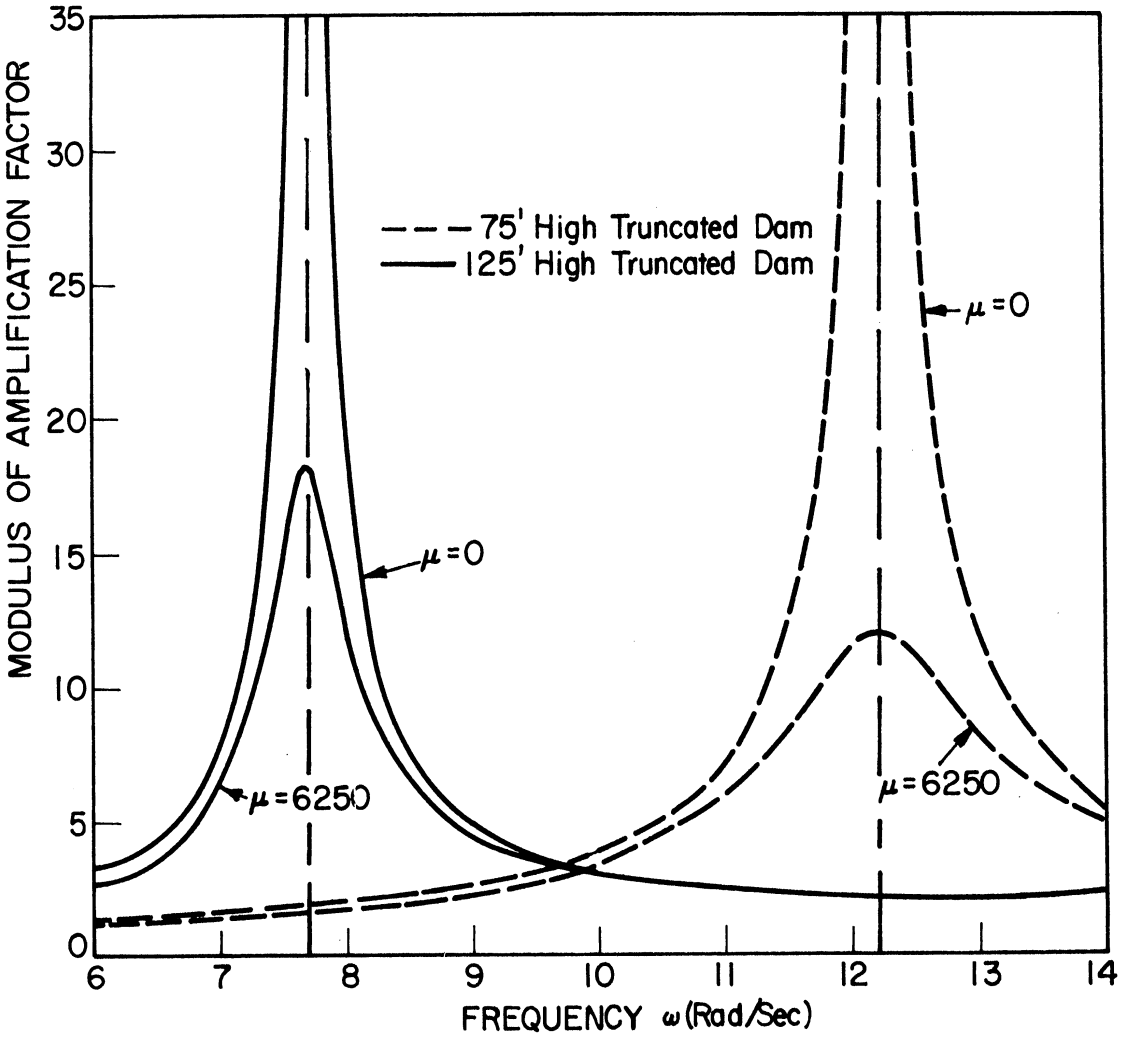

Figure 19. Response curves for two viscously damped truncated dams.

frequency would be less than 12.22 rad/sec. The undamped natural frequency of the whole 100 ft high wedge from Equation (85) is 10.99 rad/sec. The natural frequency of the 125 ft high truncated dam for both viscosity values was found to be ω_n = 7.70 rad/sec. The undamped natural frequency of the corresponding 150 ft high wedge is ω_n = 7.33 rad/sec.

Response curves of the type of Figure 19 are very useful in studying resonance effects in dams.

Characteristics Method

The same basic partial differential equations governing the propagation of shear waves through tapered cross sections are used in the following analysis, namely the equation of motion (Eq. 67) and the equation of state (Eq. 68). If Equation (68) is differentiated with respect to time, it can be written in terms of the horizontal particle velocities V:

$$\frac{\partial \tau}{\partial t} - G \frac{\partial V}{\partial z} - \mu \frac{\partial^2 V}{\partial z \partial t} = 0 \qquad (86)$$

The equation of motion (Eq.67) can also be written in terms of the horizontal particle velocities V:

$$\frac{\partial \tau}{\partial z} + \frac{\tau}{z} - \rho \frac{\partial V}{\partial t} = 0 \qquad (87)$$

The third term of Equation (86) containing the viscosity μ may be represented by a finite difference approximation as:

$$\mu \frac{\partial^2 V}{\partial z \partial t} = \mu \frac{1}{\Delta t} \left[\frac{\partial V}{\partial z} - \left(\frac{\partial V}{\partial z} \right)_C \right] \qquad (88)$$

where Δt is a selected time interval and the subscript C refers to the value determined at point C on the z-t diagram of Figure 20. Combination of Equations (86) and (88) gives:

$$\frac{\partial \tau}{\partial t} - (G + \frac{\mu}{\Delta t}) \frac{\partial V}{\partial z} + \mu (\frac{\partial V}{\partial z})_C = 0 \qquad (89)$$

Equations (87) and (89) can be transformed into four ordinary differential equations by the method of characteristics. Equation (87) is multiplied by an unknown multiplier θ and is added to Equation (89) to give:

$$[\theta \frac{\partial \tau}{\partial z} + \frac{\partial \tau}{\partial t}] - \theta\rho[\frac{1}{\theta\rho}(G + \frac{\mu}{\Delta t})\frac{\partial V}{\partial z} + \frac{\partial V}{\partial t}] + \theta \frac{\tau}{z} + \frac{\mu}{\Delta t}(\frac{\partial V}{\partial z})_C = 0 \qquad (90)$$

The bracketed terms in Equation (90) become total derivatives if:

$$\frac{dz}{dt} = \theta = \frac{1}{\theta\rho} (G + \frac{\mu}{\Delta t}) \qquad (91)$$

Equation (91) solved for θ gives:

$$\theta = \pm \sqrt{\frac{G}{\rho} + \frac{\mu}{\rho \Delta t}} = \pm v_s \qquad (92)$$

where v_s is the apparent shear wave velocity in ft/sec. Two pairs of ordinary differential equations originate from Equation (90), one pair with the positive value of θ (C^+) and the other pair with the negative value of θ (C^-):

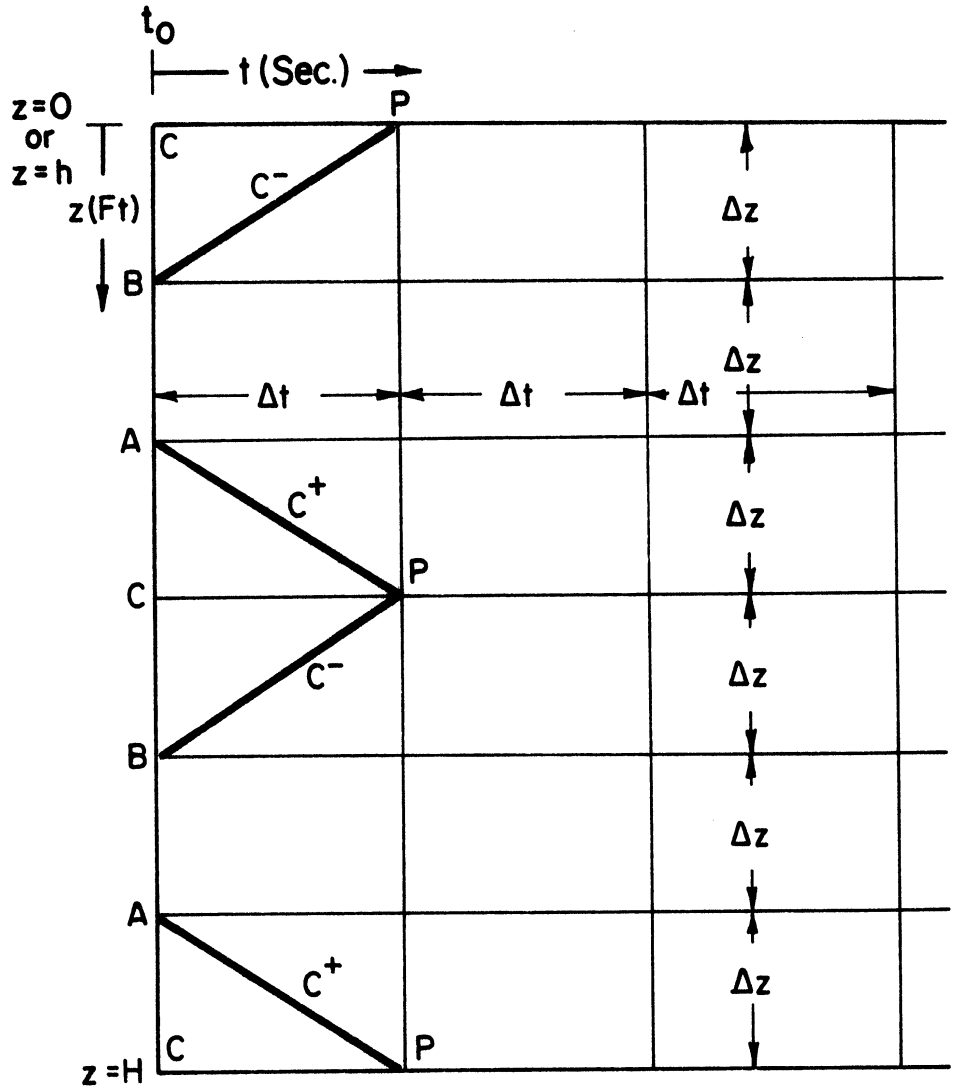

Figure 20. z-t diagram. Method of characteristics.

$$C^+ \begin{cases} \frac{d\tau}{dt} - \rho v_s \frac{dV}{dt} + v_s \frac{\tau}{z} + \frac{\mu}{\Delta t} \left(\frac{\partial V}{\partial z}\right)_C = 0 & (93) \\ \frac{dz}{dt} = v_s & (94) \end{cases}$$

$$C^- \begin{cases} \frac{d\tau}{dt} + \rho v_s \frac{dV}{dt} - v_s \frac{\tau}{z} + \frac{\mu}{\Delta t} \left(\frac{\partial V}{\partial z}\right)_C = 0 & (95) \\ \frac{dz}{dt} = -v_s & (96) \end{cases}$$

In a central finite difference form using a second order approximation, Equations (93) and (95) reduce to:

$$C^+: \tau_P - \tau_A - \rho v_s (V_P - V_A) + v_s \Delta t \frac{\tau_P + \tau_A}{z_P + z_A} + \mu \frac{V_B - V_A}{2\ \Delta z} = 0 \quad (97)$$

$$C^-: \tau_P - \tau_B + \rho v_s (V_P - V_B) - v_s \Delta t \frac{\tau_P + \tau_B}{z_P + z_B} + \mu \frac{V_B - V_A}{2\ \Delta z} = 0 \quad (98)$$

where the subscripts A, B, and P refer to values at the corresponding points of the z-t diagram (Figure 20). Equations (97) and (98) apply in both cases of a wedge-shaped cross section and of a cross section with truncated top.

In cases where the dam crest is of finite width ($h \neq 0$), a better approximation of the third term of Equations (93) and (95) emanated from Professor Wylie's suggestion that only τ should be approximated. This term

if integrated becomes:

$$\int \frac{\tau}{z} v_s \, dt = \int \frac{\tau}{z} \, dz = \frac{\tau_P+\tau_A}{2} \ln\frac{z_P}{z_A} \quad \text{(for } C^+\text{)} \tag{99}$$

$$= \frac{\tau_P+\tau_B}{2} \ln\frac{z_B}{z_P} \quad \text{(for } C^-\text{)} \tag{100}$$

By using this approximation, Equations (97) and (98) may be rewritten as:

$$C^+: \quad \tau_P - \tau_A - \rho v_s (V_P - V_A) + \frac{\tau_P+\tau_A}{2} \ln\frac{z_P}{z_A} + \mu \frac{V_B-V_A}{2\,\Delta z} = 0 \tag{101}$$

$$C^-: \quad \tau_P - \tau_B + \rho v_s (V_P - V_B) - \frac{\tau_P+\tau_B}{2} \ln\frac{z_B}{z_P} + \mu \frac{V_B-V_A}{2\,\Delta z} = 0 \tag{102}$$

All quantities with subscripts A and B refer to the previous time increment and are known. Also:

$$z_P = z_A + \Delta z = z_B - \Delta z \tag{103}$$

where

$$\Delta z = \Delta t \sqrt{\frac{G}{\rho} + \frac{\mu}{\rho \Delta t}} \tag{104}$$

The method is not restricted to constant values of G, ρ or μ. For example, in case the shear modulus is considered to be a function of depth, the distance intervals computed from Equation (104) will not be equal. However, G should be considered constant within each layer having the value calculated at mid-thickness of the layer.

To determine the unknowns τ_P and V_P, Equations (101) and (102) are solved conveniently by grouping all known quantities for each of these two equations and calling them CP and CM:

$$CP = \tau_A - \frac{\tau_A}{2} \ln\frac{z_P}{z_A} - \mu \frac{V_B - V_A}{2\,\Delta z} - \rho v_s V_A \tag{105}$$

$$CM = \tau_B + \frac{\tau_B}{2} \ln\frac{z_B}{z_P} - \mu \frac{V_B - V_A}{2\,\Delta z} + \rho v_s V_B \tag{106}$$

Equations (101) and (102) then yield:

$$\tau_P = (CP + CM)/\left(2 + \ln\frac{z_P}{\sqrt{z_A z_B}}\right) \tag{107}$$

$$V_P = \left[\tau_P\left(1 + 0.5 \ln\frac{z_P}{z_A}\right) - CP\right]/\rho v_s \tag{108}$$

At the crest where $z_P = h$, the boundary condition is expressed as $\tau_P = 0$. The C^- characteristic equation becomes:

$$-\tau_B + \rho v_s (V_P - V_B) - \frac{\tau_B}{2} \ln\frac{z_B}{h} + \mu \frac{V_B - V_C}{\Delta z} = 0 \tag{109}$$

The particle velocity V_P at the crest of the dam is readily available from Equation (109). At the base of the dam where $z_P = H$, the boundary condition is that V_P is known as a function of time for the seismic motion under consideration . The C^+ characteristic equation becomes:

$$\tau_P - \tau_A - \rho v_s (V_P - V_A) + \frac{\tau_A + \tau_P}{2} \ln\frac{H}{z_A} + \mu \frac{V_C - V_A}{\Delta z} = 0 \tag{110}$$

The shearing stress τ_p at the base of the dam is obtained by solving Equation (110). The next step is to compute τ_p and V_p for all layer interfaces for the next time interval and repeat the procedure stepwise in the time domain. A computer program in FORTRAN IV Language which performs the necessary step-by-step calculations is presented in Appendix 8.

Case Studies

Four tapered dam cross sections were selected for study. Cross Section III is a whole wedge. The other three cross sections present a truncated crest (Figure 21). Examples 2 and 3 are of a rather academic nature since soil properties were selected in such a way as to facilitate a comparative analysis, and a study of the influence of an earth dam height on its frequency responses. However, it should be noted that the methodology developed previously is applicable for any selected realistic data.

Example 1. The analytical method and the method of characteristics were compared in the case of harmonic vibrations. Cross Section I was used having h = 5 feet, and H = 50 feet. The average value of the density of the earth material was assumed to be $\rho = 4.0$ slugs/ft^3 and the average shear modulus $G = 10^6$ psf. The base developed a horizontal sinusoidal velocity of the form $V = 0.2 \sin 4\pi t$ in feet per second. The dam material was considered to be elastic ($\mu = 0$). A time interval of $\Delta t = 0.01$ seconds was used in the method of

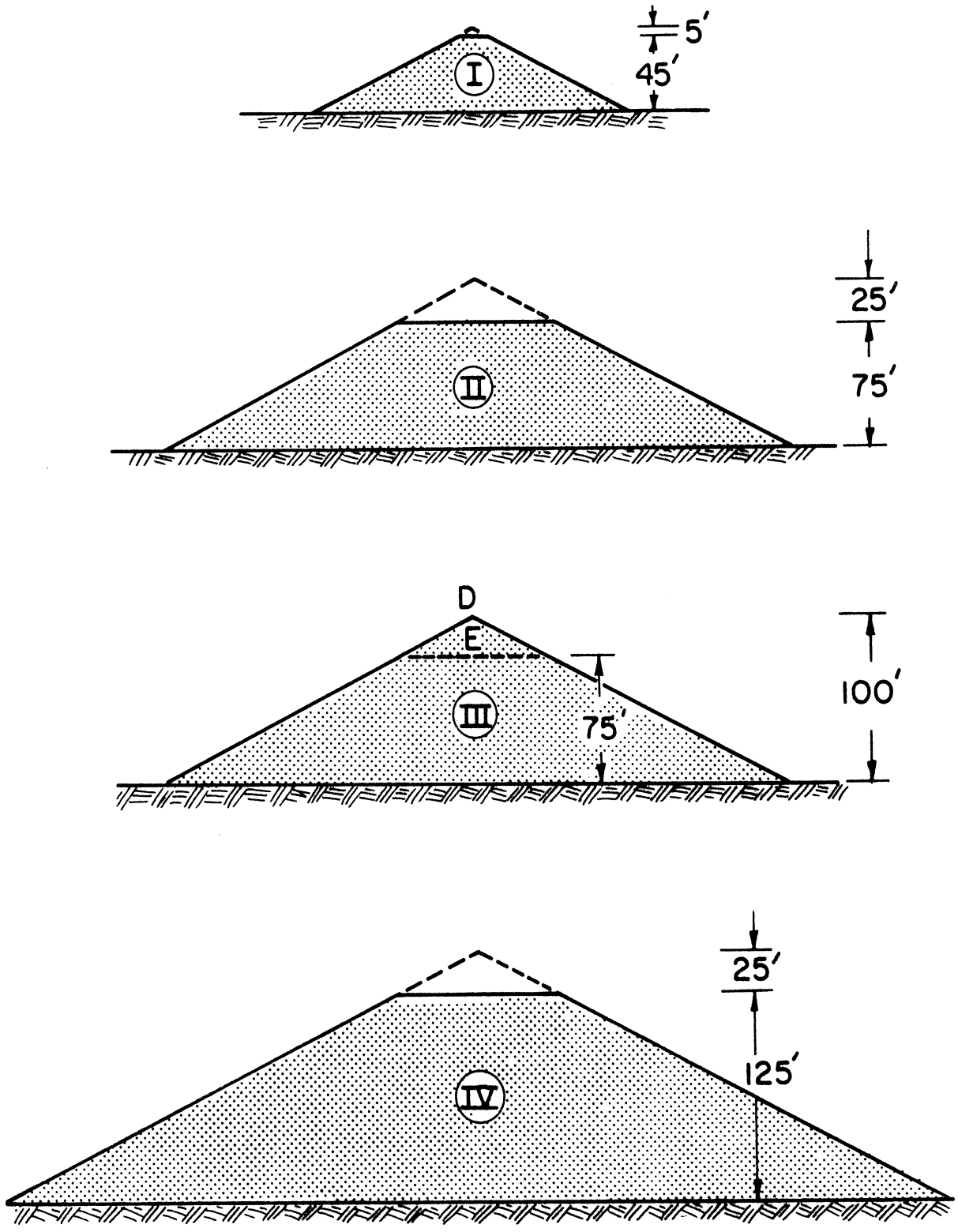

Figure 21. Tapered dam cross-sections.

characteristics which resulted in a distance interval $\Delta z = 5$ feet (9 reaches) and a shear wave velocity $v_s = 500$ ft/sec. Applying the method of characteristics, the generation of an initial transient should be avoided since there is no damping mechanism to dissipate it. For this purpose, the values of shearing stresses and velocities calculated by the analytical method at time $t = 0$ were adopted as initial conditions for the method of characteristics. The two methods were in perfect agreement for all subsequent time steps in calculating the particle velocities at the dam crest (Figure 22).

The same example was examined considering the dam material to be viscoelastic. Viscosity $\mu = 20000$ lb·sec/ft^2, soil mass density $\rho = 4$ slugs/ft^3, and shear modulus $G = 800000$ psf were assumed constant throughout the dam. A time interval of $\Delta t = 0.01$ sec was used in the method of characteristics. The distance interval was found to be 5 feet and the apparent wave velocity was 500 ft/sec. For the same excitation at the dam base, initial conditions for the method of characteristics were considered the static shear stresses and velocities at time $t = 0$, all equal to zero. The initial transient generated, dissipated after 18 cycles. The particle velocities at the dam crest computed by the analytical method and the method of characteristics appear in Figure 23 at the beginning of the 19th cycle. The agreement between the two methods was satisfactory.

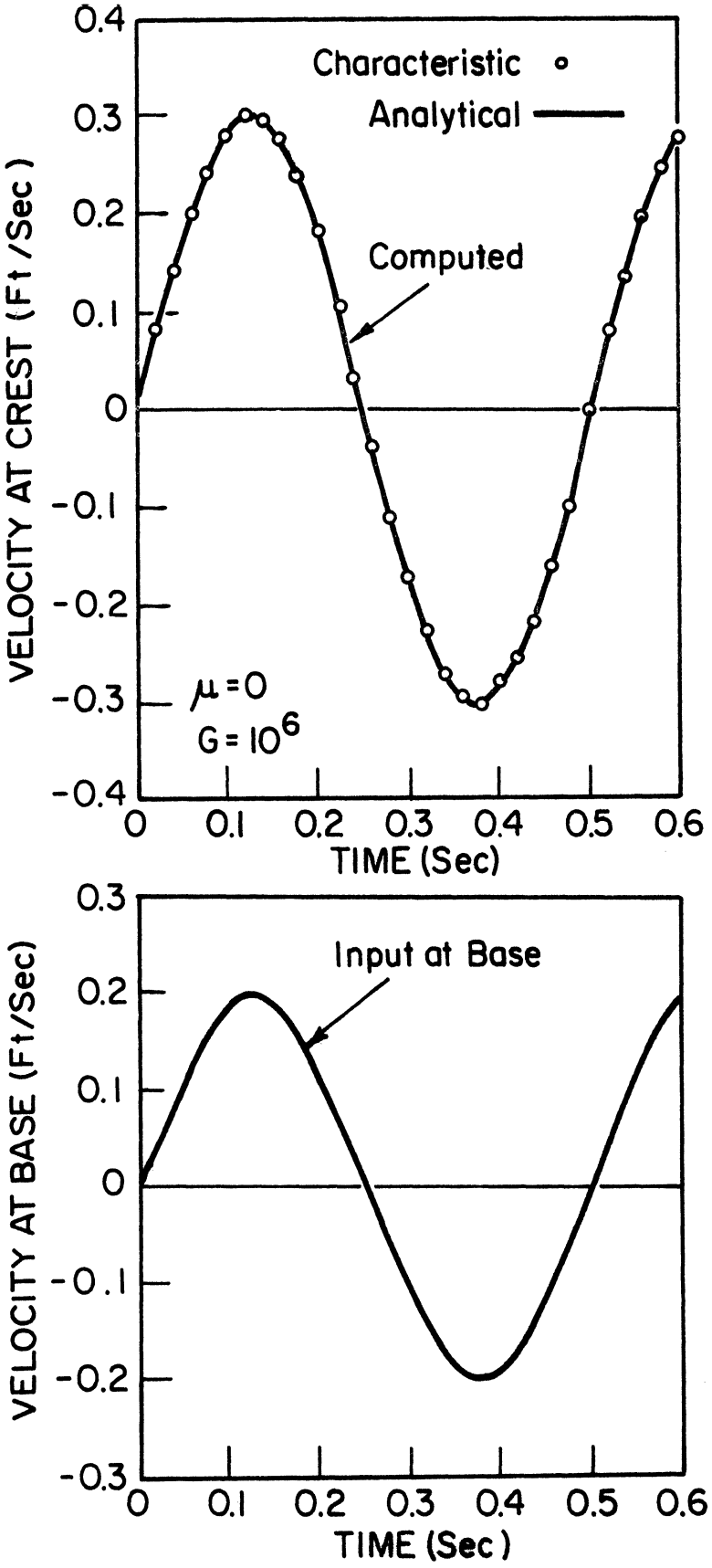

Figure 22. Velocity response at crest of dam I. Elastic material. Analytical method vs. characteristics.

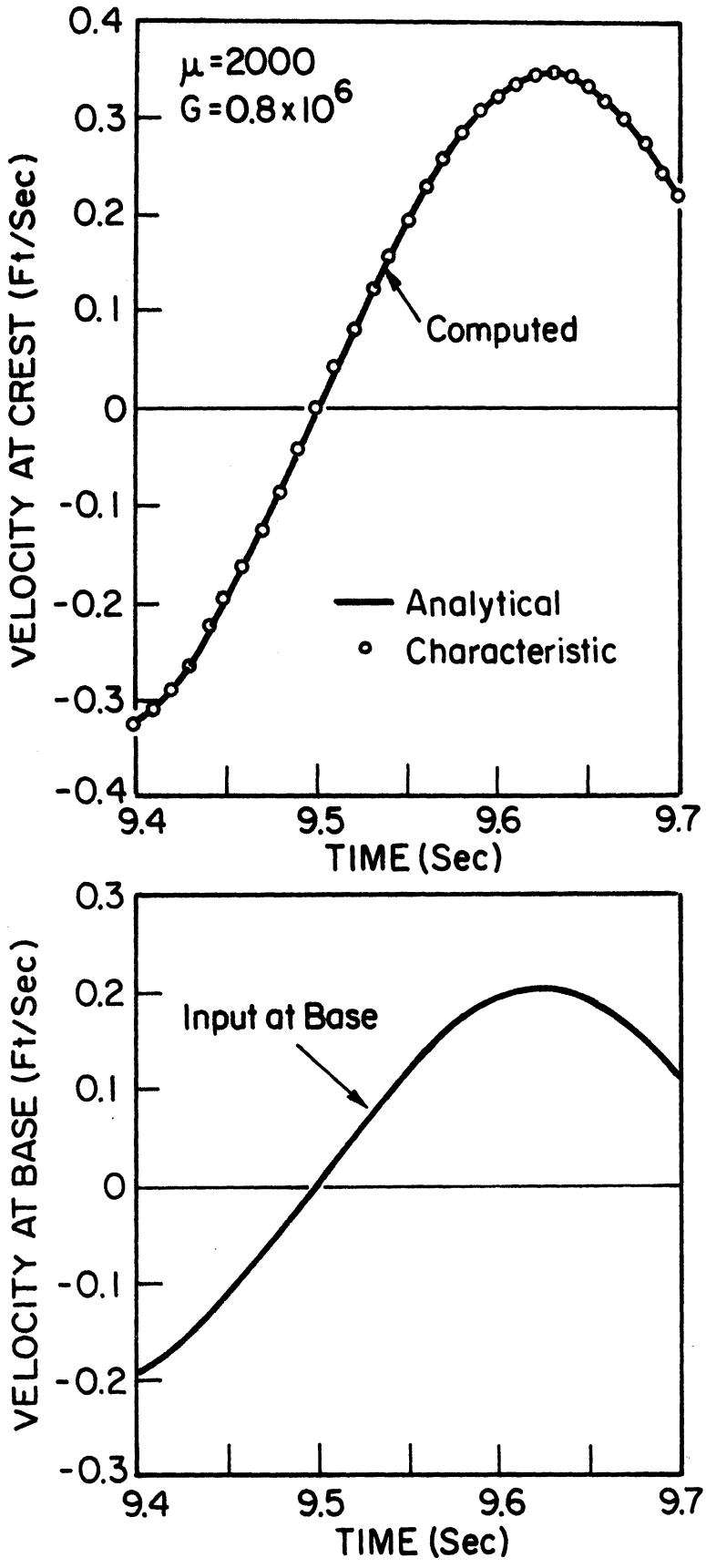

Figure 23. Velocity response at crest of dam I. Viscoelastic material. Analytical method vs. characteristics.

Example 2. A 75 feet high dam with truncated crest (Cross Section II, Figure 21) was considered resting on a horizontal rock base subjected to the S69°E component of the Taft, 1952, earthquake. The first 12 seconds of the accelerogram appear in Figure 24. Shear modulus G = 650000 psf, viscosity μ = 6250 lb·sec/ft^2 and soil mass density ρ = 3.1 slugs/ft^3 were considered constant throughout the dam. A time increment of 0.05 sec was used in the method of characteristics. The apparent wave velocity was 500 ft/sec and the dam was divided into three reaches, each 25 feet thick. The displacement and velocity responses at the crest of the dam are plotted in Figures 25 and 26. The shearing stresses developed at the base of the dam appear in Figure 27a.

The analytical method was also used to solve the above problem. Displacements at the base of the dam were obtained every 0.05 sec by twice integrating numerically the accelerogram of Figure 24. The result is presented in the lower graph of Figure 25. This displacement diagram was analyzed into 24 harmonics by using Fourier transform in conjunction with a least squares criterion (Appendix 2). The amplification factor at the dam crest for each harmonic was computed from Equation (82) and an Inverse Fourier Transform reconstituted the transient response which is plotted in the upper graph of Figure 25. The comparison with the displacements obtained by the method of characteristics was considered unsatisfactory. The reason that smoother results were obtained by the analytical method was that the

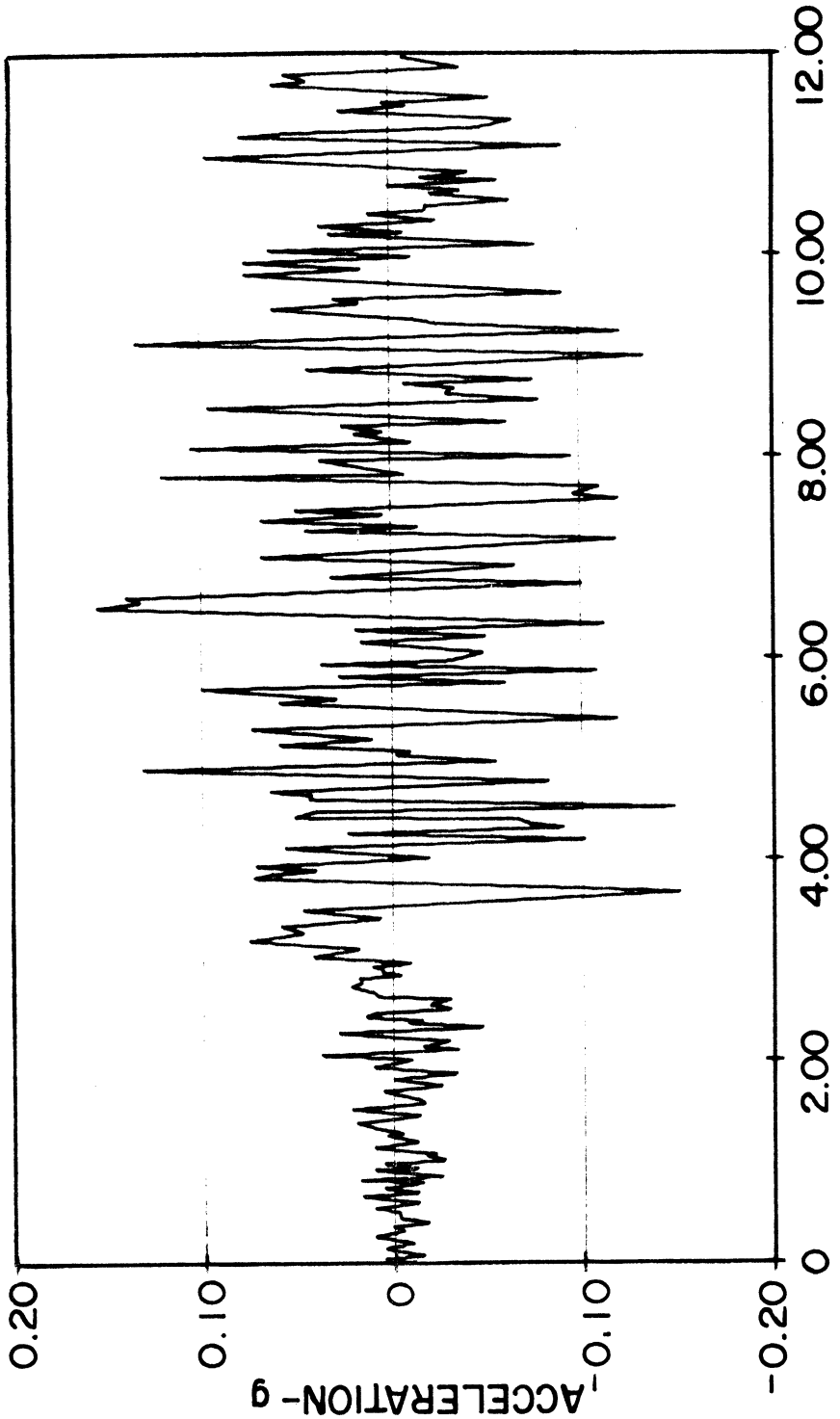

Figure 24. Accelerogram of Taft earthquake, 1952, S69°E component.

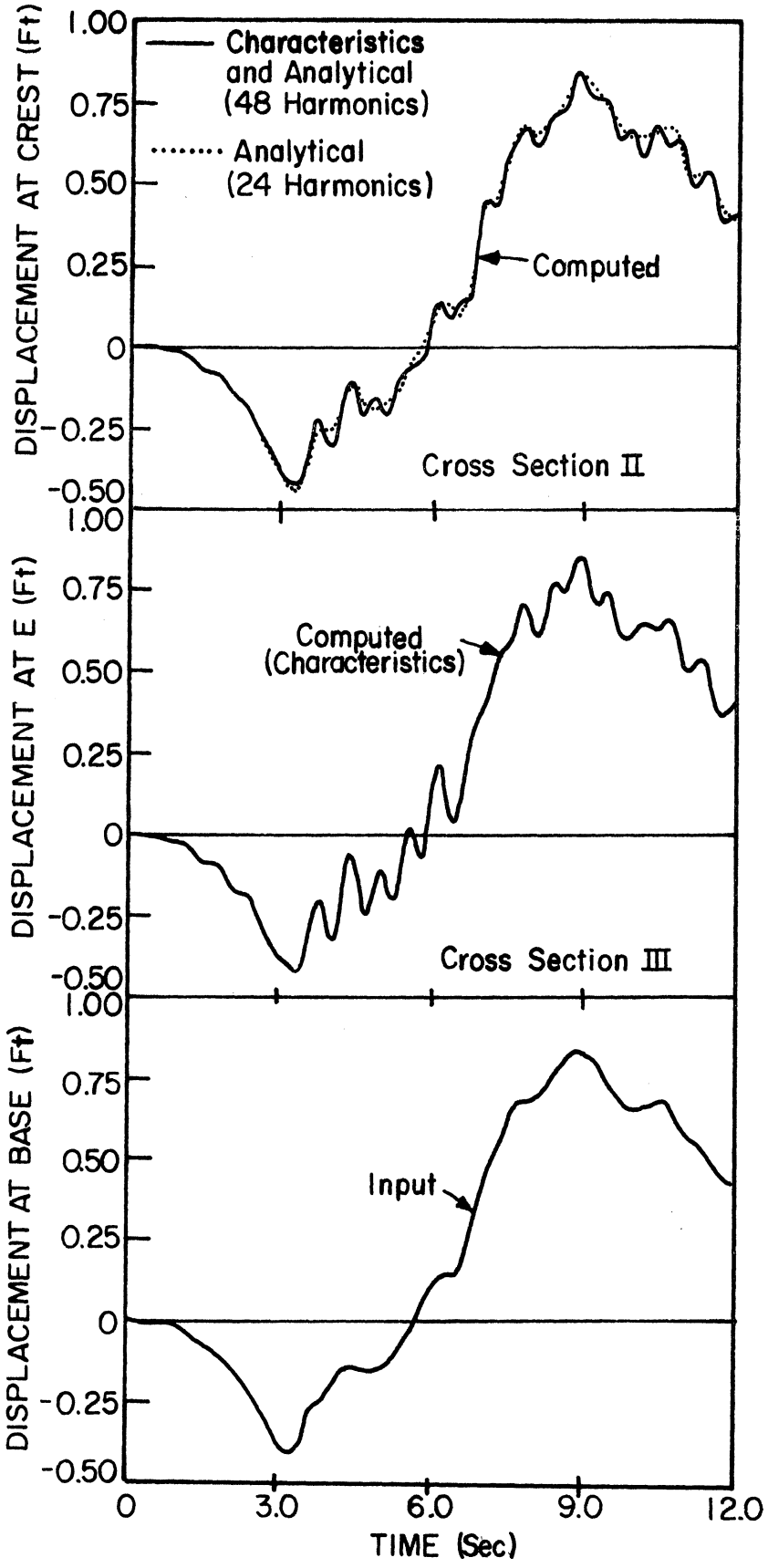

Figure 25. Displacement response of truncated and wedge shaped dams to Taft S69°E earthquake.

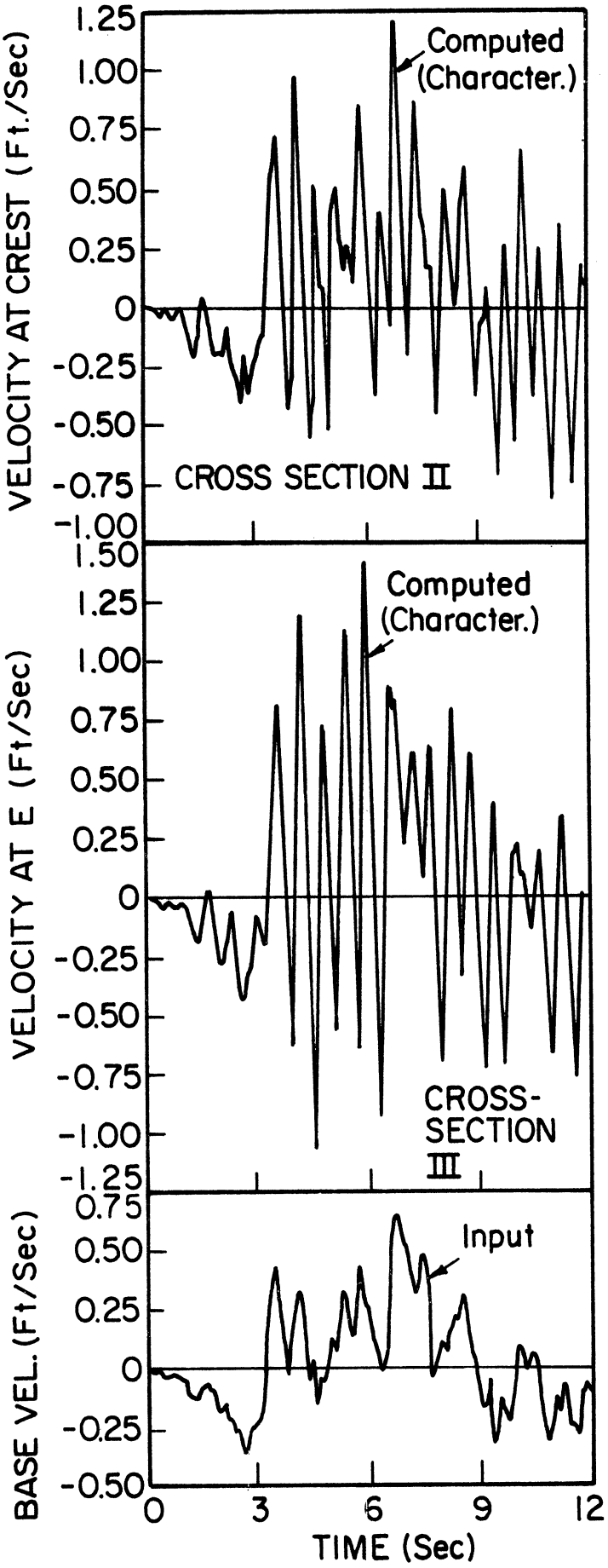

Figure 26. Velocity responses of truncated and wedge shaped dams to Taft S69°E earthquake.

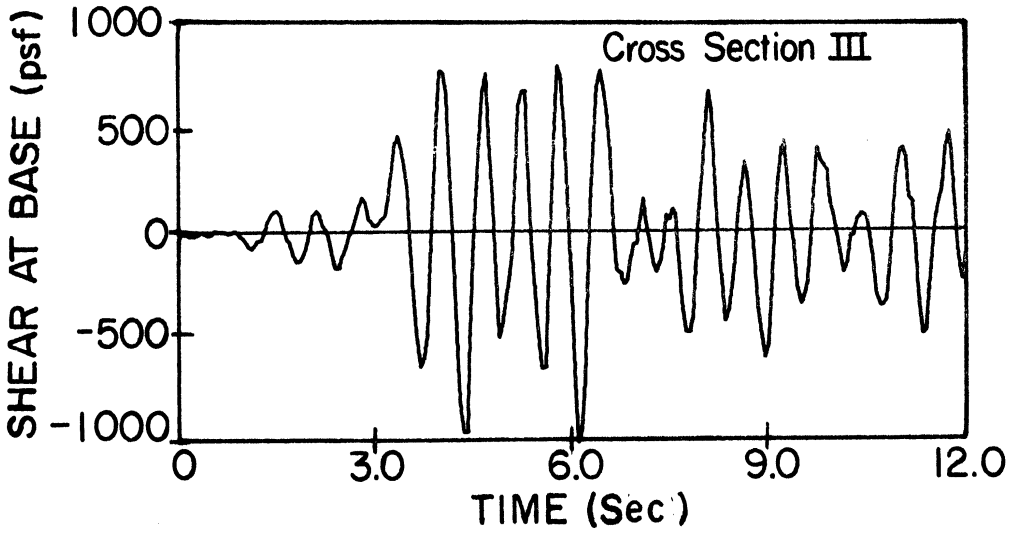

Figure 27a. Shearing stress at the base of a 100 ft high wedge shaped dam. Taft S69°E earthquake.

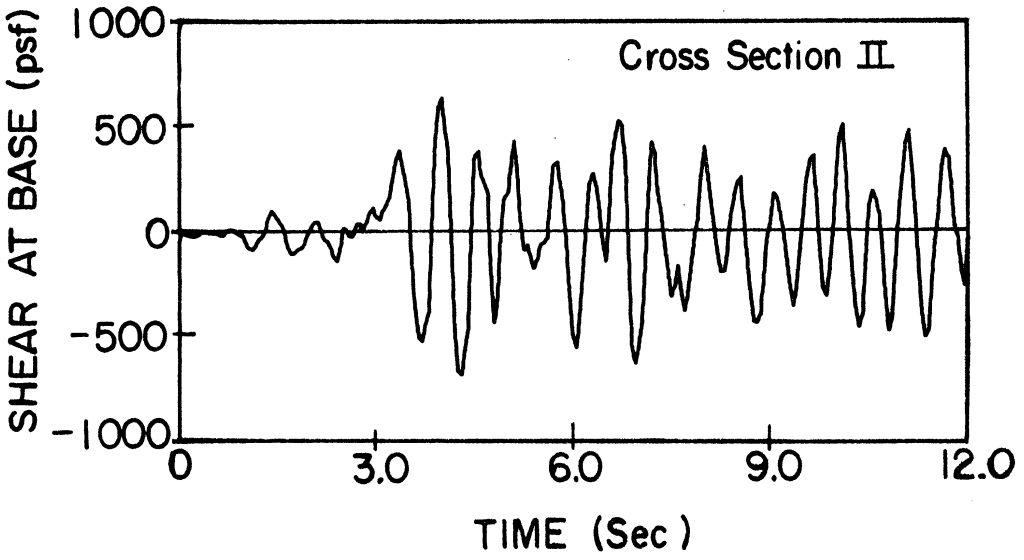

Figure 27b. Shearing stress at the base of a 75 ft high truncated dam. Taft S69°E earthquake.

24 harmonics did not model frequencies less than 0.625 sec. Therefore, the problem was solved again by analyzing the base motion into 48 harmonics. The response at the crest found from the analytical solution was substantially the same as that found from the method of characteristics (Figure 25). In both cases, the base rock displacement record which was analyzed into 24 or 48 harmonics, was extended to 15 seconds with the displacements dropping gradually to zero. This resulted in better Fourier transforms especially for the time intervals from 0.0 to 1.0 sec and from 11.0 to 12.0 sec.

A dam of Cross Section III (Figure 21) was selected to study the influence of a truncated crest on the responses of a dam to a seismic disturbance. This cross section is similar to the Cross Section II previously used, the difference being that Cross Section II is truncated. The same soil properties were retained. The response of the dam at elevation E, 75 feet above the base (at the same elevation with the crest of Cross Section II), to the S69°E component of the Taft 1952 earthquake was found using the method of characteristics. Displacements and velocities at E are presented in the middle plot of Figures 25 and 26. Shear stress at the base of the dam is plotted in Figure 27b. It is observed that all values obtained are larger than the corresponding values at the crest of the dam with Cross Section II. The two cross sections have different natural

frequencies but it seems that concentration of stresses and a stronger reflection pattern at the crest D of the Cross Section III accounts for part of the differences.

Example 3. A 125 feet high dam with truncated crest (Cross Section IV, Figure 21) was selected to demonstrate resonance effects. The dam material was assumed to have ρ = 3.1 slug/ft^3, G = 650000 psf, μ = 6250 lb·sec/ft^2 and the time increment used was Δt = 0.05 sec (then Δz = 25 ft and v_s = 500 ft/sec). The dam rested on a horizontal rock base subjected to the S69°E component of the Taft earthquake, 1952. The response spectrum of this earthquake reveals a predominant frequency of about 7.4 rad/sec. The natural frequency of the structure from Figure 19 was found to be 7.7 rad/sec. The displacements and velocities at the crest and the shearing stresses at the base of the dam, computed by the method of characteristics, are presented in Figures 28 and 29. The excessive magnification of these responses is in accordance with the closeness of the natural periods of the excitation and the structure.

Example 4. A 100 feet high wedge-shaped dam (Cross Section III, Figure 21) has a constant shear modulus G = 4 x 10^6 psf and a density of 130 lb/ft^3. The base of the dam is subjected to the North-South component of the 1940 El Centro earthquake accelerogram. Two methods were used to obtain

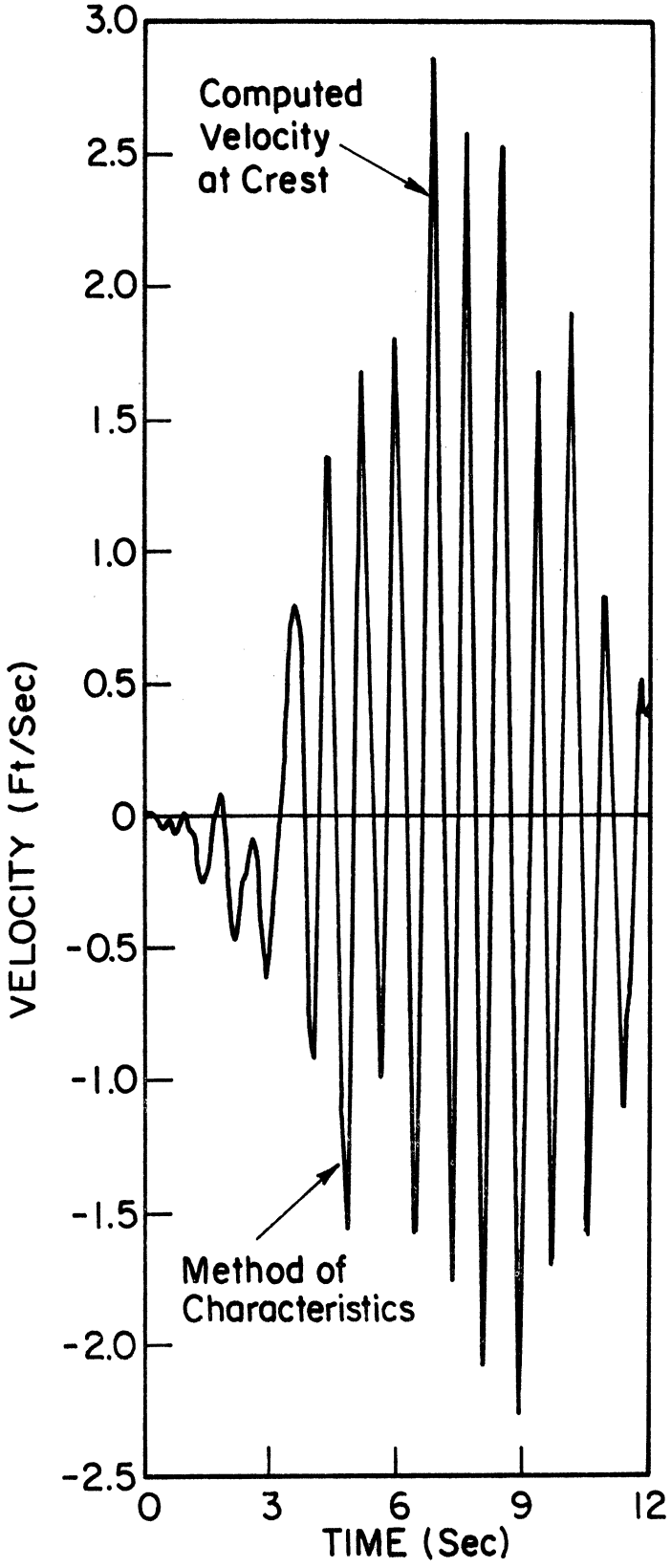

Figure 28. Particle velocities computed at crest of a 125 ft high dam (cross section IV) subjected at its base to Taft S69°E earthquake.

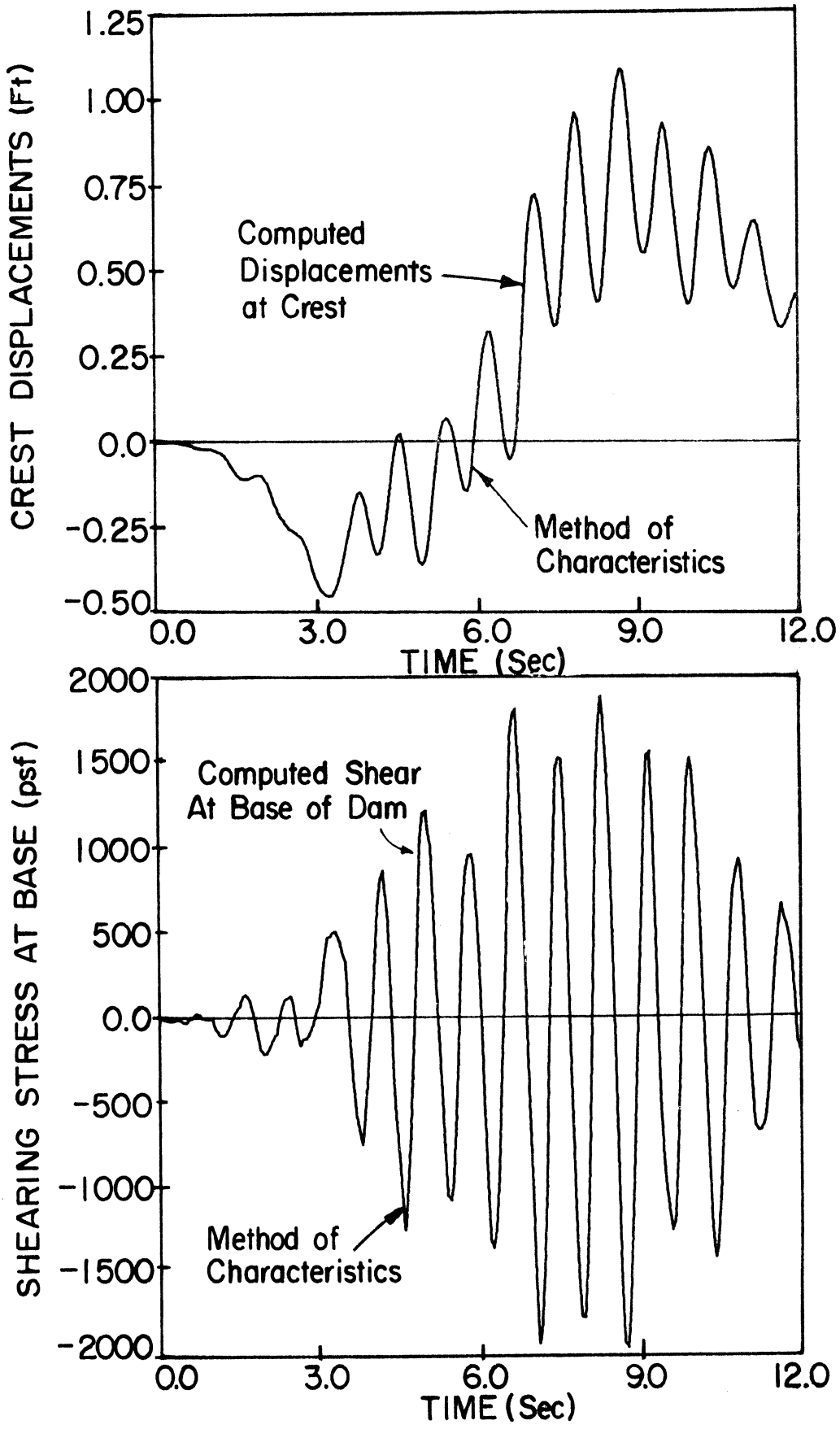

Figure 29. Computed responses of a 125 ft high dam (cross section IV) to Taft S69°E earthquake.

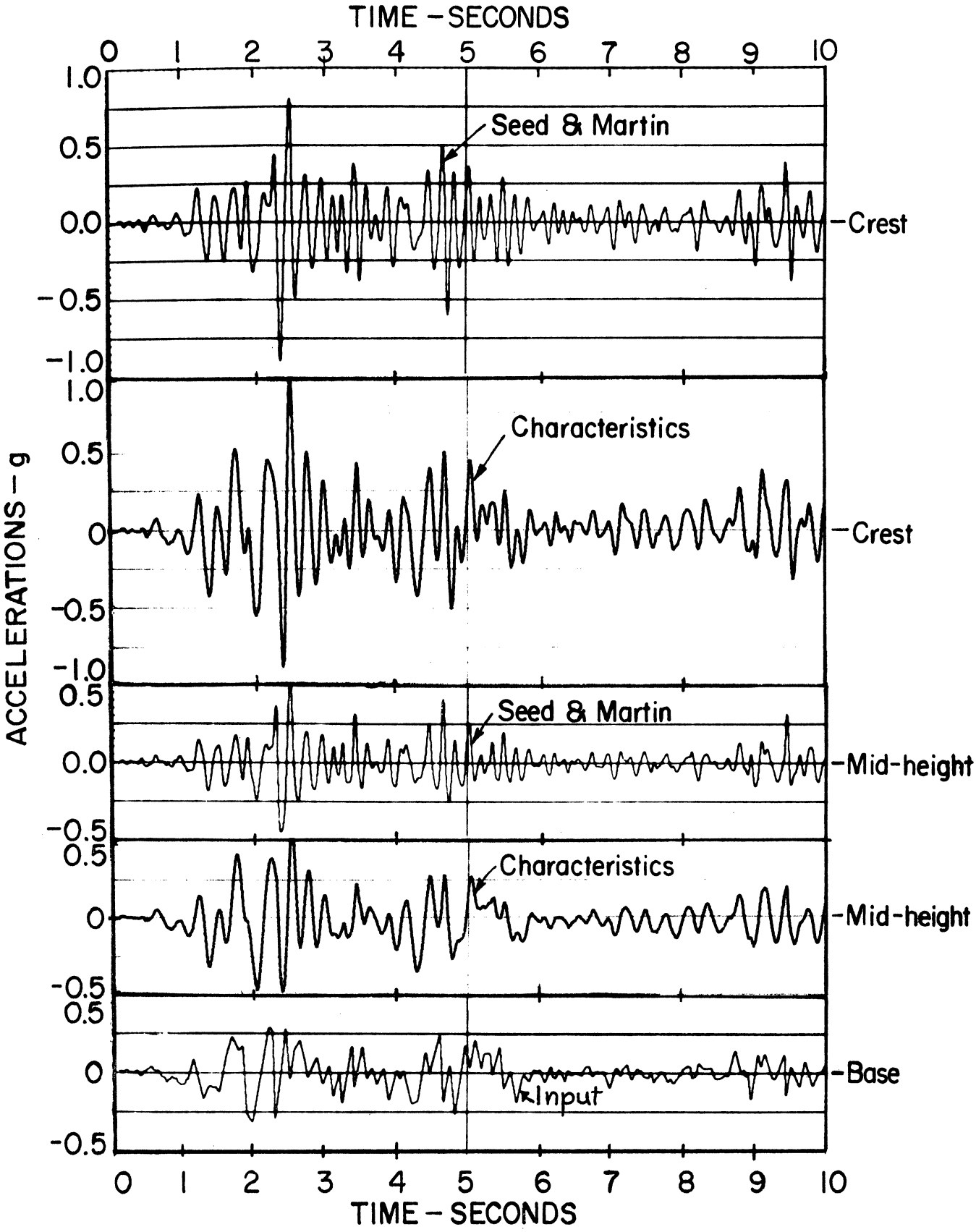

Figure 30. Response of a dam (cross section III) to El Centro, 1940, N-S earthquake. Comparison between Seed and Martin's solution and method of characteristics.

the response accelerations at midheight and at the crest of the dam: the method of characteristics and Seed and Martin's analytical solution [63].

A time increment $\Delta t = 0.01$ sec was used in the method of characteristics. Soil viscosity was assumed to have a constant value $\mu = 71250$ lb·sec/ft^2. Six reaches were used, each of thickness $\Delta z = 16.67$ ft. The apparent wave velocity was found to be $v_s = 1667.71$ ft/sec.

A time increment $\Delta t = 0.02$ sec was used in Seed and Martin's solution. A damping factor of 0.2 was assumed, constant for each mode. Equation (6) of reference [63] was used and the responses for the first six modes of vibration were superimposed.

The results obtained by both methods are plotted in Figure 30, and are of a very similar form despite the differences. Since the damping mechanisms used by the two methods were different and the first six modes were only considered in the analytical solution, quantitatively the results obtained by the two methods were in unexpectedly good agreement.

CHAPTER VI

ONE-DIMENSIONAL PRESSURE WAVE PROPAGATION THROUGH SATURATED SOIL DEPOSITS

Review of Literature

In evaluating the response of saturated soil deposits under seismic loading, a method for the determination of pore pressures and intergranular stresses is necessary. Due to lack of such a method early attempts were made [14,33] to model the saturated soil by an equivalent solid with the same total properties.

Another approach to the problem of wave propagation through saturated porous media was to assume that the porous material consisted of a homogeneous and elastic frame with the pores filled with liquid. Zwikker and Kosten [75] studied the propagation of one-dimensional pressure waves through porous materials with the pores filled with air. They mainly used the concept of impedance to examine problems of sound absorption.

Biot [9] presented in 1956 the most complete treatment of the problem. The three-dimensional propagation of shear and pressure waves in an infinite fluid saturated porous solid with elastic properties was analyzed. The fluid was considered to be viscous, compressible and free to flow through the pores. Stress-strain relationships were developed for the material in terms of the elastic constants of the fluid and the solid frame and two additional constants relating to the coupling between the fluid and solid constituents. These relationships were introduced to the

equation of motion whose solution as developed holds only for cases of harmonic vibrations of a medium of infinite extent. Ishihara [38,39] using the continuity equation and some specific test conditions succeeded to relate Biot's coupling coefficients to the compressibilities of the individual constituent materials. Ishihara's results made Biot's approach more realistic.

In 1960, Deresiewicz [17] treated the problem of the one-dimensional propagation of elastic waves in a semi-infinite non-dissipative liquid-filled porous solid. A general solution of Biot's differential equations was deduced. These field equations govern the relationship between the displacements in the solid and the displacements in the liquid. An approach used to solve similar equations of linear thermoelasticity was employed, namely the resolution of each of the solid and liquid displacements into a lamellar and a solenoidal part (Helmholtz resolution). However, the solution obtained did not find any practical application.

Biot [10,11] incorporated internal dissipation to his theory considering the solid frame to be viscoelastic. The theory of deformation in a porous viscoelastic medium was developed on the basis of the thermodynamics of irreversible processes. Biot stated that "the equations governing the mechanics of porous media are formally the same for an elastic or viscoelastic system, provided that the elastic coefficients are replaced by the corresponding operators." Thus, the effects of viscous damping were included into the

elastic constants and the coupling coefficients by introducing two relaxation constants. According to this approach, the solid was considered elastic for rapid deformations while it was considered viscous for slow deformations (type of Maxwell solid). However, a theoretical or experimental procedure to define these new constants was not presented and still none is available, seriously restricting the application of this theory.

Ghaboussi and Wilson [22,23] in 1971 developed a numerical method for the dynamic analysis of a saturated porous solid. The field equations of Biot's theory [9] were used to systematically develop a Gurtin-type variational formulation of the problem. The response of a half-space to a step loading applied to the free surface was examined. The system consisted of a sequence of one-dimensional elements along the vertical axis. Wave reflections at the base rock were not considered since the fixed boundary was located at such a distance from the surface that it was not reached from the motion during the time of interest.

It becomes apparent that solution techniques have lagged behind the development of the theory for nearly a decade. Experimental work to evaluate the effects of void ratio, degree of saturation, grain characteristics, and confining pressure on the shear and pressure wave velocities in granular materials was carried out by Hardin and Richart [26].

Analytical Method

Assuming a conservative physical system statistically isotropic, comprised of an elastic solid skeleton and of compressible liquid free to flow through the pores, Biot [9] derived stress-strain relations containing four distinct elastic constants. These relations in the vertical z-direction reduce to:

$$\sigma = (2G+\lambda) \frac{\partial w}{\partial z} + Q \frac{\partial \bar{w}}{\partial z} \tag{111}$$

$$s = -np = Q \frac{\partial w}{\partial z} + R \frac{\partial \bar{w}}{\partial z} \tag{112}$$

where σ = stress at the z-direction on the solid part of a unit area, positive when tension; s = stress on the fluid part per unit area, negative when pressure; p = porewater pressure; n = effective porosity; G and λ = Lame's constants, G being the modulus of rigidity; Q and R = coupling coefficients relating to the coupling between the fluid and solid constituents; w = vertical displacement of solid particles at a depth z from the ground surface; $\bar{w}$ = vertical displacement of liquid particles defined in such a way that the product of this displacement by the cross-sectional fluid area represents the volume flow.

If the total volume of the aggregate is held constant, R is a measure of the pressure required to push a certain additional volume of fluid into the aggregate. The constant Q is a coupling coefficient between the volume change of the solid and that of the fluid. Ishihara [38] by using the

equation of continuity and an expression for the internal energy of the system plus some rather theoretical specific states of stress (unjacketed compression test, jacketed test), arrived at the same equations of state as Biot (Equations 111 and 112). However, in the process of doing so, Ishihara obtained expressions for the coupling coefficients relating them to the compressibilities of each of the system's substances:

$$Q = \frac{-n[(n-1)C_p + C_s]}{C_b(C_\ell - C_s) + C_p C_s} \tag{113}$$

$$R = \frac{nC_b}{C_b(C_\ell - C_s) + C_p C_s} \tag{114}$$

and also

$$\lambda = \frac{(n-1)^2 C_p + (n-1)C_s + C_\ell}{C_b(C_\ell - C_s) + C_p C_s} - \frac{2}{3} G \tag{115}$$

where C_s = compressibility of the soil particles; C_p = pore compressibility; C_ℓ = fluid compressibility, and C_b = $n C_p + C_s$ = bulk compressibility of the soil skeleton.

Biot derived the dynamic equations of equilibrium using Lagrange's equation. The concept of generalized coordinates was employed according to which the position of every particle is completely determined when the values of the independent variables (or generalized coordinates) w and $\bar{w}$ are known. Biot's dynamic equations of equilibrium in the vertical z-direction neglecting the effect of gravity forces are:

$$\frac{\partial^2}{\partial t^2}(\rho_{11}w+\rho_{12}\bar{w}) + b\frac{\partial}{\partial t}(w-\bar{w}) = \frac{\partial \sigma}{\partial z} \tag{116}$$

$$\frac{\partial^2}{\partial t^2}(\rho_{12}w+\rho_{22}\bar{w}) - b\frac{\partial}{\partial t}(w-\bar{w}) = \frac{\partial s}{\partial z} \tag{117}$$

where

$$\rho_{11} = (1-n)\rho_S + \rho_a \tag{118}$$

$$\rho_{22} = n\rho_L + \rho_a \tag{119}$$

$$\rho_{12} = -\rho_a \tag{120}$$

$$b = \frac{\mu_L n^2}{K} \tag{121}$$

In the above relations ρ_{11} and ρ_{22} = mass of solid and liquid per unit volume of aggregate, respectively; ρ_S and ρ_L = mass densities of the solid and liquid respectively; ρ_a = apparent mass density due to the fluid, considered to be zero at low frequencies by Ishihara; μ_L = dynamic viscosity of the fluid in $lb \cdot sec/ft^2$; and K = intrinsic permeability, a characteristic of the medium alone, in ft^2.

The author, working with Eulerian coordinates, assuming Darcy's friction as the dissipation mechanism, derived the equations of motion for the solid and the fluid constituents respectively including the effect of gravity forces (Appendix 4). These equations prove to be identical with Biot's equations of equilibrium (116) and (117) if the gravity effect was neglected.

Because of the assumption of statistical isotropy of the material, Biot concluded that the rotational or shear waves are uncoupled from the dilatational or pressure waves

and obey independent equations of propagation. This is correct, since elastic materials do not undergo changes in volume when subjected to shear. The presence of fluid in the pores little affects the propagation of shear waves. Therefore, the subsequent analysis is concentrated on the pressure waves.

By substituting the equations of state (111) and (112) into the equations of equilibrium (116) and (117), Biot [9] obtained the following two differential equations (reduced here to the z-direction):

$$\frac{\partial^2}{\partial z^2}[(\lambda+2G)w + Q\bar{w}] = \frac{\partial^2}{\partial t^2}(\rho_{11}w + \rho_{12}\bar{w}) + b\,\frac{\partial(w-\bar{w})}{\partial t} \qquad (122)$$

$$\frac{\partial^2}{\partial t^2}[Qw + R\bar{w}] = \frac{\partial^2}{\partial t^2}(\rho_{12}w + \rho_{22}\bar{w}) - b\,\frac{\partial(w-\bar{w})}{\partial t} \qquad (123)$$

The bulk mass density is $\rho = \rho_{11} + 2\rho_{12} + \rho_{22}$ and the bulk modulus of compressibility is $\bar{B} = M + R + 2Q$ where $M = \lambda + 2G$ is the constrained modulus of elasticity. It is convenient to introduce the following non-dimensional parameters:

$$C_1 = M/\bar{B}, \qquad C_2 = R/\bar{B}, \qquad C_3 = Q/\bar{B}$$

and

$$F_1 = \rho_{11}/\rho, \qquad F_2 = \rho_{22}/\rho, \qquad F_3 = \rho_{12}/\rho$$

where $C_1 + C_2 + 2C_3 = 1$ and $F_1 + F_2 + 2F_3 = 1$, i.e. there are only four independent parameters. The parameters C_j define the elastic properties of the material and the parameters F_j its dynamic properties.

Substitution back into Equations (122) and (123) yields:

$$C_1\frac{\partial^2 w}{\partial z^2} + C_3\frac{\partial^2 \bar{w}}{\partial z^2} = \frac{1}{v_c^2}\left(F_1\frac{\partial^2 w}{\partial t^2} + F_3\frac{\partial^2 \bar{w}}{\partial t^2}\right) + \frac{b}{\rho v_c^2}\frac{\partial (w-\bar{w})}{\partial t} \qquad (124)$$

$$C_3\frac{\partial^2 w}{\partial z^2} + C_2\frac{\partial^2 \bar{w}}{\partial z^2} = \frac{1}{v_c^2}\left(F_3\frac{\partial^2 w}{\partial t^2} + F_2\frac{\partial^2 \bar{w}}{\partial t^2}\right) - \frac{b}{\rho v_c^2}\frac{\partial (w-\bar{w})}{\partial t} \qquad (125)$$

where $v_c = \sqrt{\bar{B}/\rho}$ is a characteristic wave velocity depending on the bulk properties of the material. In Equations (124) and (125) the elastic properties and the densities of the aggregate constituents were considered to be constant with depth. Therefore, the only unknown quantities are the displacements w and $\bar{w}$.

Biot and Ishihara studied the propagation of elastic waves through a saturated medium of infinite extent. If horizontal bedrock is underlying a saturated soil deposit and if a free surface exists where stresses should be zero, a more general solution is needed. Such a solution is presented in the following and accounts for wave reflections at the boundaries. Normal incidence is assumed, so incident waves are reflected back as themselves not accompanied by waves of other types.

Assuming that the harmonic excitation applied at the bedrock has a circular frequency ω, steady state solutions to Equations (124) and (125) may be written as:

$$w(z,t) = A \exp(i\omega t + i\omega z/v_d) \qquad (126)$$

$$\bar{w}(z,t) = B \exp(i\omega t + i\omega z/v_d) \qquad (127)$$

where A and B are constants to be found from the boundary conditions; and v_d is the dilational wave velocity. Calling $x_0 = v_c/v_d$ and

$$X = \frac{ib}{\rho\omega} = \frac{i\mu n^2}{\rho K\omega} \tag{128}$$

and substituting Equations (126) and (127) into Equations (124) and (125), two compatibility relationships are obtained:

$$(F_1 - x_0^2C_1 - X)A = (x_0^2C_3 - F_3 - X)B \tag{129}$$

$$(F_3 - x_0^2C_3 + X)A = (x_0^2C_2 - F_2 + X)B \tag{130}$$

Division of these two equations by parts gives:

$$\frac{F_1 - x_0^2C_1 - X}{F_3 - x_0^2C_3 + X} = \frac{x_0^2C_3 - F_3 - X}{x_0^2C_2 - F_2 + X} \tag{131}$$

or

$$(C_1C_2-C_3^2)x_0^4-(C_2F_1+C_1F_2-2C_3F_3)x_0^2+(F_1F_2-F_3^2)+X(x_0^2-1)=0 \tag{132}$$

Four roots x_1', $-x_1'$, x_2', and $-x_2'$ are obtained from the solution of the biquadratic equation:

$$(C_1C_2-C_3^2)x_0^4 - (C_2F_1+C_1F_2-2C_3F_3)x_0^2 + (F_1F_2-F_3^2) = 0 \tag{133}$$

Then, Equation (132) can be written as:

$$(x_0^2-x_1'^2)(x_0^2-x_2'^2) + \frac{X(x_0^2-1)}{(C_1C_2-C_3^2)} = 0 \tag{134}$$

From Equation (134) four complex roots x_1, $-x_1$, x_2 and $-x_2$ are obtained. Since $x_0 = v_c/v_d$, four complex values of the pressure wave velocity v_d emerge:

$$\left.\begin{aligned} v_{d_1} &= v_c/x_1 \quad , \quad v_{d_2} = v_c/x_2 \\ v_{d_3} &= v_c/(-x_1) = -v_{d_1}, \quad v_{d_4} = v_c/(-x_2) = -v_{d_2} \end{aligned}\right\} \quad (135)$$

Three factors β', β_1, β_2 are introduced for convenience, as follows:

$$\beta' = i\omega t, \qquad \beta_1 = i\omega z/v_{d_1}, \qquad \beta_2 = i\omega z/v_{d_2} \quad (136)$$

Equations (124) and (125) are linear partial differential equations and superposition of solutions of the form of Equations (126) and (127) results in the following general solutions:

$$w=A_1\exp(\beta'+\beta_1)+A_1'\exp(\beta'-\beta_1)+A_2\exp(\beta'+\beta_2)+A_2'\exp(\beta'-\beta_2) \quad (137)$$

$$\bar{w}=B_1\exp(\beta'+\beta_1)+B_1'\exp(\beta'-\beta_1)+B_2\exp(\beta'+\beta_2)+B_2'\exp(\beta'-\beta_2) \quad (138)$$

where A_1, A_1', A_2, A_2', B_1, B_1', B_2, and B_2' are coefficients to be evaluated from the boundary conditions.

From Equations (137) and (138) it is observed that there are two pressure waves propagating through the saturated medium with wave velocities v_{d_1} and v_{d_2}. The first two terms of Equations (137) and (138) represent the incident and reflected waves traveling with a velocity v_{d_1} through the medium. The other two remaining terms represent the incident and reflected waves of phase velocity v_{d_2}. Many investigators refer to the two pressure waves as the fluid wave and the frame wave although there is coupled motion of the fluid and the frame in both waves. Therefore, both waves travel through both the solid skeleton and the liquid except in cases of a very weak coupling.

The constant coefficients of Equations (137) and (138) are computed from the boundary conditions available. At the upper surface (z = 0) of a saturated soil layer of thickness H, stresses should be zero (s = 0 and σ = 0). At the lower boundary (z = H) liquid and solid displacements are known functions of time from the prescribed harmonic excitation in the form:

$$w(H,t) = \bar{w}(H,t) = \mathrm{Re}(W\, e^{i\omega t}) = W \cos\omega t \qquad (139)$$

where Re means "real part of" and is dropped in the following.

In order to have a traction free surface at z = 0, it should be $s(0,t) = \sigma(0,t) = 0$. Then differentiation of Equations (137) and (138) with respect to z and substitution back into the equations of state (111) and (112) yields:

$$\frac{M}{v_{d_1}}(A_1-A_1') + \frac{M}{v_{d_2}}(A_2-A_2') + \frac{Q}{v_{d_1}}(B_1-B_1') + \frac{Q}{v_{d_2}}(B_2-B_2') = 0 \qquad (140)$$

$$\frac{Q}{v_{d_1}}(A_1-A_1') + \frac{Q}{v_{d_2}}(A_2-A_2') + \frac{R}{v_{d_1}}(B_1-B_1') + \frac{R}{v_{d_2}}(B_2-B_2') = 0 \qquad (141)$$

For any value of M, Q, and R these two equations are only satisfied when $A_1 = A_1'$, $B_1 = B_1'$, $A_2 = A_2'$, and $B_2 = B_2'$. Then, Equations (137) and (138) become:

$$w=\left\{A_1[\exp(\beta_1)+\exp(-\beta_1)] + A_2[\exp(\beta_2)+\exp(-\beta_2)]\right\}\exp(\beta') \qquad (142)$$

$$\bar{w}=\left\{B_1[\exp(\beta_1)+\exp(-\beta_1)] + B_2[\exp(\beta_2)+\exp(-\beta_2)]\right\}\exp(\beta') \qquad (143)$$

The compatibility relationships (129) and (130) relate A_1 to B_1 and A_2 to B_2 as follows:

$$A_1 = B_1\left[\frac{x_1^2C_3-F_3-X}{F_1-x_1^2C_1-X}\right] = B_1\phi_1 \qquad (144)$$

$$A_2 = B_2\left[\frac{x_2^2C_3-F_3-X}{F_1-x_2^2C_1-X}\right] = B_2\phi_2 \qquad (145)$$

where ϕ_1 and ϕ_2 are introduced only for convenience and have known values. Using the lower boundary condition, the displacements at the bedrock elevation are given by Equations (139). Substitution in Equations (142) and (143) yields:

$$\text{if} \qquad \beta_{11} = i\omega H/v_{d_1} \quad \text{and} \quad \beta_{22} = i\omega H/v_{d_2} \qquad (146)$$

$$W=A_1[\exp(\beta_{11})+\exp(-\beta_{11})]+A_2[\exp(\beta_{22})+\exp(-\beta_{22})] \qquad (147)$$

$$W=B_1[\exp(\beta_{11})+\exp(-\beta_{11})]+B_2[\exp(\beta_{22})+\exp(-\beta_{22})] \qquad (148)$$

By dividing Equations (147) and (148) by parts and by substituting B_1 and B_2 from Equations (144) and (145), it is obtained that:

$$\frac{A_1}{A_2} = \frac{\exp(\beta_{22})+\exp(-\beta_{22})}{\exp(\beta_{11})+\exp(-\beta_{11})}\,\frac{\phi_1(1-\phi_2)}{\phi_2(\phi_1-1)} \qquad (149)$$

Then, Equation (147) becomes:

$$A_1 = \frac{W}{[\exp(\beta_{11}) + \exp(-\beta_{11})]\left\{1 + \frac{\phi_2(\phi_1-1)}{\phi_1(1-\phi_2)}\right\}} \qquad (150)$$

Since the amplitude A_1 is obtainable from Equation (150), the amplitude A_2 is computed from Equation (149). The fluid displacement amplitudes B_1 and B_2 are obtained from Equations (144) and (145). Finally, displacements w and $\bar{w}$ are computed from Equations (142) and (143), the right hand side parts of which contain all known quantities.

The liquid particle velocities U and the solid particle velocities V are:

$$V = \partial w/\partial t = i\omega w \qquad (151)$$

$$U = \partial\bar{w}/\partial t = i\omega\bar{w} \tag{152}$$

The stresses σ and s acting on the solid and liquid parts respectively are:

$$\sigma = i\omega \exp(\beta') \left\{ [\exp(\beta_1) - \exp(-\beta_1)] \frac{MA_1 + QB_1}{v_{d_1}} + [\exp(\beta_2) - \exp(-\beta_2)] \frac{MA_2 + QB_2}{v_{d_2}} \right\} \tag{153}$$

$$s = i\omega \exp(\beta') \left\{ [\exp(\beta_1) - \exp(-\beta_1)] \frac{QA_1 + RB_1}{v_{d_1}} + [\exp(\beta_2) - \exp(-\beta_2)] \frac{QA_2 + RB_2}{v_{d_2}} \right\} \tag{154}$$

The stresses computed from Equations (153) and (154) are dynamic, i.e. are changes of stress from the initial static conditions. The analysis presented above is also valid for the case of no dissipation with the fluid dynamic viscosity considered zero, which however is not a realistic situation. In this case $X = 0$, $x_1 = x_1'$, $x_2 = x_2'$ and x_1, x_2, v_{d_1} and v_{d_2} are not complex but real.

The analysis presented above only applies to harmonic motions. If n equidistant displacement values are available from a digitized seismogram for the transient motion of the bedrock, a Fourier transform with a least squares criterion (Appendix 2) could be used to analyze the transient motion in a selected number of harmonics. Superposition of the solutions obtained for each harmonic provides the transient response of the system to the seismic action considered. A computer program to perform all necessary calculations is presented in Appendix 9.

Characteristics Method

The particle velocities of the solid and liquid constituents of a saturated soil deposit are denoted by $V=\partial w/\partial t$ and $U=\partial \bar{w}/\partial t$ respectively. Biot's equations of equilibrium in the z-direction (Equations 116 and 117) may be written as:

$$\frac{\partial \sigma}{\partial z} - \rho_{11} \frac{\partial V}{\partial t} - b\,(V - U) = 0 \qquad (155)$$

$$\frac{\partial s}{\partial z} - \rho_{22} \frac{\partial U}{\partial t} + b\,(V - U) = 0 \qquad (156)$$

The apparent mass was omitted from Equations (155) and (156) since the particles are of small size and the relative velocities are also small. If Biot's equations of state (111) and (112) are differentiated with respect to time, they may be written in terms of the particle velocities V and U as:

$$\frac{\partial \sigma}{\partial t} - M \frac{\partial V}{\partial z} - Q \frac{\partial U}{\partial z} = 0 \qquad (157)$$

$$\frac{\partial s}{\partial t} - Q \frac{\partial V}{\partial z} - R \frac{\partial U}{\partial z} = 0 \qquad (158)$$

where $M = \lambda + 2G$ is the constrained modulus of elasticity.

In case the soil is dry, the parameters s, ρ_{22}, U, μ_L, b, Q, and R become zero. Equations (155), (156), (157), and (158) degenerate to two equations for the one-dimensional propagation of pressure waves through elastic unsaturated soil:

$$\frac{\partial \sigma}{\partial z} - \rho_{11} \frac{\partial V}{\partial t} = 0 \qquad (159)$$

$$\frac{\partial \sigma}{\partial t} - M \frac{\partial V}{\partial z} = 0 \qquad (160)$$

Equations (159) and (160) present a striking similarity to Equations (39) and (41) which model one-dimensional shear wave propagation. The normal stress σ and the constrained modulus M are used instead of the shear stress τ and the shear modulus G. Therefore, by solving Equations (155) to (158), both cases of one-dimensional propagation of pressure waves through saturated or unsaturated elastic porous media can be studied.

Equations (155) and (156) and therefore Equation (159) do not include the effect of gravity forces. Thus, solutions obtained by using these equations are purely dynamic. However, since the equations are linear, superposition of static stresses would provide the real stress response of the system, if desired.

Equations (155) and (157) are transformed into four ordinary differential equations by the method of characteristics. Equation (155) is multiplied by an unknown multiplier θ_1 and is added to Equation (157) to give:

$$\left[\theta_1\frac{\partial\sigma}{\partial z} + \frac{\partial\sigma}{\partial t}\right] - \theta_1\rho_{11}\left[\frac{M}{\theta_1\rho_{11}}\frac{\partial V}{\partial z} + \frac{\partial V}{\partial t}\right] - b\theta_1(V-U) - Q\frac{\partial U}{\partial z} = 0 \quad (161)$$

The bracketed terms become total derivatives if:

$$\frac{dz}{dt} = \theta_1 = \frac{M}{\theta_1\rho_{11}} \quad (162)$$

From the solution of Equation (162), the pressure wave velocity v_M through the soil skeleton is obtained:

$$\theta_1 = \pm\sqrt{M/\rho_{11}} = \pm v_M \quad (163)$$

The four ordinary differential equations then are:

$$C_M^+ \begin{cases} \frac{d\sigma}{dt} - v_M\rho_{11}\frac{dV}{dt} - bv_M(V-U) - Q\left(\frac{\partial U}{\partial z}\right)_C = 0 & (164) \\ \frac{dz}{dt} = v_M & (165) \end{cases}$$

$$C_M^- \begin{cases} \frac{d\sigma}{dt} + v_M\rho_{11}\frac{dV}{dt} + bv_M(V-U) - Q\left(\frac{\partial U}{\partial z}\right)_C = 0 & (166) \\ \frac{dz}{dt} = -v_M & (167) \end{cases}$$

The subscript C indicates the value determined at point C of the z-t diagram in Figure 31. Using the same approach, Equation (156) is multiplied by an unknown multiplier θ_2 and is added to Equation (158) to give:

$$\left[\theta_2\frac{\partial s}{\partial z} + \frac{\partial s}{\partial t}\right] - \theta_2\rho_{22}\left[\frac{R}{\theta_2\rho_{22}}\frac{\partial U}{\partial z} + \frac{\partial U}{\partial t}\right] + \theta_2 b(V-U) - Q\frac{\partial V}{\partial z} = 0 \quad (168)$$

The bracketed terms become total derivatives if:

$$\frac{dz}{dt} = \theta_2 = \frac{R}{\theta_2\rho_{22}} \quad (169)$$

From the solution of Equation (169), the pressure wave velocity v_L through the liquid part is:

$$\theta_2 = \pm\sqrt{R/\rho_{22}} = \pm v_L \quad (170)$$

Equations (156) and (158) are transformed into the following four ordinary differential equations:

$$C_L^+ \begin{cases} \frac{ds}{dt} - v_L\rho_{22}\frac{dU}{dt} + bv_L(V-U) - Q\left(\frac{\partial V}{\partial z}\right)_C = 0 & (171) \\ \frac{dz}{dt} = v_L & (172) \end{cases}$$

$$C_L^- \begin{cases} \frac{ds}{dt} + v_L\rho_{22}\frac{dU}{dt} - bv_L(V-U) - Q\left(\frac{\partial V}{\partial z}\right)_C = 0 & (173) \\ \frac{dz}{dt} = -v_L & (174) \end{cases}$$

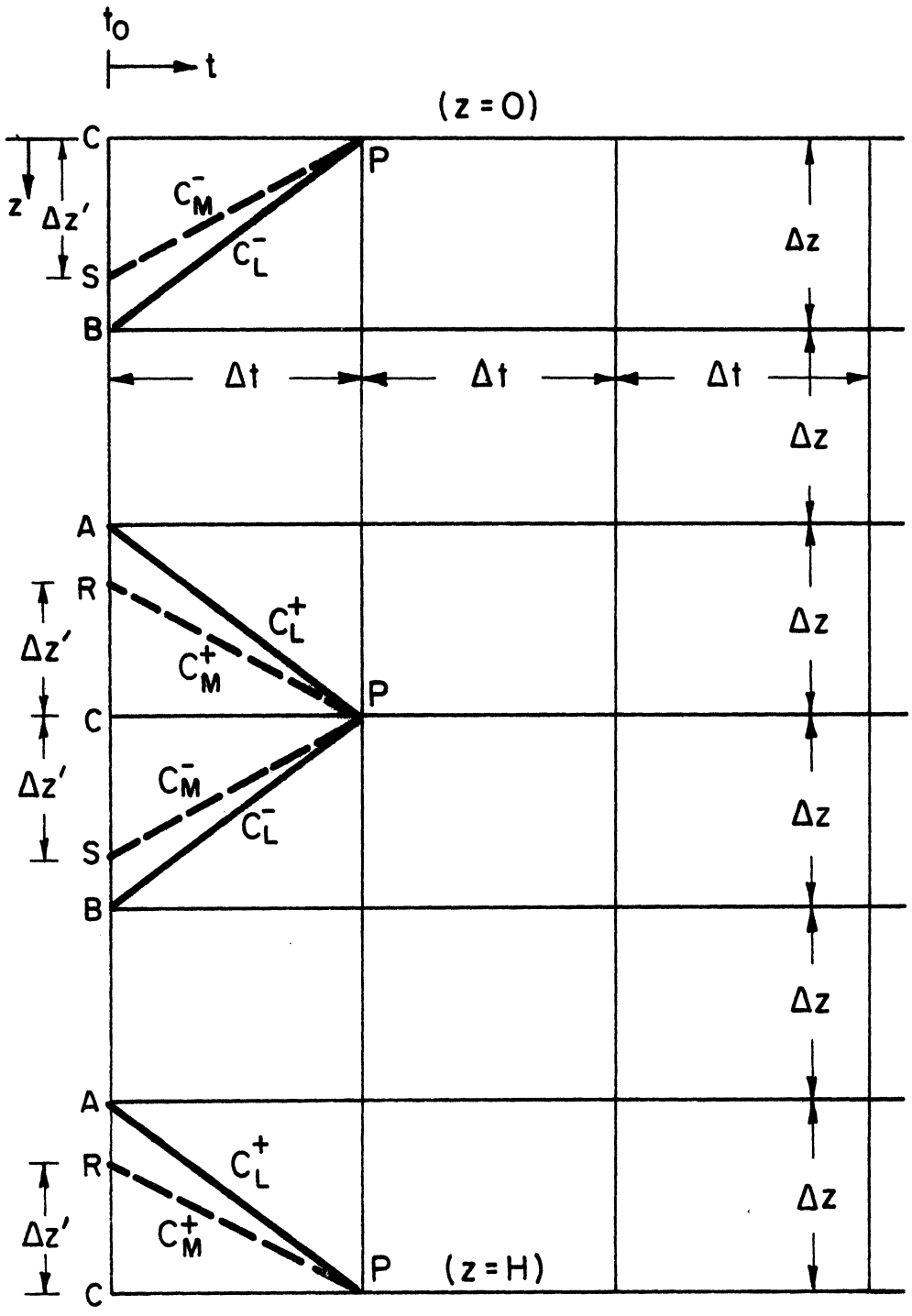

Figure 31. z-t diagram. Saturated porous media. Method of characteristics.

In Figure 31 the time (t) - distance (z) grid for the finite difference approximation is shown. Since v_M is always smaller than v_L, the saturated soil layer is partitioned into distance intervals equal to $\Delta z = v_L \Delta t$ where Δt is a selected time interval to be kept constant throughout the calculations. Then $v_M \Delta t = \Delta z' < \Delta z$ at all times, a condition necessary to satisfy stability criteria of the method of characteristics.

For the interior points of the z-t diagram (Figure 31), the central finite difference form of Equations (164), (166), (171), and (173) using a second order approximation is:

$$C_M^+: \quad \sigma_P-\sigma_R-\rho_{11}v_M(V_P-V_R)-bv_M\frac{\Delta t}{2}(V_P+V_R-U_P-U_R)-Q\Delta t\frac{U_S-U_R}{2\Delta z'} = 0 \quad (175)$$

$$C_M^-: \quad \sigma_P-\sigma_S+\rho_{11}v_M(V_P-V_S)+bv_M\frac{\Delta t}{2}(V_P+V_S-U_P-U_S)-Q\Delta t\frac{U_S-U_R}{2\Delta z'} = 0 \quad (176)$$

$$C_L^+: \quad s_P-s_A-\rho_{22}v_L(U_P-U_A)+bv_L\frac{\Delta t}{2}(V_P+V_A-U_P-U_A)-Q\Delta t\frac{V_B-V_A}{2\Delta z} = 0 \quad (177)$$

$$C_L^-: \quad s_P-s_B+\rho_{22}v_L(U_P-U_B)-bv_L\frac{\Delta t}{2}(V_P+V_B-U_P-U_B)-Q\Delta t\frac{V_B-V_A}{2\Delta z} = 0 \quad (178)$$

All quantities with subscripts A, B, C, R and S refer to the previous time step (z-t diagram, Figure 31). Using specified time intervals Δt, the conditions at points R and S can be evaluated by linear interpolations as follows:

$$\left.\begin{aligned} U_R &= U_C-(U_C-U_A)v_M/v_L, \quad & U_S &= U_C-(U_C-U_B)v_M/v_L \\ V_R &= V_C-(V_C-V_A)v_M/v_L, \quad & V_S &= V_C-(V_C-V_B)v_M/v_L \\ \sigma_R &= \sigma_C-(\sigma_C-\sigma_A)v_M/v_L, \quad & \sigma_S &= \sigma_C-(\sigma_C-\sigma_B)v_M/v_L \end{aligned}\right\} (179)$$

The four unknowns σ_P, s_P, V_P, and U_P are obtained from the solution of Equations (175) to (178) and (179). All known quantities in each of Equations (175) to (178) are grouped together for convenience:

$$CP1 = \sigma_R - \rho_{11} v_M V_R + b v_M \frac{\Delta t}{2}(V_R - U_R) + Q\Delta t \frac{U_S - U_R}{2\Delta z} \tag{180}$$

$$CM1 = \sigma_S + \rho_{11} v_M V_S - b v_M \frac{\Delta t}{2}(V_S - U_S) + Q\Delta t \frac{U_S - U_R}{2\Delta z} \tag{181}$$

$$CP2 = s_A - \rho_{22} v_L U_A - b v_L \frac{\Delta t}{2}(V_A - U_A) + Q\Delta t \frac{V_B - V_A}{2\Delta z} \tag{182}$$

$$CM2 = s_B + \rho_{22} v_L U_B + b v_L \frac{\Delta t}{2}(V_B - U_B) + Q\Delta t \frac{V_B - V_A}{2\Delta z} \tag{183}$$

also

$$\left.\begin{aligned} \psi_1 &= b v_L \Delta t/2 \quad , & \psi_2 &= b v_M \Delta t/2 \\ \psi_3 &= \psi_1 + \rho_{22} v_L \quad , & \psi_4 &= \psi_2 + \rho_{11} v_M \end{aligned}\right\} \tag{184}$$

The solution of Equations (175) to (178) written in terms of the above quantities is:

$$\sigma_P = (CP1 + CM1)/2 \tag{185}$$

$$s_P = (CP2 + CM2)/2 \tag{186}$$

$$U_P = \frac{\psi_1 (CP1 - CM1) + \psi_4 (CP2 - CM2)}{2(\psi_1 \psi_2 - \psi_3 \psi_4)} \tag{187}$$

$$V_P = \frac{\psi_3 (CP1 - CM1) + \psi_2 (CP2 - CM2)}{2(\psi_1 \psi_2 - \psi_3 \psi_4)} \tag{188}$$

At the surface ($z = 0$), the boundary conditions are expressed by $\sigma_P = 0$ and $s_P = 0$. The C_M^- and C_L^- characteristics Equations (176) and (178) are solved to find the particle velocities V_P and U_P at the surface. Equations (176) and (178) can be written as:

$$\psi_4 V_P - \psi_2 U_P = \sigma_S + \rho_{11} v_M V_S - \psi_2 (V_S - U_S) + Q\Delta t \frac{U_S - U_C}{\Delta z} = CCM1 \qquad (189)$$

$$\psi_3 U_P - \psi_1 V_P = s_B + \rho_{22} v_L U_B + \psi_1 (V_B - U_B) + Q\Delta t \frac{V_B - V_C}{\Delta z} = CCM2 \qquad (190)$$

The solutions are:

$$U_P = \frac{\psi_1 \cdot CCM1 + \psi_4 \cdot CCM2}{\psi_3 \psi_4 - \psi_1 \psi_2} \qquad (191)$$

$$V_P = (CCM1 + \psi_2 \cdot U_P)/\psi_4 \qquad (192)$$

At the bedrock (z = H) the particle velocities V_P and U_P are equal and known as a function of time for the seismic motion considered. The C_M^+ and C_L^+ Equations (175) and (177) are solved to find σ_P and s_P at the bedrock:

$$\sigma_P = \psi_4 V_P - \psi_2 U_P + \sigma_R - \rho_{11} v_M V_R + \psi_2 (V_R - U_R) + Q\Delta t \frac{U_C - U_R}{\Delta z} \qquad (193)$$

$$s_P = \psi_3 U_P - \psi_1 V_P + s_A - \rho_{22} v_L U_A - \psi_1 (V_A - U_A) + Q\Delta t \frac{V_C - V_A}{\Delta z} \qquad (194)$$

It should be noted that using the method of characteristics, the guantities M, Q, R, ρ_{11}, ρ_{22} and b can vary with depth; they should be considered constant only within each reach of thickness Δz. The method, as developed herein is applicable to cases where there are more than one saturated or unsaturated soil layer present in the soil formation. This method is not restricted to harmonic vibration cases. Appendix 10 includes a program written in FORTRAN IV Language which performs all necessary calculations.

Case Studies

Example 1 A saturated sand layer 200 feet thick rests on a horizontal rock base subjected to a harmonic excitation of the form $V(H,t) = U(H,t) = 0.2 \sin 4\pi t$ or $w(H,t) = \bar{w}(H,t) = -0.016 \cos 4\pi t$. Specific mass densities are assumed to be $\rho_S = 5.11$, $\rho_L = 1.94$, $\rho_a = 0.5$, $\rho = 4.0$ in slugs/ft^3. Elastic constants are $G = 4 \times 10^6$, $\lambda = 37.5 \times 10^6$, $R = 20 \times 10^6$, $Q = 10 \times 10^6$ in psf. Two cases are examined, with and without dissipation.

The influence of porosity n is studied in the case of no dissipation, which however is not a realistic situation. The pressure wave velocities were found to be $v_{d_1} = 2820$ ft/sec, $v_{d_2} = 5100$ ft/sec for $n = 0.35$ and $v_{d_1} = 2668$ ft/sec, $v_{d_2} = 4958$ ft/sec for $n = 0.45$. The water and solid particle velocities at the surface of the deposit were computed from the analytical method and are presented in Figure 32. The difference between solid and fluid velocity ampitudes (relative velocity) decreases for increasing n, since increased porosity reduces the resistance to the flow of the fluid through the pores. No difference in phase is obsered since dissipation is absent.

Disipation is next introduced by assuming that water viscosity is $\mu_L = 1.8 \times 10^{-5}$ lb·sec/ft^2 and intrinsic permeability is $K = 14.4 \times 10^{-9}$ ft^2. Porosity is assumed to be equal to 0.35. The damped pressure wave velocities were computed as $v_{d_1} = 677$ ft/sec and $v_{d_2} = 4624$ ft/sec. The water and solid particle velocities at the surface of the

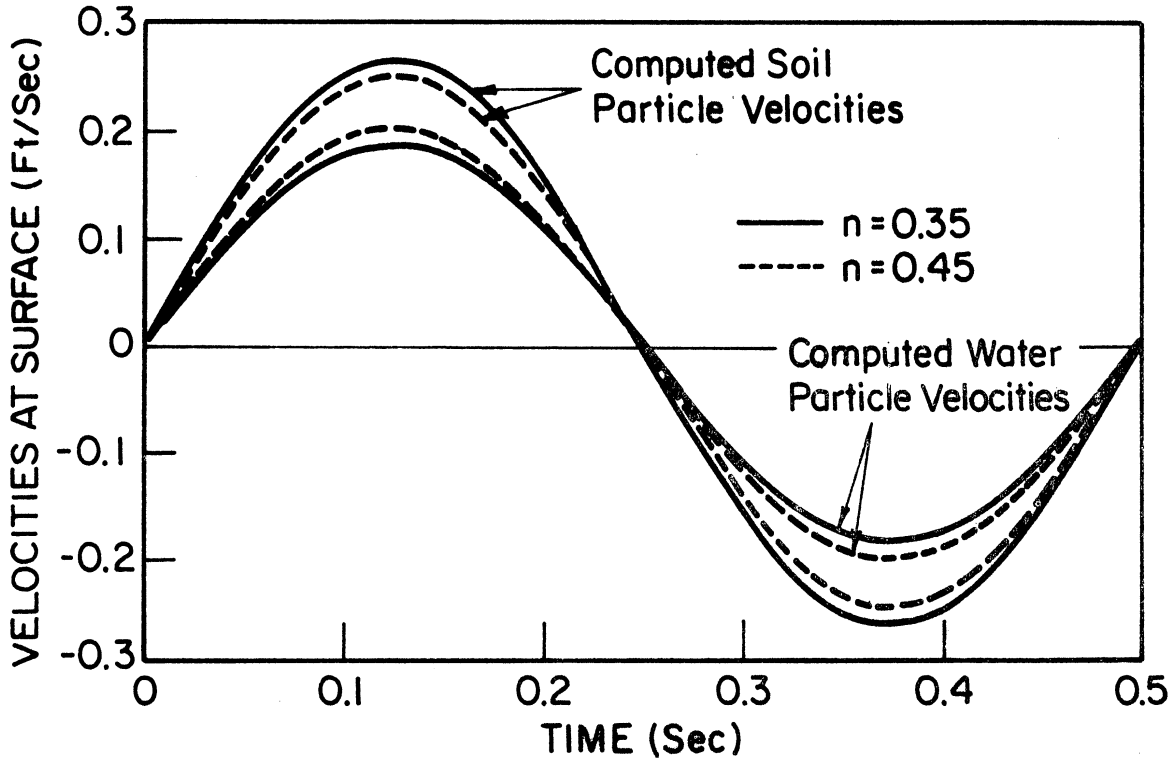

Figure 32. Water and soil particle velocities at surface of a 200 ft thick saturated soil deposit, for different values of porosity. No dissipation ($\mu_L = 0$).

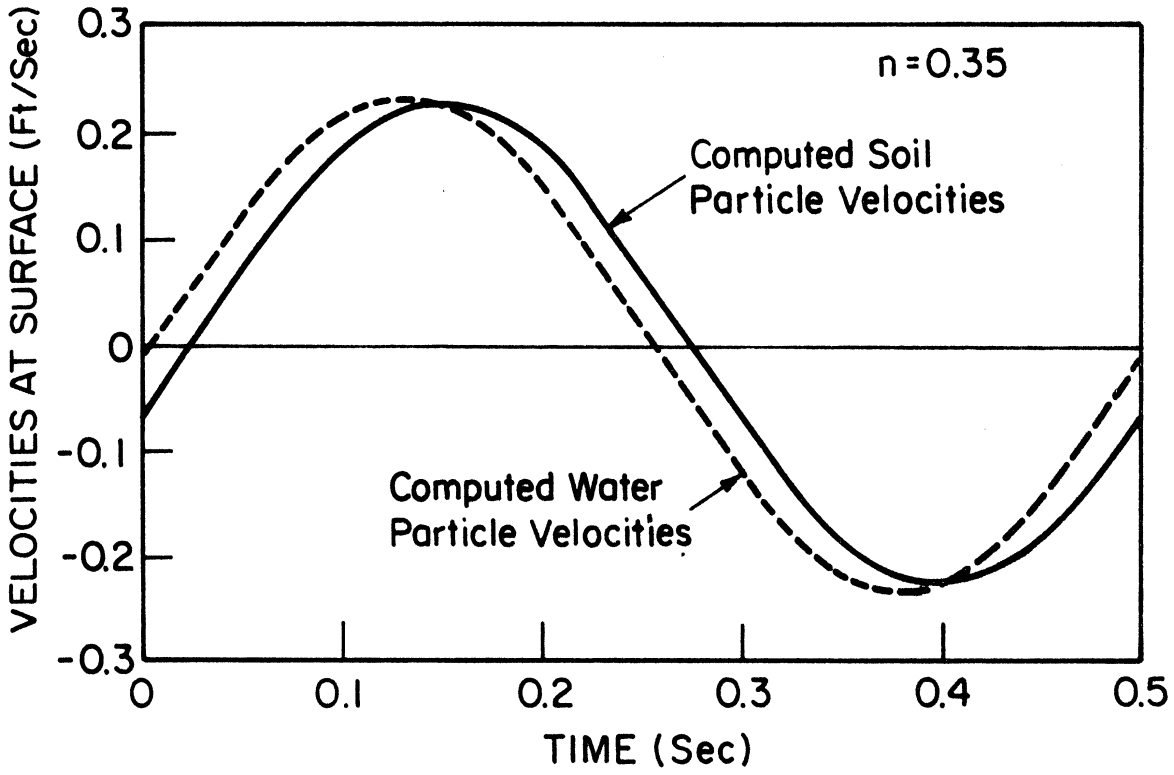

Figure 33. Water and soil particle velocities at surface of a 200 ft thick saturated soil deposit, $\mu_L = 1.8 \times 10^{-5}$ lb-sec/ft^2.

saturated soil deposit were computed by using the analytical method and are presented in Figure 33. The solid and water particle velocities have about the same amplitudes, with the amplitude of the latter being larger. However, because of the phase difference due to the presence of dissipation, relative velocities are of considerable magnitude. From several other similar examples, it was observed that an increase in permeability decreases the phase difference, i.e. for very large permeability values the solid and fluid constituents tend to move together.

Example 2 A 200 feet thick saturated sand layer is resting on horizontal bedrock which develops a sinusoidal velocity of the form $V(H,t) = U(H,t) = 0.2 \sin 4\pi t$ (ft/sec). Porosity is assumed equal to $n = 0.30$. Specific mass densities are assumed: $\rho_S = 5.13$, $\rho_L = 1.94$, $\rho_a = 0.0$, and $\rho = 4.173$ slugs/ft^3. Elastic constants are $G = 6 \times 10^6$, $\lambda = 56 \times 10^6$, $R = 27 \times 10^6$ and $Q = 11 \times 10^6$ in psf. Two cases are examined, with and without dissipation and the results obtained by the analytical method and the method of characteristics are compared.

For zero dissipation, the sand layer was divided into five 40-feet thick reaches with the time interval selected for the method of characteristics being $\Delta t = 0.00587$ seconds. The pressure wave velocities computed are $v_L = 6811$ ft/sec and $v_M = 4351$ ft/sec. The dynamic pressure σ on the soil skeleton computed 80 feet below the surface by the analytical method is plotted in Figure 34. To avoid the generation of

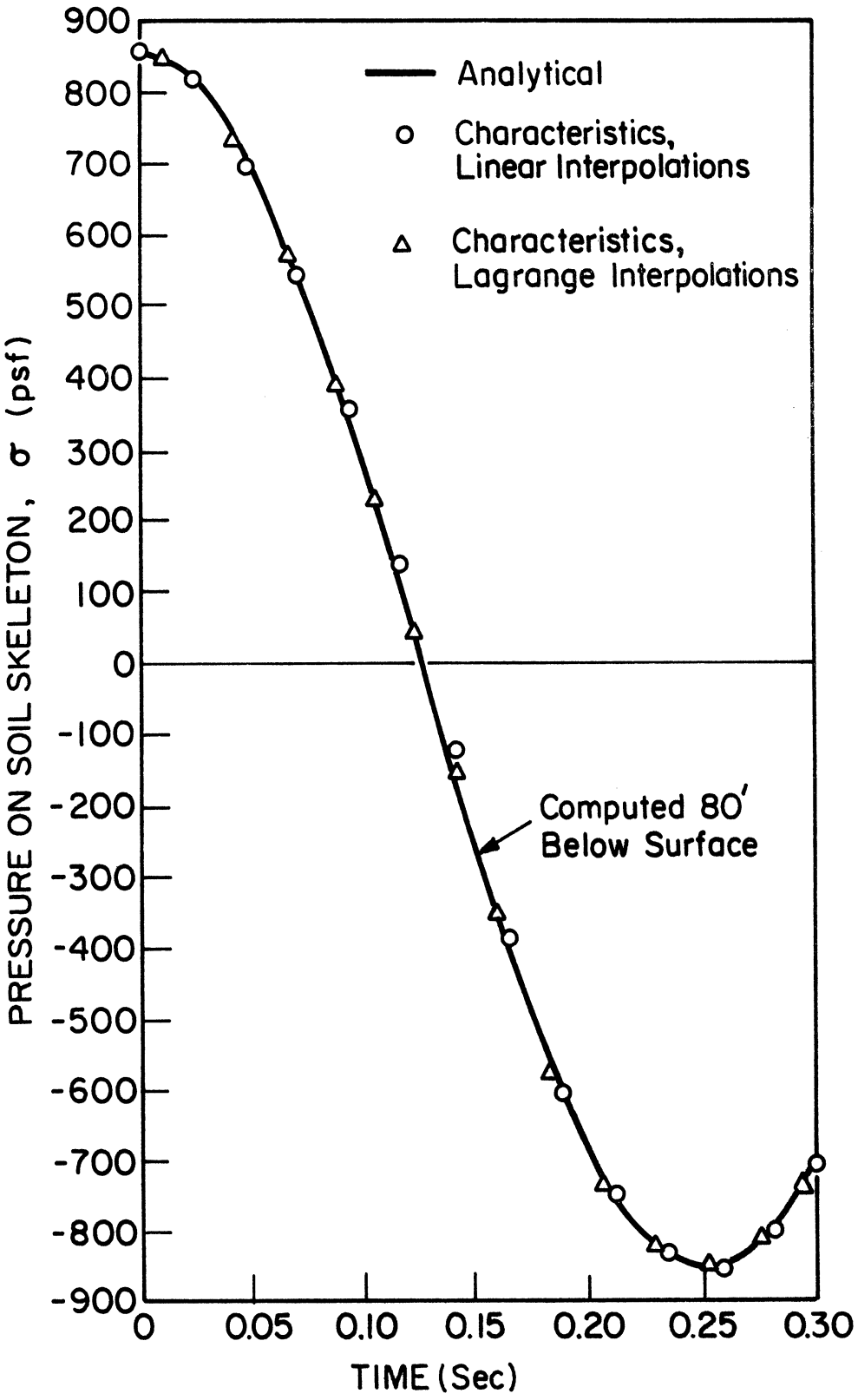

Figure 34. Dynamic pressure on soil skeleton computed 80 ft below surface of a 200 ft thick saturated soil deposit. No dissipation ($\mu_L = 0$).

an initial transient, conditions found at time zero throughout the layer by the analytical method were used as initial conditions for the method of characteristics. Linear interpolations and fifth order Lagrange interpolations were used in conjunction with the method of characteristics. The dynamic pressure on the soil skeleton computed by the method of characteristics for both interpolation schemes is in agreement with the analytical solution as shown in Figure 34.

Dissipation is next introduced by assuming that the water viscosity is $\mu_L = 1.8 \times 10^{-5}$ lb·sec/ft^2 and intrinsic permeability is $K = 15 \times 10^{-9}$ ft^2. For a time increment $\Delta t = 0.00587$ sec the saturated soil layer was divided into five 40-feet thick reaches. For a time increment $\Delta t = 0.00293$ sec the soil layer was divided into ten 20-feet thick reaches. The dynamic pressure on the soil skeleton 80 feet below the surface computed by the method of characteristics using linear interpolations was substantially the same for the two time increments selected. Fifth order Lagrangian interpolations did not improve the results obtained by using linear interpolations. The initial transient generated because of the use of initial conditions zero throughout the layer, vanished after 2.3 seconds due to the presence of the dissipation. The dynamic pressure on the soil skeleton 80 feet below the surface computed by the analytical method is plotted in Figure 35. Linear interpolations and numerical approximations in the method of characteristics accounted for the differences in the results (maximum 5%). The effect of

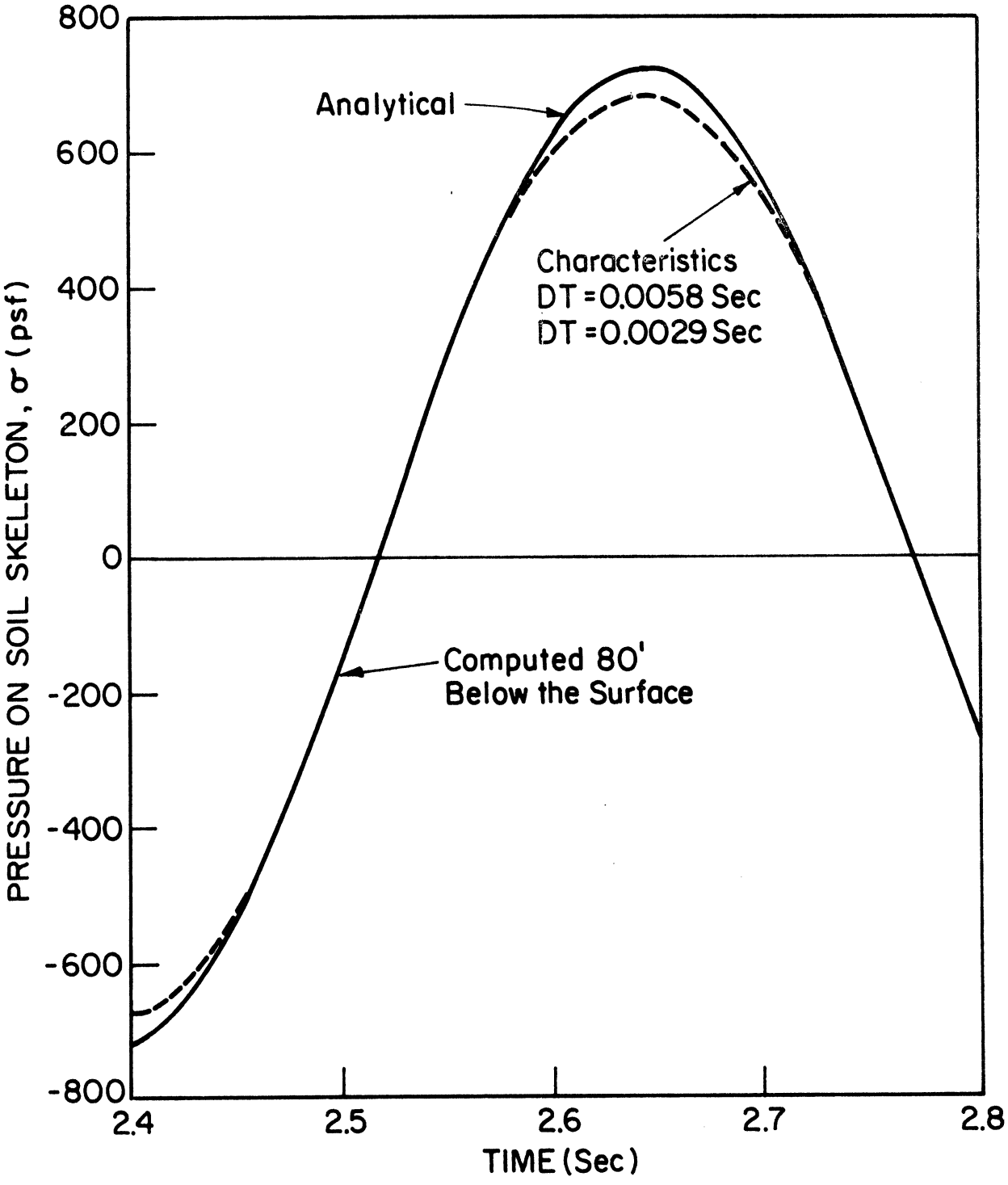

Figure 35. Dynamic pressure on soil skeleton computed at 80 ft below surface of a 200 ft thick saturated soil deposit. Dissipation μ_L = 1.8×10^{-5} lb-sec/ft^2.

dissipation on the peak magnitudes of σ can be observed by comparing Figures 34 and 35. In the presence of dissipation the amplitude is considerably reduced.

Example 3 A transient problem involving a real earthquake motion is solved by the method of characteristics. The first 7.5 seconds of the vertical component of the 1952 Taft earthquake (Figure 36) act at the base rock of a saturated sand deposit 1953 feet thick. Water viscosity is $\mu_L = 1.8 \times 10^{-5}$ lb·sec/ft^2, intrinsic permeability is $K = 15 \times 10^{-9}$ ft^2, porosity is $n = 0.35$, mass densities are $\rho_S = 5.11$, $\rho_L = 1.94$, $\rho_a = 0.0$, $\rho = 4.0$ slugs/ft^3 and elastic constants are $R = 20 \times 10^6$, $Q = 10 \times 10^6$, $\lambda = 37.5 \times 10^6$, $G = 4 \times 10^6$ psf. The pressure wave velocities computed are $v_L = 5427$ ft/sec and $v_M = 3701$ ft/sec. A time increment $\Delta t = 0.015$ sec is assumed constant throughout the computations. The layer is partitioned into 24 distance intervals of 81.4 feet. Linear interpolations were used.

The dynamic stress on the soil skeleton σ and the pore water pressure p, 81.4 feet below the ground surface, calculated by the method of characteristics are plotted in Figure 37. It can be observed that increase in pore water pressure results to a decrease in stress on the soil skeleton. The soil and water particle velocities computed 81.4 feet below the ground surface are plotted in Figure 38. These two velocities are of about the same magnitude but are slightly out of phase.

The method of characteristics provides the means to evaluating the transient pore water pressure in a saturated

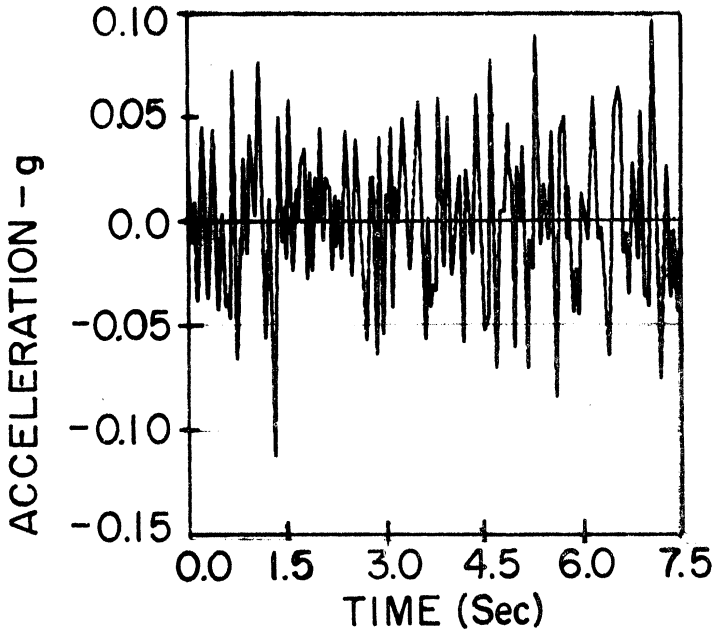

Figure 36. Taft earthquake accelerogram vertical component, 1952.

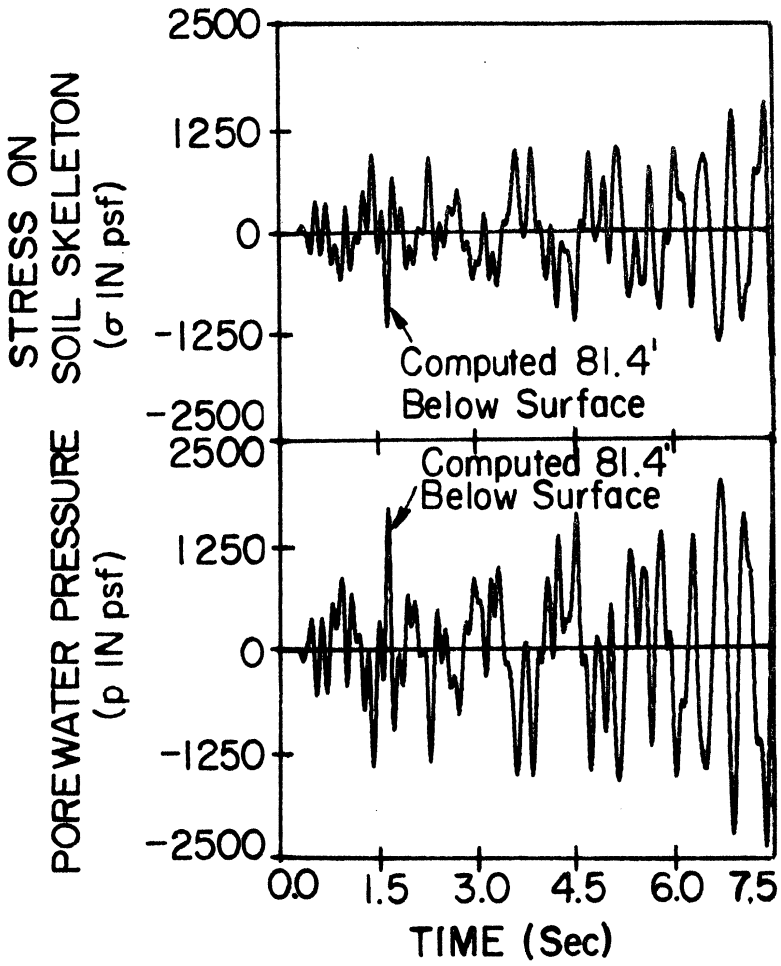

Figure 37. Dynamic stress on soil skeleton and porewater pressure calculated 81.4 feet below ground surface.

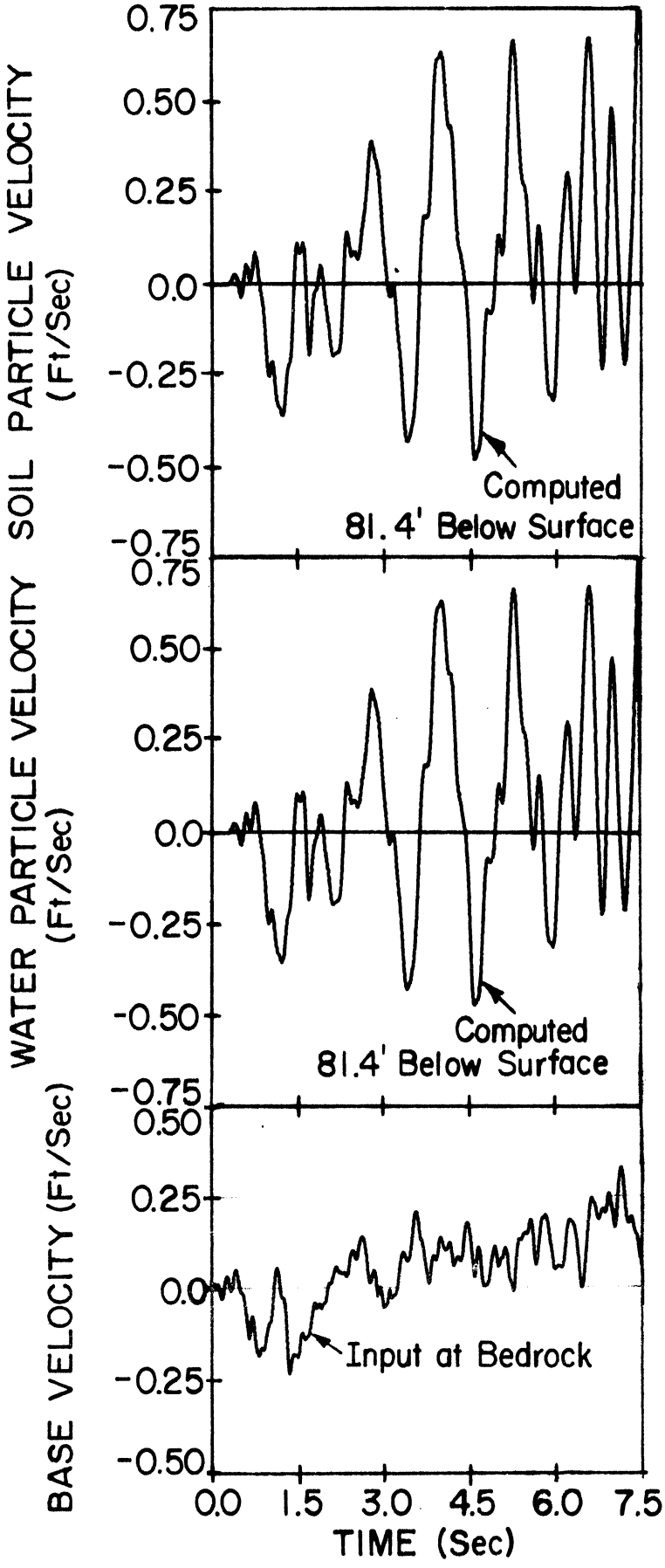

Figure 38. Water and soil particle velocities applied at base and computed 81.4 ft below the surface of a 1953 feet thick saturated soil deposit.

soil deposit. If pore water pressure builds up to the point that the effective stress becomes zero, the sand completely loses its strength and liquefies. Since Biot's equations hold for an elastic soil skeleton, it is obvious that only instantaneous liquefaction can be modeled. Permanent deformations and plastic rebound of the soil skeleton due to readjustment of soil grains should be incorporated to solve successfully the problem of liquefaction. At low pressure ranges, soil still reacts as a "strain-softening" material and a "locking-up" model for the soil is not necessary. Future investigations on the subject should try to incorporate a Ramberg-Osgood type of stress-strain curves in the analysis. Thus, the constrained modulus for the soil at a particular instant will be represented by the slope of the tangent to the corresponding stress-strain curve. The variation of the coupling coefficients R and Q under dynamic conditions of loading and unloading should also be studied. Such a model would definitely provide a more realistic solution to the problem of potential liquefaction under dynamic conditions.

CHAPTER VII

TWO-DIMENSIONAL PROPAGATION OF SHEAR AND PRESSURE WAVES THROUGH SOIL

Review of Literature

The Finite Element method is a mathematical discretization technique (basic variation of the Ritz method) where the governing differential equations are replaced by a related system of simultaneous algebraic equations. The material properties of the prototype are retained in the individual elements so that varying material properties and geometric configurations may readily be handled. Since the advent of high speed computers, this method has been widely used. The initial application of the Finite Element method to the solution of linear elasto-dynamic soil problems in two dimensions is due to Clough and Chopra [14]. They studied the response of earth fill dams to earthquakes.

Idriss and Seed [34] in 1967 studied the response of earth banks to earthquakes. The earth banks were idealized by a number of triangular elements and the Finite Element method was used. The problem was complicated by the necessity of extending the finite element mesh a sufficient distance from the area of the slope in order to obtain an accurate response picture [60]. In 1969, Dibaj and Penzien [20] used the Finite Element method and a step-by-step integration method to study the nonlinear response of two-dimensional earth structures to earthquakes.

The nonlinear problem was reduced to a number of successive linear problems. Relative differences between linear and nonlinear solutions were discussed.

Dezfulian and Seed [18] applied the method of Finite Elements to linear-viscoelastic soil deposits underlain by sloping rock boundaries. The analysis incorporated strain compatible values of moduli and damping factors. This method was applied to analyze the response of the valley passing through the Palos Grandes area during the Caracas earthquake of July 29, 1967 [73,62,64]. The actual elastic continuum was idealized as an assemblage of triangular elements interconnected at a finite number of nodal points. In these analyses, the rock motions were treated as a time dependent phenomenon with the same motions developed at all points in the rock at a given time. Spacial variations in rock motions, due to wave propagation effects, were studied by Dezfulian and Seed [19]. The interaction between soil and embedded foundations during earthquakes was studied by Isenberg and Adham [37] in the case of an embedded nuclear reactor building. A finite element solution was obtained considering a two-dimensional, dynamic, elastic continuum representation of the soil, embedded foundation, walls, and containment and support structures.

Results obtained by the Finite Element method near the edges of valleys or at the toes of earth dams tend to be erratic [18,62]. The reasons behind these inaccuracies are: that stresses are small near these regions compared

with the stresses in the earth structure itself; and that triangular finite elements adjacent to these regions are stiffer, thus restricting deformations. The computer time required to obtain solutions by the Finite Element method is rather excessive. Realizing the need for a more economical method, Streeter, Wylie and Richart [71] replaced the visco-elastic continuum with a latticework of one-dimensional linear elements as used in hydraulics [70]. The linear elements of the latticework transmitted shear and pressure waves to the interior nodes of the latticework where an imaginary nodal transfer element received and transmitted all shear and pressure waves. The nodal element was considered to be rigid, weightless and free to move horizontally and vertically but not to rotate. The rigidity of the nodal element was responsible for the lack of coupling between shear and pressure waves. A force balance was written in the x and z directions and two equations (the C^+ and C^- characteristics equations) were used from each linear element correlating pressure or shear with the corresponding velocity. For the interior nodes, there were 5 equations in 5 unknowns for each of the x and z directions. Soil deposits with uniform properties were considered. Cases with a shear wave velocity being half of the pressure wave velocity were examined (i.e., $\nu = 1/3$ for $\mu = 0$). This method is termed in the following "10-Latticework method," the number referring to the number of equations at each internal node.

Latticework Method

To create a coupling between shear and pressure waves, Professor Streeter's suggestion that the nodal transfer elements of a latticework (Figure 39) should be deformable was adopted. Sixteen simultaneous linear equations were obtained for each interior nodal transfer element. Two equations represent the force balance in the x and z direction. A pair of equations (C^+ and C^- characteristics) from each surrounding linear element relate pressure and shear to the corresponding velocities. Two equations model the deformation of the transfer element in the x and z directions including the Poisson ratio effects. The last four equations relate the velocities of the four faces of the transfer element to the velocities of the element itself in the x and z directions. This method is termed herein "16-Latticework method," the number referring to the equations used, and it is explicit in the solution of the equations involved at each node, which explains the low computer cost associated with the method.

A nodal transfer element and the sixteen unknown quantities (shearing stresses, pressures and velocities) are shown in Figure 40. Each of the unknowns has a two capital alphabetic character subscript. The first character refers to the face of the nodal element (up, down, left, right) and the second refers to the corresponding position on the x-t or z-t diagram (Figures 41 and 42).

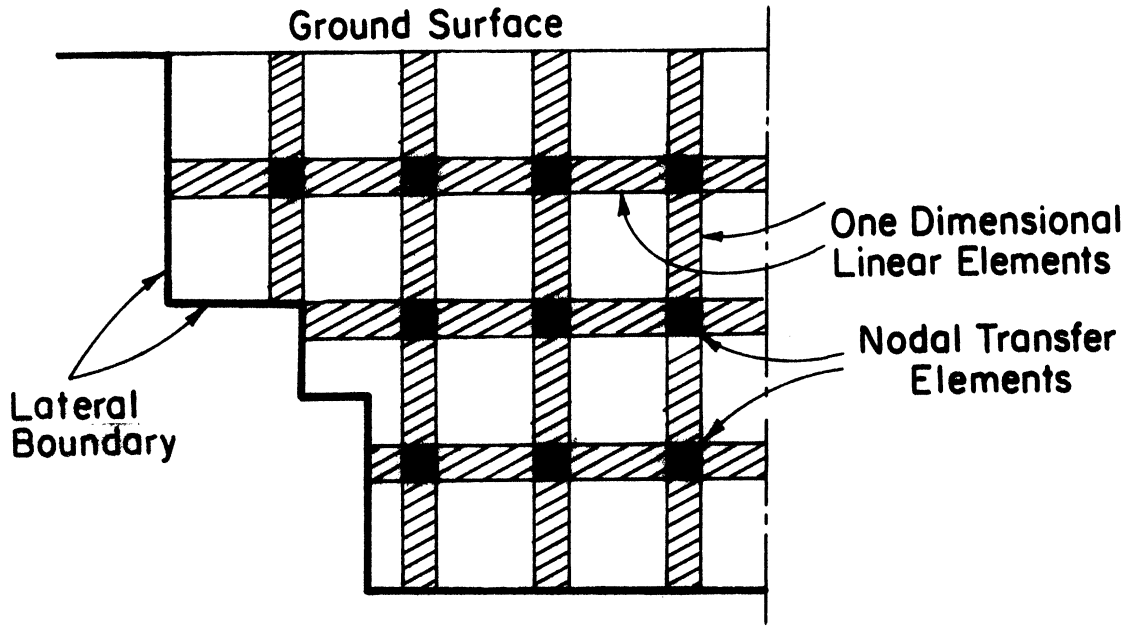

Figure 39. Two-dimensional latticework with linear and nodal elements.

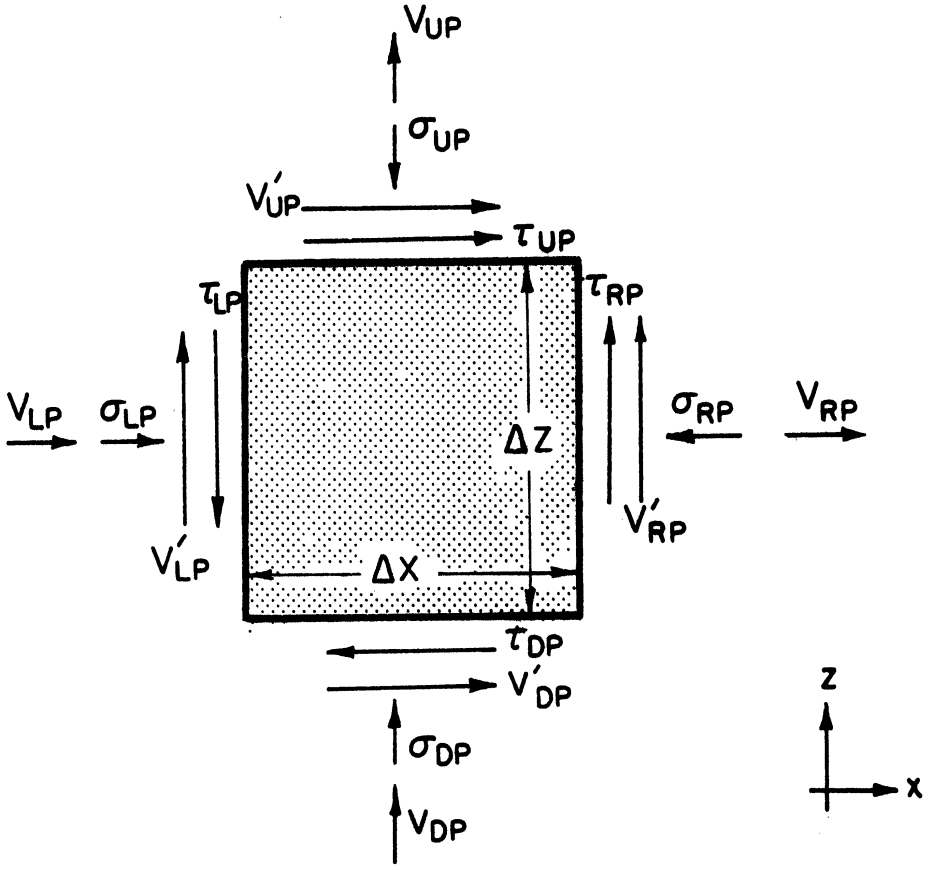

Figure 40. Transfer element and the eight unknowns for each of the two coordinates.

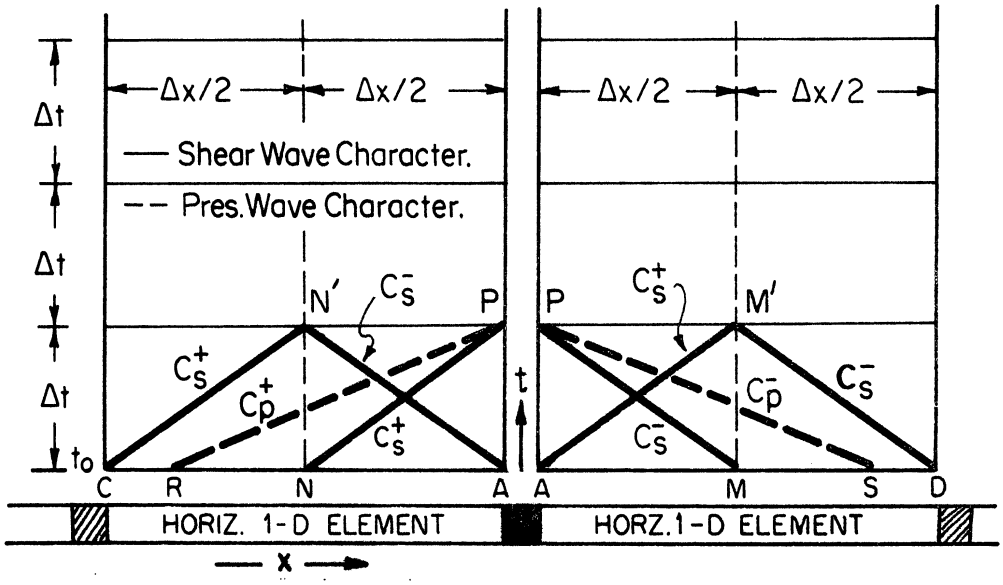

Figure 41. Characteristics in x-t plane for horizontal one-dimensional elements.

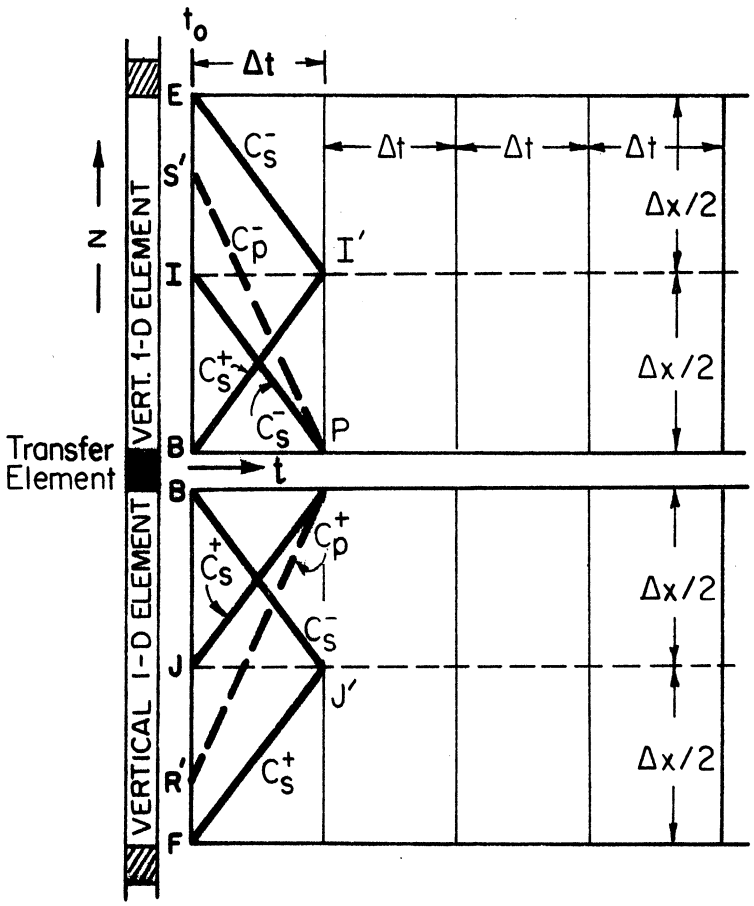

Figure 42. Characteristics in z-t plane for vertical one-dimensional elements.

The force balance in the x and z direction yields:

$$(\sigma_{LP}-\sigma_{RP})\Delta Z + (\tau_{UP}-\tau_{DP})\Delta X = 0 \tag{195}$$

$$(\sigma_{DP}-\sigma_{UP})\Delta X + (\tau_{RP}-\tau_{LP})\Delta Z = 0 \tag{196}$$

where ΔX and ΔZ are the dimensions of the nodal transfer element which is considered to be weightless, deformable and free to move in the x and z directions but not to rotate. Therefore, the relations between the vertical and parallel velocities of the four faces of the transfer element are:

$$V'_{DP} = V'_{UP} = (V_{RP}+V_{LP})/2 \tag{197}$$

$$V'_{LP} = V'_{RP} = (V_{UP}+V_{DP})/2 \tag{198}$$

Since there are stresses in both principal directions x and z of the transfer element, the strain in either direction will depend not only upon the stress in that direction but also upon the stress in the orthogonal direction because of the Poisson ratio effect. Differentiation of the total strains with respect to time yields:

$$\frac{dV_x}{dx} = -\frac{1}{E}\frac{d\sigma_x}{dt} + \frac{\nu}{E}\frac{d\sigma_z}{dt} \tag{199}$$

$$\frac{dV_z}{dz} = -\frac{1}{E}\frac{d\sigma_z}{dt} + \frac{\nu}{E}\frac{d\sigma_x}{dt} \tag{200}$$

where ν is the Poisson ratio and E is the modulus of

elasticity. Subscripts indicate the two principal directions x and z. Equations (199) and (200) in finite difference form become:

$$\frac{V_{RP}-V_{LP}}{\Delta X} = -\frac{\sigma_{RP}+\sigma_{LP}-\sigma_{RA}-\sigma_{LA}}{2E\Delta t} + \frac{\nu}{E}\frac{\sigma_{UP}+\sigma_{DP}-\sigma_{UB}-\sigma_{DB}}{2\ \Delta t} \qquad (201)$$

$$\frac{V_{UP}-V_{DP}}{\Delta Z} = -\frac{\sigma_{UP}+\sigma_{DP}-\sigma_{UB}-\sigma_{DB}}{2E\Delta t} + \frac{\nu}{E}\frac{\sigma_{PR}+\sigma_{LP}-\sigma_{RA}-\sigma_{LA}}{2\ \Delta t} \qquad (202)$$

where ΔX and ΔZ are the transfer element's dimensions which may be considered equal. However, they subsequently cancel out and they do not appear in the final solution.

Assuming that the soil material is linear viscoelastic, the partial differential euqations governing the propagation of shear waves through the vertical one-dimensional linear elements of the latticework are:

$$\frac{\partial \tau}{\partial z} - \rho\frac{\partial V}{\partial t} = 0 \qquad (203)$$

$$\frac{\partial \tau}{\partial t} - G\frac{\partial V}{\partial z} - \mu\frac{\partial^2 V}{\partial z \partial t} = 0 \qquad (204)$$

The same equations hold for the horizontal one-dimensional linear elements if x is substituted for z. The partial differential equations governing the propagation of pressure waves through the vertical one-dimensional linear elements of the latticework are:

$$\frac{\partial \sigma}{\partial z} - \rho g - \rho\frac{\partial V}{\partial t} = 0 \qquad (205)$$

$$\frac{\partial \sigma}{\partial t} - M\frac{\partial V}{\partial z} - \mu\frac{\partial^2 V}{\partial z \partial t} = 0 \qquad (206)$$

where M is the constrained modulus and the term ρg introduces the effect of gravity. The same equations hold for the vertical one-dimensional linear elements if x is substituted for z and if the gravity term ρg is omitted. If dynamic stress conditions are sought the gravity term ρg should be also omitted from Equation (205). In this case, total stresses are obtained from the superposition of dynamic and static stresses.

The method of characteristics is employed to solve Equations (203), (204), and (205), (206) as well as the corresponding equations in the x direction. A common time step Δt is selected. After transforming the partial differential equations to ordinary differential equations by the usual procedure, the apparent shear and pressure wave velocities are obtained:

$$v_s = \sqrt{\frac{G}{\rho} + \frac{\mu}{\rho \Delta t}} \tag{207}$$

$$\text{and} \quad v_p = \sqrt{\frac{M}{\rho} + \frac{\mu}{\rho \Delta t}} \tag{208}$$

The lengths of the vertical and horizontal one-dimensional linear elements are assumed to be:

$$\Delta x = \Delta z = 2 v_s \Delta t \tag{209}$$

The one-dimensional linear elements are therefore partitioned into two reaches for the case of shear wave propagation. For pressure waves the condition required to

satisfy stability criteria of the method of characteristics is:

$$\Delta x \geq v_p \Delta t > \Delta x/2 \qquad (209a)$$

and should be always satisfied. If $\mu = 0$, condition (209a) holds for any $\nu \leq 1/3$. For values of $\mu > 0$, higher values of ν satisfy condition (209a). Usual Poisson ratio ranges are: for sandy soils $0.25 \geq \nu \geq 0.35$; for clay with some sand and silt $0.30 \geq \nu \geq 0.40$; and for clays $0.35 \geq \nu \geq 0.45$. Therefore, condition (209a) holds for all practical purposes. Linear interpolations are required in this case. Figures 41 and 42 show the x-t and z-t diagrams for the two horizontal and the vertical linear elements surrounding a transfer element.

The finite difference expressions of the ordinary differential equations emanating from the method of characteristics for the case of shear waves are:

Hor.

$$C_s^+: \quad \tau_{LP}-\tau_N-\rho v_s(V'_{LP}-V_N) + \frac{2\mu}{\Delta x}(V'_{LA}-V_N) = 0 \qquad (210)$$

$$C_s^-: \quad \tau_{RP}-\tau_M+\rho v_s(V'_{RP}-V_M) + \frac{2\mu}{\Delta x}(V_M-V'_{RA}) = 0 \qquad (211)$$

Vert.

$$C_s^+: \quad \tau_{DP}-\tau_J-\rho v_s(V'_{DP}-V_J) + \frac{2\mu}{\Delta x}(V'_{DB}-V_J) = 0 \qquad (212)$$

$$C_s^-: \quad \tau_{UP}-\tau_I+\rho v_s(V'_{UP}-V_I) + \frac{2\mu}{\Delta x}(V_I-V'_{UB}) = 0 \qquad (213)$$

where v_s is the apparent shear wave velocity. The first character of the two capital alphabetic character subscripts

refers to the face of the transfer element and the second to the corresponding position on the x-t or z-t diagram. Single alphabetic character subscripts refer to positions on the x-t and z-t diagram.

The finite difference expressions of the ordinary differential equations emanating from the method of characteristics for the case of pressure waves are:

$$\text{Hor.}\begin{cases} C_p^+: & \sigma_{LP}-\sigma_R+\rho v_p(V_{LP}-V_R) - \frac{\mu}{\Delta x}(V_{LA}-V_R) = 0 \quad (214) \\ C_p^-: & \sigma_{RP}-\sigma_S-\rho v_p(V_{RP}-V_S) - \frac{\mu}{\Delta x}(V_S-V_{RA}) = 0 \quad (215) \end{cases}$$

$$\text{Vert.}\begin{cases} C_p^+: & \sigma_{DP}-\sigma_{R'}+\rho v_p(V_{DP}-V_{R'})-\frac{\mu}{\Delta x}(V_{DB}-V_{R'})+\rho g v_p \Delta t=0 \quad (216) \\ C_p^-: & \sigma_{UP}-\sigma_{S'}-\rho v_p(V_{UP}-V_{S'})-\frac{\mu}{\Delta x}(V_{S'}-V_{UB})-\rho g v_p \Delta t=0 \quad (217) \end{cases}$$

By calling $r = v_p/2v_s$, the necessary linear interpolations are written as:

$$\left.\begin{aligned} \sigma_R &= \sigma_{LA} - r\,(\sigma_{LA}-\sigma_{RC}) \\ V_R &= V_{LA} - r\,(V_{LA}-V_{RC}) \\ \sigma_S &= \sigma_{RA} - r\,(\sigma_{RA}-\sigma_{RD}) \\ V_S &= V_{RA} - r\,(V_{RA}-V_{RD}) \\ \sigma_{R'} &= \sigma_{DB} - r\,(\sigma_{DB}-\sigma_{UF}) \\ V_{R'} &= V_{DB} - r\,(V_{DB}-V_{UF}) \\ \sigma_{S'} &= \sigma_{UB} - r\,(\sigma_{UB}-\sigma_{DE}) \\ V_{S'} &= V_{UB} - r\,(V_{UB}-V_{DE}) \end{aligned}\right\} \quad (218)$$

The 16 unknowns that appear in Figure 40 are obtained from the solution of the linear simultaneous Equations (195) to (198), (201), (202), (210) to (217) together with Equation (218). To present the solution, it becomes necessary for purposes of clarity to group known quantities under different headings:

$$
\left.
\begin{aligned}
C0 &= \rho(v_s+v_p) \\
C1 &= \mu/\Delta x \\
C2 &= 2\mu/\Delta x \\
CC &= \rho g v_p \Delta t \\
CM &= \rho v_s - 2\mu/\Delta x \\
CCM &= \rho v_p - \mu/(v_p \Delta t) \\
F1 &= \sigma_S - CCM \cdot V_S - C1 \cdot V_{RA} \\
F2 &= \sigma_R + CCM \cdot V_R + C1 \cdot V_{LA} \\
F3 &= \sigma_{R'} + CCM \cdot V_{R'} + C1 \cdot V_{DB} - CC \\
F4 &= \sigma_{S'} - CCM \cdot V_{S'} - C1 \cdot V_{UB} + CC \\
F5 &= \tau_N - CM \cdot V_N - C2 \cdot V'_{LA} \\
F6 &= \tau_M + CM \cdot V_M + C2 \cdot V'_{RA} \\
F7 &= \tau_J - CM \cdot V_J - C2 \cdot V'_{DB} \\
F8 &= \tau_I + CM \cdot V_I + C2 \cdot V'_{UB} \\
B1 &= (F2+F8-F1-F7)/C0 \\
B2 &= (F3-F4+F6-F5)/C0
\end{aligned}
\right\} \quad (219)
$$

$$
\left.
\begin{aligned}
G1 &= 2+\rho v_p/(E\cdot\Delta t) \\
G2 &= \nu\rho v_p/(E\cdot\Delta t) \\
G3 &= \frac{1}{E\cdot\Delta t}\left[\nu(F1+F2-\sigma_{RA}-\sigma_{LA})-F3-F4+\sigma_{UB}+\sigma_{DB}\right] \\
G4 &= \frac{1}{E\cdot\Delta t}\left[\nu(F3+F4-\sigma_{UB}-\sigma_{DB})-F1-F2+\sigma_{RA}+\sigma_{LA}\right] \\
A1 &= (G2\cdot G3+G1\cdot G4)/(G2^2-G1^2) \\
A2 &= (G2\cdot G4+G1\cdot G3)/(G2^2-G1^2)
\end{aligned}
\right\} \text{(219 cont.)}
$$

The velocites perpendicular to the faces of the transfer element are:

$$V_{LP} = (A1+B1)/2 \tag{220}$$

$$V_{DP} = (A2+B2)/2 \tag{221}$$

$$V_{RP} = (B1-A1)/2 \tag{222}$$

$$V_{UP} = (B2-A2)/2 \tag{223}$$

Velocities V'_{LP}, V'_{RP}, V'_{DP}, and V'_{UP} are now obtained from Equations (197) and (198). Shearing stresses τ_{LP}, τ_{RP}, τ_{DP}, and τ_{UP} are found from Equations (210) to (213). Pressures σ_{LP}, σ_{RP}, σ_{DP}, and σ_{UP} are calculated from Equations (214) to (217) in conjunction with Equations (218).

In order to proceed to the next time step and repeat the procedure described above, the values of shearing stresses and particle velocities at points M′, N′, I′, and J′ of the x-t and z-t diagrams are needed. Shearing stress and velocity at point M′ of the x-t diagram (Figure

41) are obtained from the equations:

$$C_s^+: \quad \tau_{M'}-\tau_{RA}-\rho v_s(V_{M'}-V'_{RA}) + \frac{2\mu}{\Delta x}(V_M-V'_{RA}) = 0 \qquad (224)$$

$$C_s^-: \quad \tau_{M'}-\tau_{LP}+\rho v_s(V_{M'}-V'_{LD}) + \frac{2\mu}{\Delta x}(V'_{LD}-V_M) = 0 \qquad (225)$$

From the similar C_s^+ and C_s^- characteristics equations, shearing stress and velocity at point N′ of the x-t diagram can be found. Shear and velocity at point J′ of the z-t diagram (Fiture 42) are obtained from the equations:

$$C_s^+: \quad \tau_{J'}-\tau_{UF}-\rho v_s(V_{J'}-V'_{UF}) + \frac{2\mu}{\Delta x}(V_J-V'_{UF}) = 0 \qquad (226)$$

$$C_s^-: \quad \tau_{J'}-\tau_{DB}+\rho v_s(V_{J'}-V'_{DB}) + \frac{2\mu}{\Delta x}(V'_{DB}-V_J) = 0 \qquad (227)$$

From the similar C_s^+ and C_s^- characteristics equations shear and velocity at point I′ of the z-t diagram (Figure 42) are computed. The procedure outlined above applies to all nodal transfer elements of the latticework and then it is repeated at any subsequent time step.

Horizontal and vertical steps make up the lateral boundaries of the latticework. Boundary conditions at the edges of the latticework where no transfer elements exist (Figure 39) are handled as in the one-dimensional propagation of shear or pressure waves. Pressure and shear are zero at earth-air interfaces and the appropriate C^+ and C^- characteristics equations are used to determine the corresponding velocities.

A computer program written in FORTRAN IV Language is presented in Appendix 11. The program is quite general

applying to latticework configurations of earth dams, earth banks and valleys. The IBM 360/67 hardware was used for the execution of the program.

Case Studies

Example 1. The study of a small soil-filled valley (Figure 43) reveals the differences between the 10-Latticework and the 16-Latticework models. The valley soil material has $\rho = 4.0$ slugs/ft^3, $G = 800000$ psf, $E = 2186560$ psf and $M = 3800000$ psf since the Poisson ratio was assumed to be $\nu = 0.367$. The soil viscosity is $\mu = 2000$ lb·sec/ft^2. The entire rock boundary surrounding the valley develops a horizontal sinusoidal velocity equal to $V = 0.2 \sin 12.5\pi t$ feet per second. The latticework modeling the soil-filled valley is comprised of 24 vertical and 16 horizontal linear elements and 14 transfer elements. The time step selected is $\Delta t = 0.01$ sec. The apparent shear wave velocity is found to be 500 ft/sec and the apparent pressure wave velocity is 1000 ft/sec. The distance between transfer elements is 10 feet.

The 10-Latticework model did not compute any vertical velocities at point A on the soil surface. This results from the assumption that the nodal transfer elements of the 10-Latticework model are rigid. Therefore, transients generated by vertical motions of the underlying rock are uncoupled from those generated by horizontal motions. The 16-Latticework model incorporating the

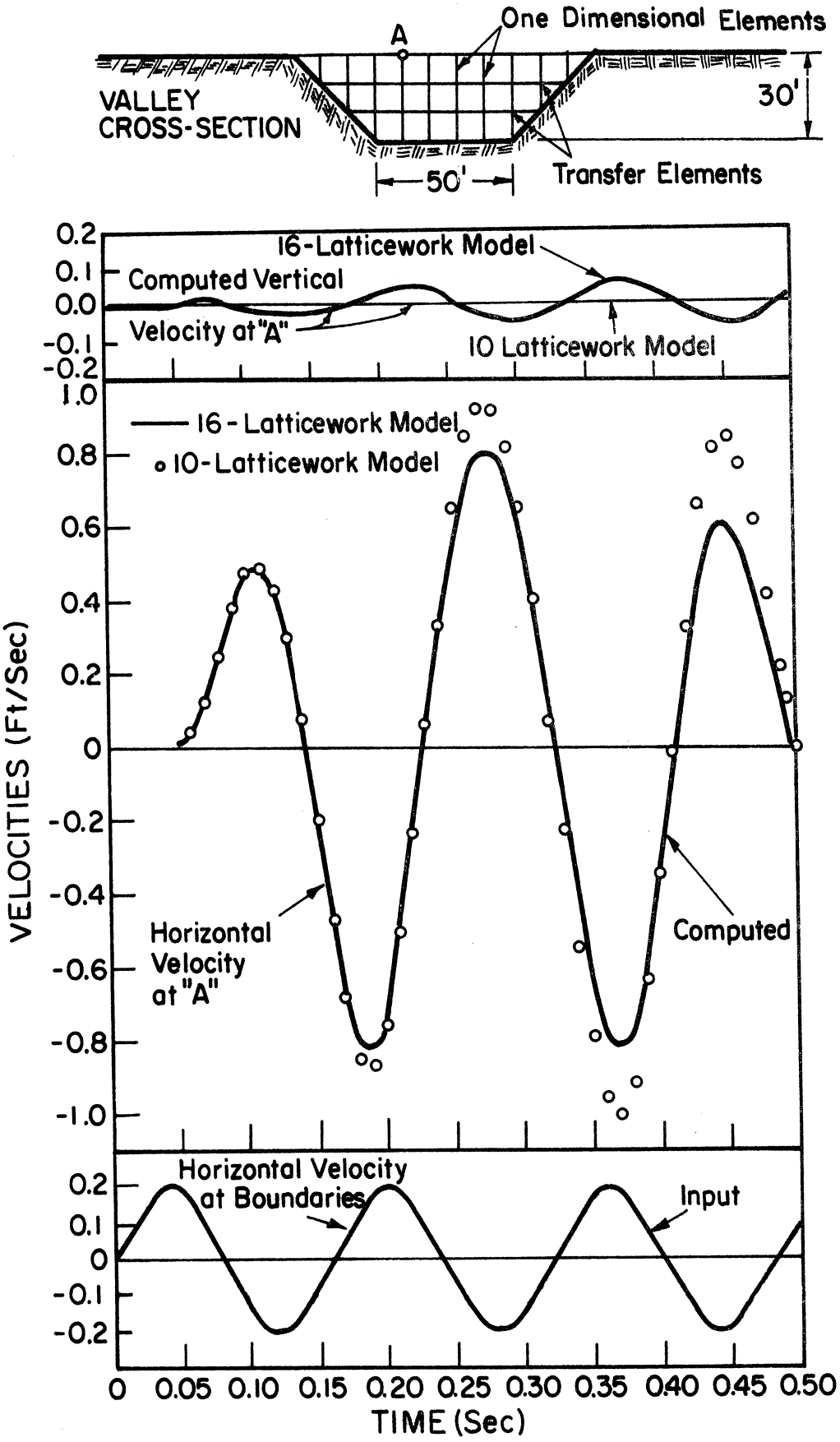

Figure 43. Horizontal and vertical velocities computed at point A by the 10- and 16-latticework models.

Poisson ratio effects, calculated a vertical response at A as shown in Figure 43. The horizontal velocities computed at A by the 16-Latticework model are smaller than the corresponding values obtained from the 10-Latticework model. The explanation is that part of the energy received in the horizontal direction by the transfer elements of the 16-Latticework model is transmitted vertically due to the Poisson ratio effect.

Example 2. The effect of the slope of the rock boundary on the response of a semi-infinite soil deposit is examined. Two semi-infinite sand layers 165 feet thick are considered having a vertical rock boundary and a 1:1 rock slope respectively. The soil properties are: mass density $\rho = 4$ slugs/ft^3; Poisson ratio $\nu = 0.25$; viscosity $\mu = 40833$ lb$\cdot$sec/ft^2; shear modulus $G = 2 \times 10^6$ psf; and modulus of elasticity $E = 5 \times 10^6$ psf. The time interval selected is $\Delta t = 0.03$ sec. The apparent shear and pressure wave velocities were found to be 916.7 ft/sec and 1356.6 ft/sec respectively. The soil deposits were modeled by latticeworks of 55 foot long linear elements (Figure 44).

The entire rock boundary was assumed to move as a rigid body. The horizontal exciting motion was the S21°W component of the Taft earthquake, 1952. The soil layers were considered to extend 9500 feet horizontally, enough to guarantee that the first 550 feet would behave as if the soil layers were actually of semi-infinite extent.

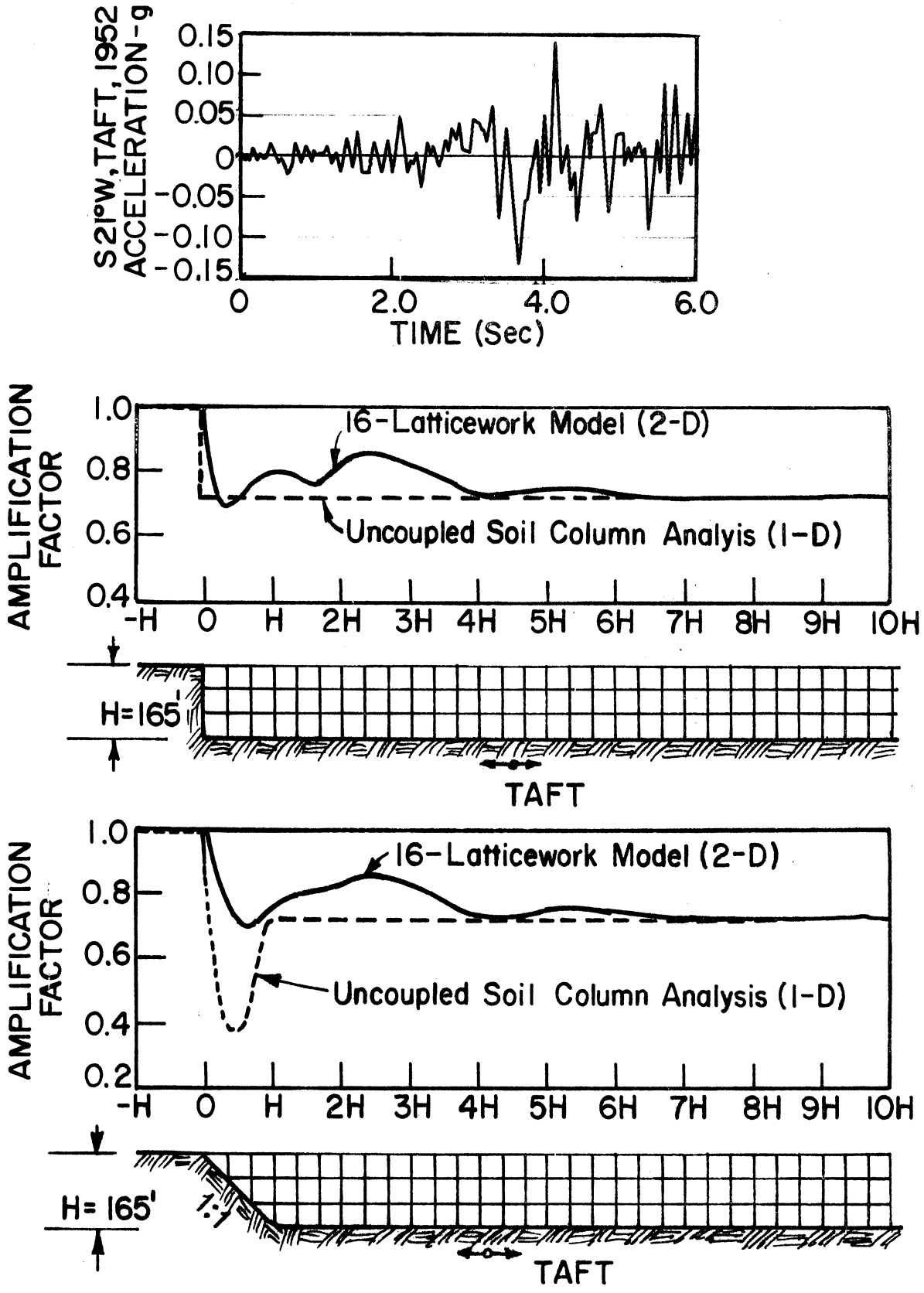

Figure 44. Influence of base slope on the response of a 165 ft thick soil deposit subjected to S21°W Taft motions.

Values of the maximum ground surface acceleration may be represented as amplification factors expressing the ratio of the maximum ground surface acceleration at any point to the maximum acceleration in the adjacent rock formation. These amplification factors were found by using the 16-Latticework model and are plotted in Figure 44 for the two layers under consideration. The results of a one-dimensional shear wave propagation analysis (shear beam, Chapter II) are also plotted for comparison. The influence of the two different slopes on the response is observed in the immediate vicinity of the slope. The influence of the slope on the accelerations obtained 350 feet beyond the toe of the slope is practically nonexistent. The amplification factors obtained from the one-dimensional and the two-dimensional analyses are in agreement for that region.

Example 3. A 300 foot high earth dam with truncated crest and side slopes 1:2 is considered resting on a horizontal base rock (Figure 45). The base rock develops the same horizontal excitation with the North-South component of the El Centro earthquake of 1940 (Figure 46). The response of the earth dam is computed by the 16-Latticework method and by the one-dimensional shear slice analysis (Chapter V). This example is rather academic since soil properties were selected in such a way as to facilitate demonstration of the comparisons between one and two-dimensional analyses.

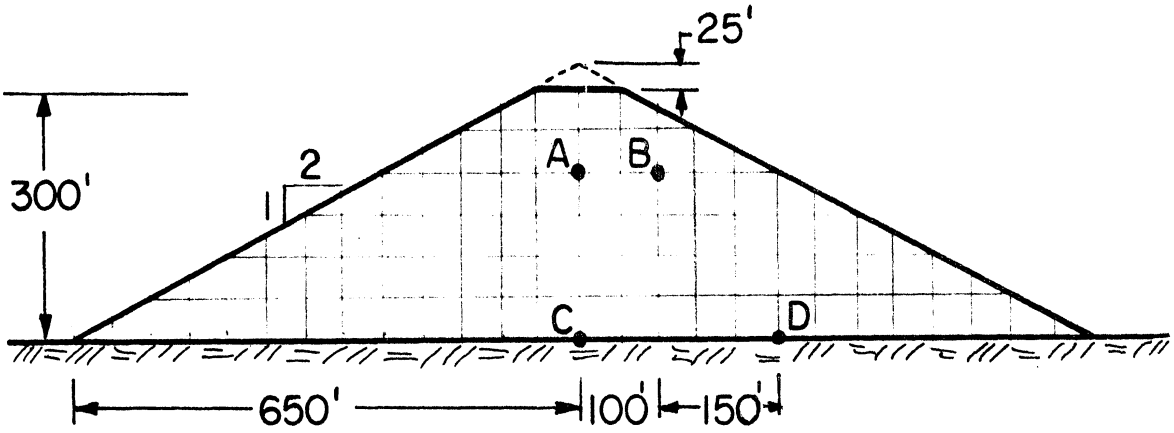

Figure 45. Rectangular latticework representation of earth dam cross section (Δx = 50 ft).

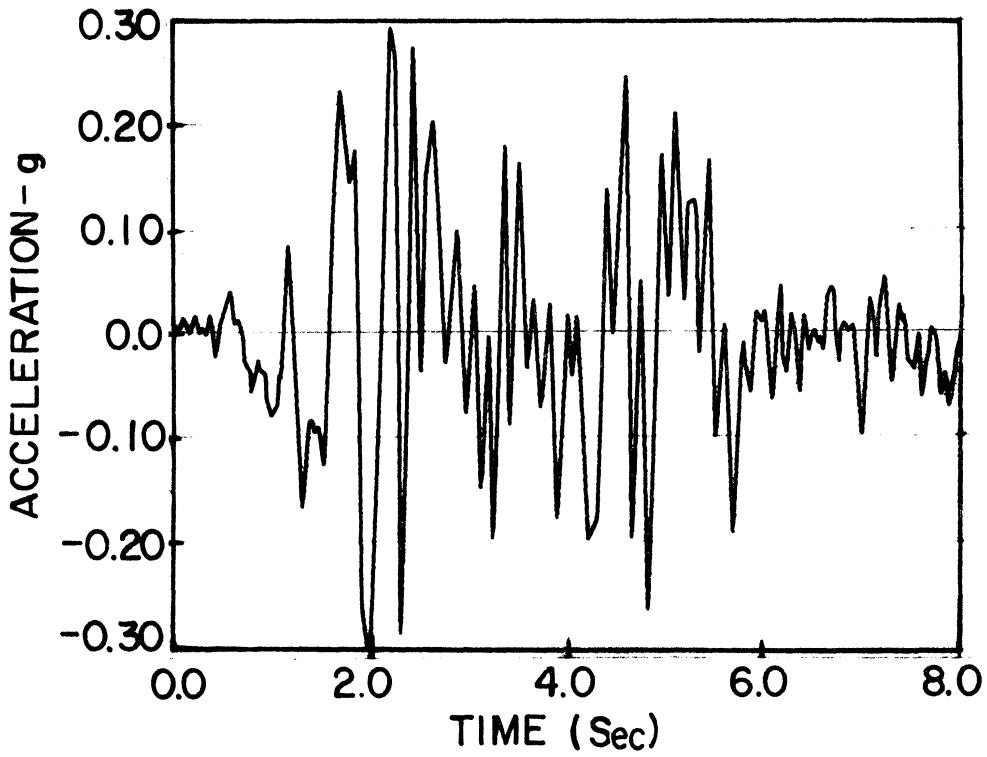

Figure 46. Base rock motion accelerogram. North-South component, El Centro earthquake, 1940.

However, the methodology associated with the Latticework model is independent of the data used with the exception of conditions (209) and (209a) required to satisfy stability criteria of the method of characteristics.

The earth dam material is assumed to be sand with the following properties: mass density ρ = 4 slugs/ft^3, viscosity μ = 15000 lb·sec/ft^2, Poisson ratio ν = 0.25, shear modulus G = 700000 psf, constrained modulus M = 2.1 x 10^6 psf and modulus of elasticity E = 1.75 x 10^6 psf. The latticework used for the two-dimensional analysis has 160 linear elements of 50 feet length and 65 transfer elements. The time increment selected is Δt = 0.05 sec. The apparent shear and pressure wave velocities were found equal to 500 ft/sec and 774.6 ft/sec respectively. For the one-dimensional analysis, the same time step was used and the dam height was partitioned into 12 reaches, each having a length of 25 feet.

Horizontal velocities and shearing stresses computed at points A and C of the dam centerline by the one-dimensional and the two-dimensional analyses are presented in Figures 47 and 48. The response pattern is very similar. However, a time delay occurs by using the latticework model. The shear wave travels through the latticework at an apparent wave speed that is less than the wave speed for a single one-dimensional element of the continuum. If the latticework did not include any transverse elements,

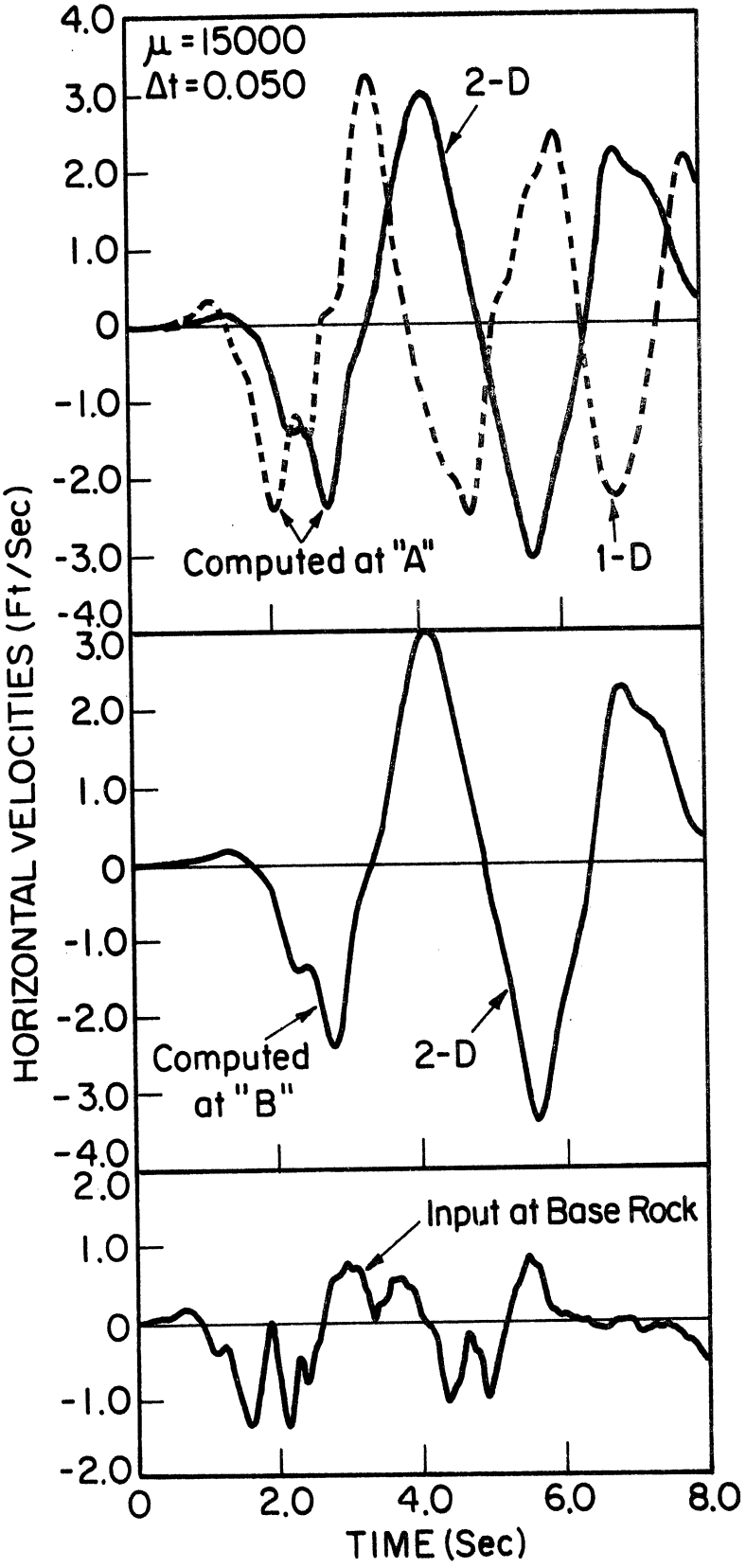

Figure 47. Particle velocities computed at points A and B by 1-D and 2-D analyses. N-S El Centro motion, 1940.

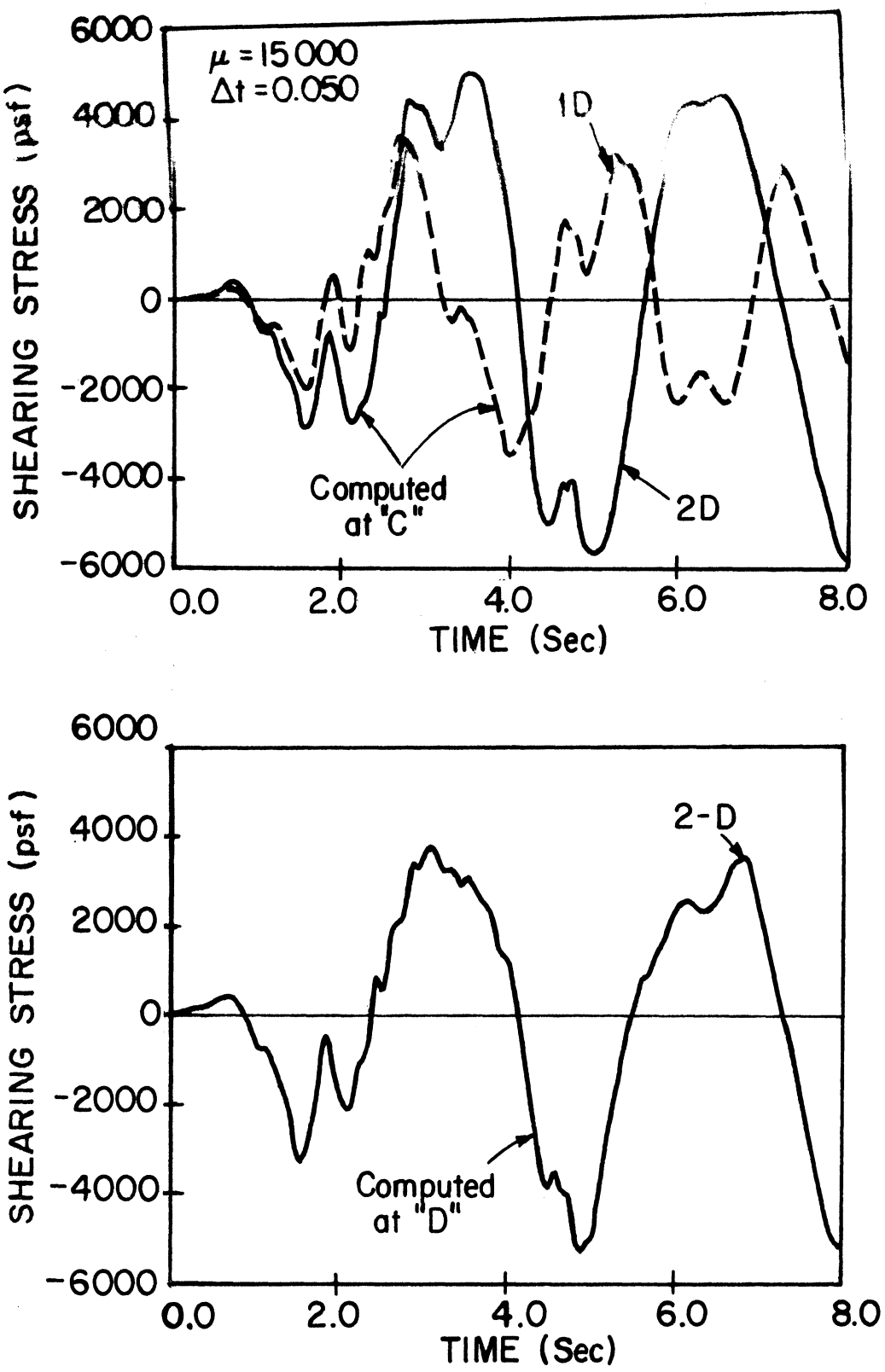

Figure 48. Dynamic shearing stresses computed at points C and D by 1-D and 2-D analyses. El Centro N-S motion. Viscosity μ = 15000 lb-sec/ft^2.

the above statement would no longer be true. The time delay is caused by the fact that a wave arriving at a node (transfer element) is transmitted as a wave of lower magnitude.

The velocities and shearing stresses computed at points B and D to the right of the dam centerline (Figure 45) by using the 16-Latticework model, are also plotted in Figures 47 and 48. As expected, the results obtained at the same elevations on the dam centerline are of higher magnitudes but similar form.

The same example was examined assuming a higher value for the soil viscosity, μ = 47000 lb·sec/ft^2. A time increment of 0.035 sec permitted the use of the same latticework. The shearing stresses at the base of the dam on its centerline (point C) computed by the one-dimensional analysis and by the two-dimensional analysis are presented in Figure 49. These results are similar and the time delay due to the latticework is again noticeable. Comparing the responses in Figures 48 and 49, it is observed that the same increase in viscosity causes a higher damping in the results obtained by the two-dimensional analysis.

The computer time for loading the object code, executing and printing the results for the above example using the 16-Latticework model (Program in Appendix 11), was approximately 65 seconds on the IBM 360/67 Computer.

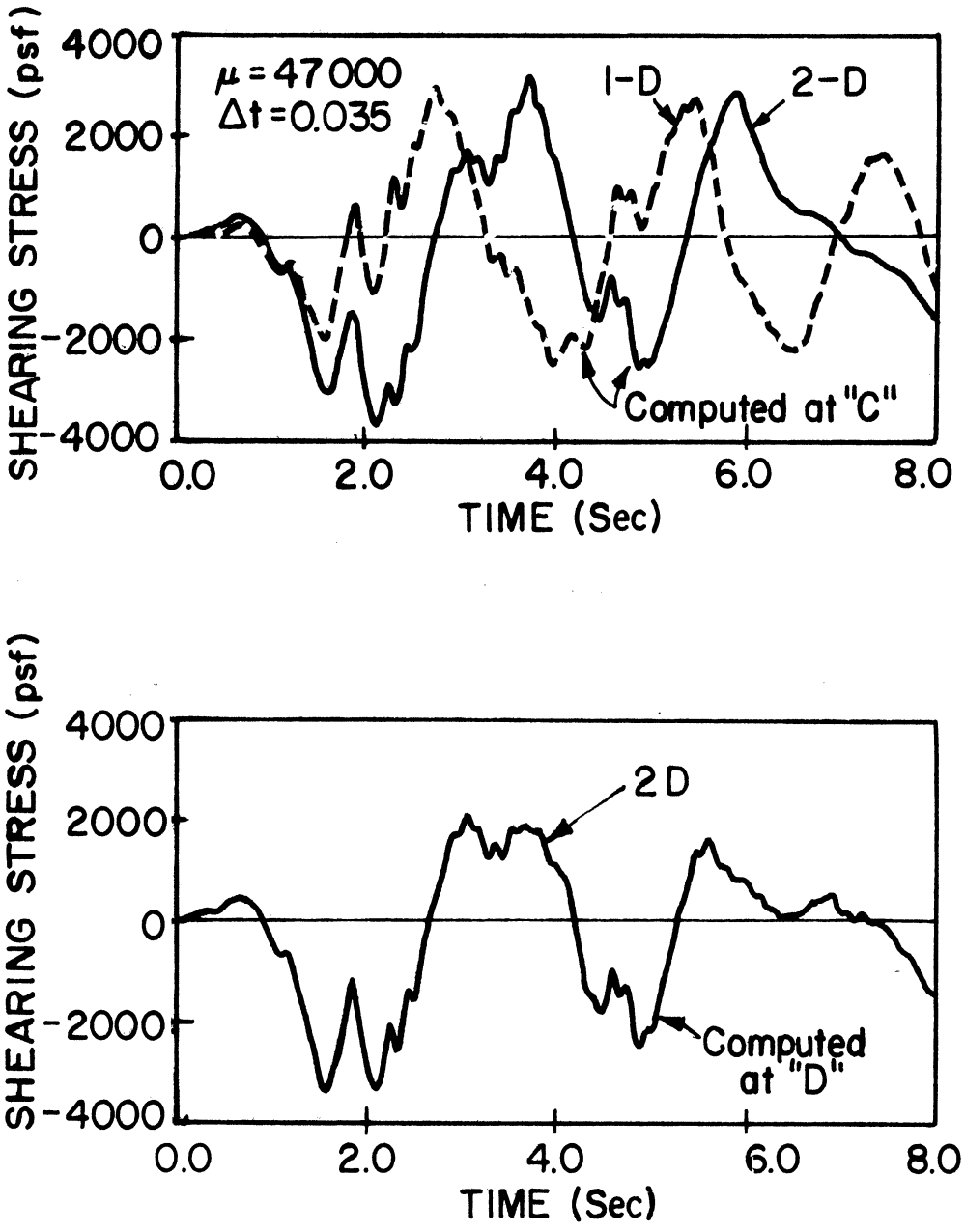

Figure 49. Dynamic shearing stresses computed at points C and D by 1-D and 2-D analyses. El Centro N-S motion. Viscosity μ = 47000 lb-sec/ft^2.

Example 4. The Caracas earthquake of July 29, 1967, although of a magnitude of 6.4, caused excessive damages to structures. Four buildings collapsed and almost all high structures suffered damage in the Palos Grandes area of east Caracas (Figure 50). Since the actual earthquake was not recorded, Seed et al. [62] proposed the use of the S21°W component of the accelerogram recorded at Taft in the Kern County (California) earthquake. This accelerogram was scaled, multiplying amplitudes by 0.166 and time by 0.9 (Figures 51 and 52). Such an accelerogram presents a maximum rock acceleration of 0.03g, and a predominant period of rock motions equal to 0.3 sec and is characteristic of a shock of magnitude 6.4 at an epicentral distance of about 35 miles.

A cross section through the Palos Grandes area (Figure 50) of the Caracas valley in the North-South direction along AA´ is shown in Figure 53. The rock underlying the valley soil deposits is assumed to move horizontally as a rigid body according to the accelerogram of Figure 51. Maximum ground surface accelerations were computed by the 16-Latticework method and compared to those obtained by the Finite Element method.

Seed et al. [62] used a shear modulus varying with the overburden pressure for the granular soils which predominate in the valley. Typical variations of shear modulus and damping ratio with shear strain were used from test data obtained in previous studies of similar materials.

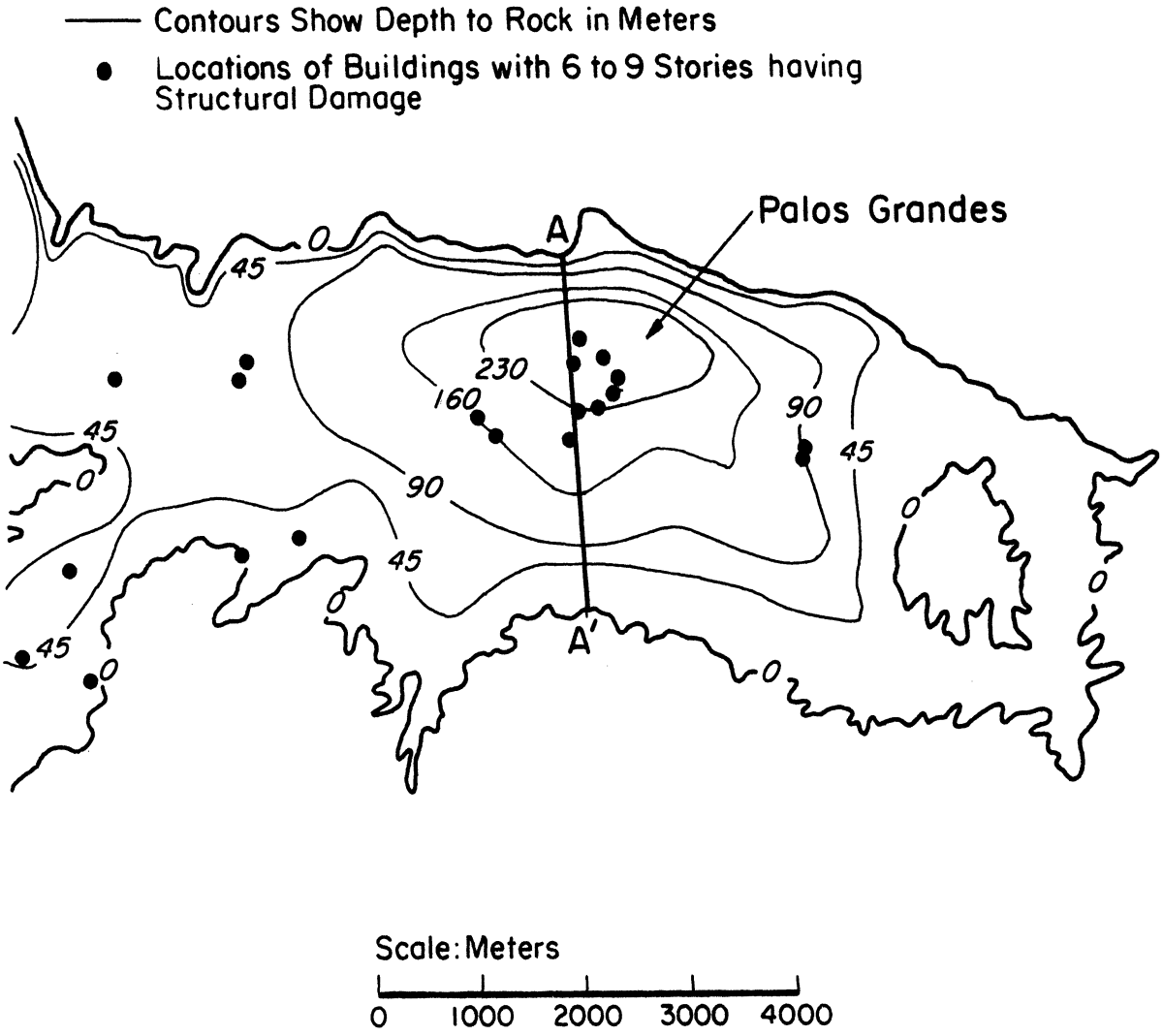

Figure 50. Topographic map of Caracas at the vicinity of Palos Grandes (Refer. 62).

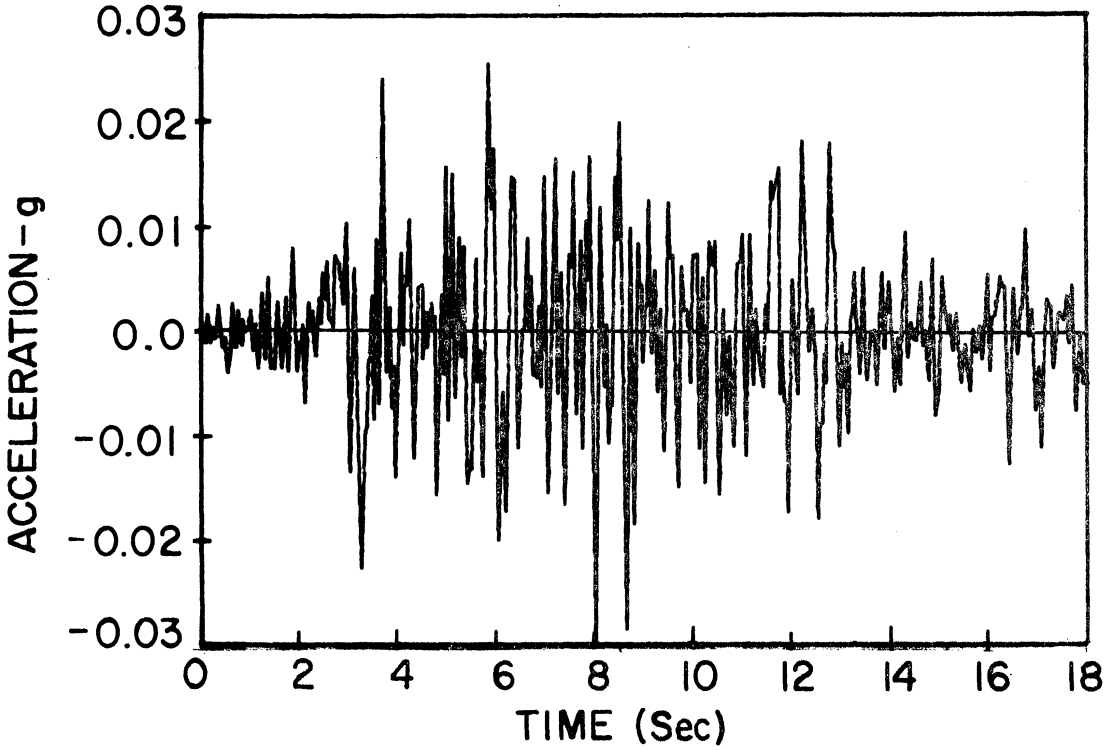

Figure 51. Estimated rock motion accelerogram for Caracas Valley in July 29, 1967 earthquake.

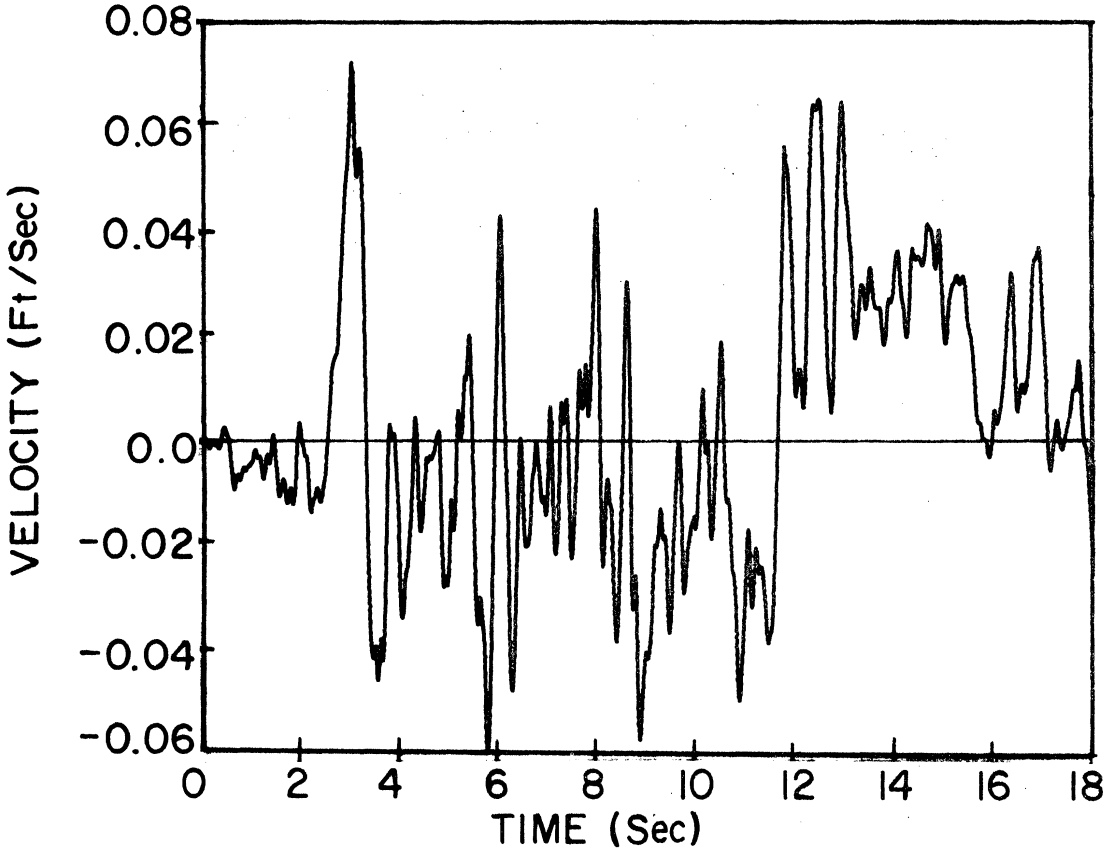

Figure 52. Rock velocity diagram for Caracas Valley in July 29, 1967 earthquake.

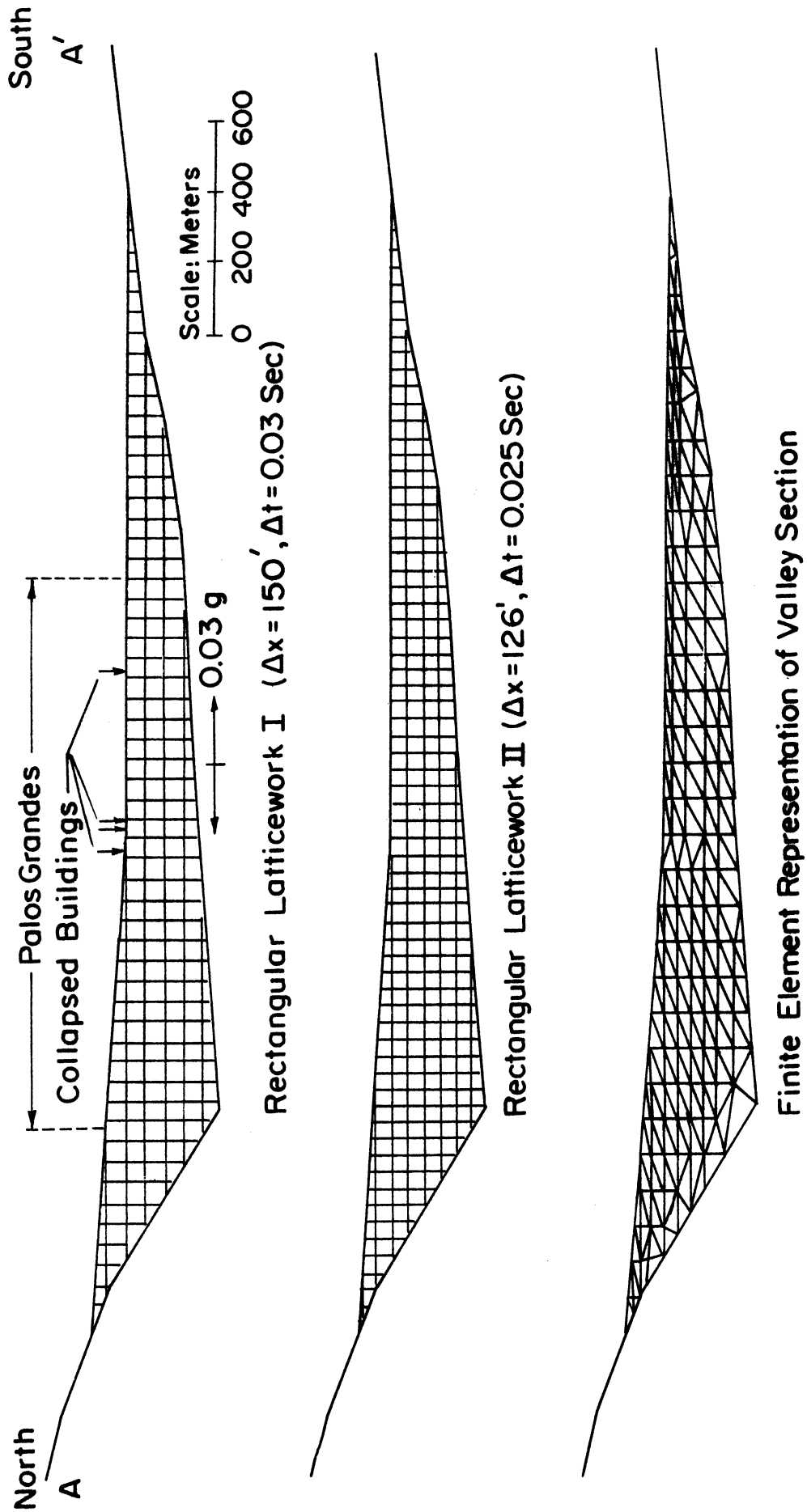

Figure 53. Rectangular latticeworks and finite element representation of cross section AA' through Palos Grandes, Caracas.

The Latticework method in its present form is applicable to problems involving constant shear modulus and viscoelastic soil behavior. This limitation neccessitated the use of average values for the Caracas valley soil properties: ρ = 4 slugs/ft^3; μ = 60000 lb·sec/ft^2; ν = 0.25; and G = 23 x 10^6 psf. A one-dimensional shear wave propagation analysis by the method of characteristics, using these average values of soil properties, resulted in approximately the same values of maximum ground surface acceleration as those obtained by Seed et al. [62] using a one-dimensional uncoupled soil column analysis (Figure 54).

Two latticeworks were used to represent the geometry of the valley section. Latticework I has 330 linear elements of length 150 feet and 133 transfer elements (Figure 53). The corresponding time increment is Δt = 0.030 sec. Latticework II has 500 linear elements of length 126 feet and 210 transfer elements (Figure 53). The corresponding time increment is Δt = 0.025 sec. Values of the maximum ground surface acceleration computed by the Latticework method are presented in Figure 54. The responses obtained by both latticeworks are in quite close agreement. The peaks of the envelope curves observed along the valley surface may be the result of focusing of reflected waves. Three of the collapsed buildings in the area are located under one of these peaks. However, definite conclusions could be made only if the acceleration time history in that location was also examined. Computer time for only

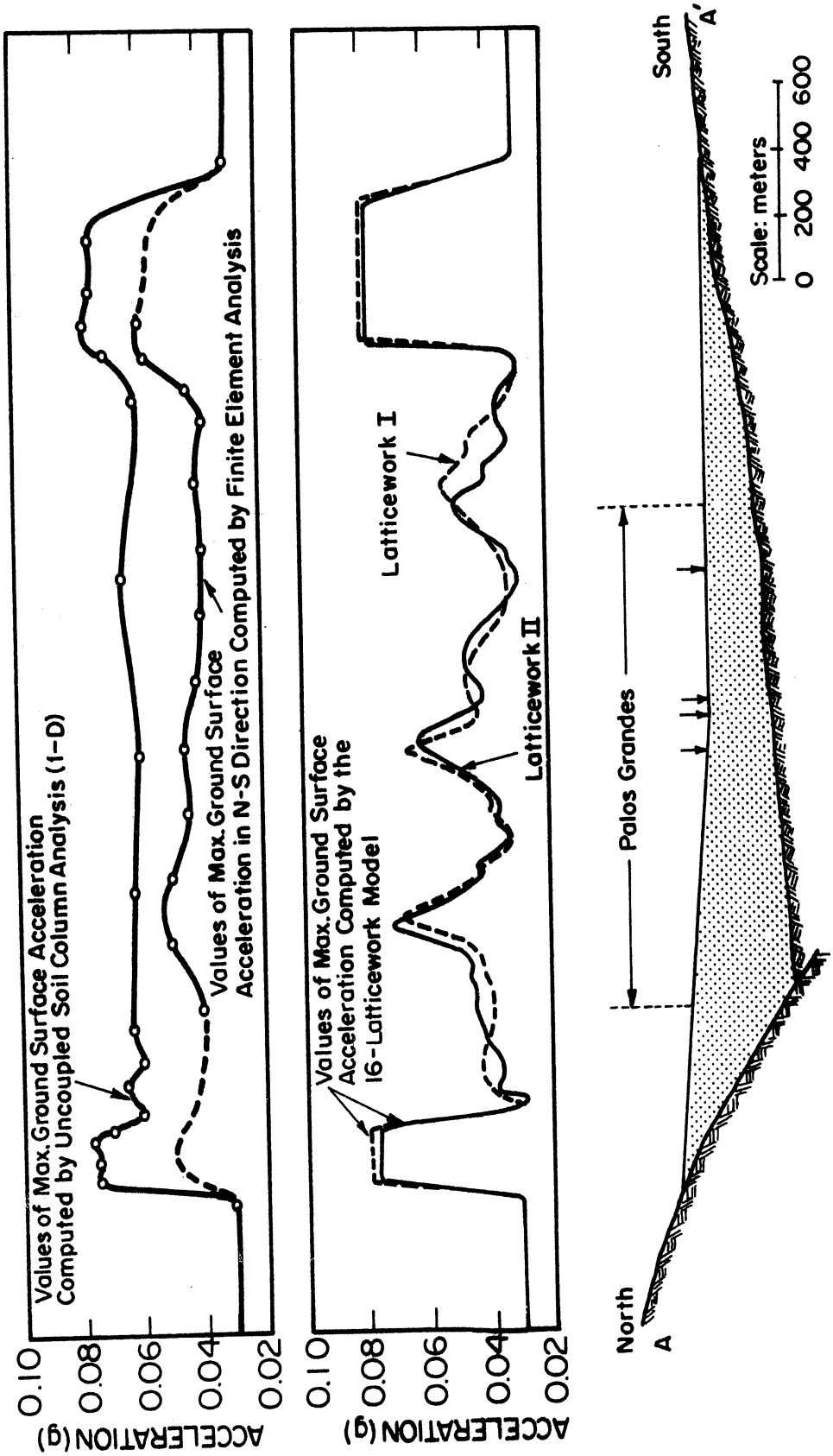

Figure 54. Comparison of computed values of maximum ground surface acceleration for section AA' through Palos Grandes, Caracas.

executing the program in the case of Latticework I was approximately 80 seconds and in the case of Latticework II was approximately 200 seconds.

Seed et al. [62] using the finite element mesh shown in Figure 53 obtained the values of the maximum ground surface acceleration plotted in Figure 54. Previous studies [18] have shown that results computed by the Finite Element method near the edges of such sections tend to be in error and estimated values are shown by the dashed lines in Figure 54. The results obtained by a one-dimensional shear wave analysis are also plotted in Figure 54 for comparison.

A standard method of assessing the adequacy of a finite element mesh is to vary systematically the mesh size and the element size[45]. The same technique was used to study the latticework adequacy. Latticeworks I and II were found to be compatible. However, results obtained by using two coarser latticeworks with $\Delta t = 0.040$ sec, $\Delta x = 198$ ft and $\Delta t = 0.050$ sec, $\Delta x = 246$ ft, differed considerably from the results obtained by using latticeworks I and II. The coarser discretized latticeworks exhibited a tendency to smooth out the envelope of maximum accelerations computed at the surface of the valley.

The results computed by using latticeworks I and II and the Finite Element method are of the same order of magnitude. However, the envelope of maximum accelerations obtained by using the Finite Element method is smoother than

the one obtained by the Latticework method. This may be partly attributed to the fact that the soil near the ground surface is considered by the Latticework method to be more rigid due to the average shear modulus used. An extention of the Latticework method to cover cases of shear modulus varying with depth is required before making any definite statements concerning its accuracy.

CHAPTER VIII

CONCLUSIONS

In the foregoing chapters the method of characteristics was applied to a variety of problems of seismic wave propagation through soil deposits. The accuracy of the method was examined and numerous examples were presented in all cases studied to demonstrate the applicability of the method and to compare solutions obtained by the characteristics method and by other methods of analysis.

The Base Motion Synthesis Method was developed by combining the method of characteristics and a centered implicit method. The Base Motion Synthesis method was shown to be applicable for computation of bedrock motions when surface motions of a viscoelastic or a "strain-softening" horizontal soil deposit were considered to be known.

The study of one-dimensional shear wave propagation through earth dams with truncated crests was carried out by using the method of characteristics. For viscoelastic material, results obtained by the characteristics method were confirmed by the shear slice theory and by an analytical method involving Hankel functions with complex arguments.

Biot's field equations, governing the propagation of pressure waves through saturated elastic soil deposits, were reduced to one-dimension and were solved by using the method of characteristics taking into account wave reflections at the boundaries of the soil formations. An

analytical solution developed for purposes of comparison was used to confirm the results obtained by the characteristics method. This development could be the basis for future extension of the studies of soil liquefaction by incorporating a Ramberg-Osgood type of stress-strain curve in the analysis to model the inelastic behavior of soils for moderate pressure ranges.

For two-dimensional shear and pressure wave propagation through viscoelastic soil material the latticework approach was used. Two-dimensional systems, i.e. earth dams, embankments, or valleys, were modeled by a latticework of one-dimensional elements and the method of characteristics was incorporated in the solution. Results obtained have indicated the applicability of this method to regional microzonation studies. Computer time economy was found to be one of the major advantages of the latticework method. This study, although of a rather preliminary nature, reveals the versatility of the method. The major disadvantage of the Latticework method is the time delay of a response resulting from the latticework used. Future investigations could incorporate the variation of shear modulus with depth by using linear interpolations for both shear and pressure waves.

Extensive application of the characteristics method to problems of earthquake generated transient disturbances traveling through soil deposits revealed that the main advantages of the method are: relative simplicity;

versatility; applicability to problems of purely transient nature; accuracy of results; and low computing cost associated with the solutions obtained.

APPENDIX 1

RAMBERG-OSGOOD HYSTERETIC MODEL

The vibration of a horizontal soil layer subjected to the horizontal motion of an earthquake is a good example of simple shear. Hardin and Drnevich [25] experimentally proved that the shearing stress-strain relationships for soils are nonlinear and that they may be represented by a hyperbola.

The hysteretic behavior of soil excited by random vibrations is most frequently represented by bilinear models [61], simplicity being their principal advantage. For dynamic studies, it is desirable to use nonlinear hysteretic stress-strain relationships which are general enough to describe yielding behavior varying between linear and elastoplastic. Structural engineers [7,41,56] have extensively studied such relationships referred to as Ramberg-Osgood models, defined by a skeleton curve equation:

$$\gamma = \frac{\tau}{G_0}\left(1 + \left|\frac{\tau}{\tau_y}\right|^{R_0-1}\right) \qquad \text{(A-1)}$$

for stresses increasing from zero, and a branch curve equation:

$$\gamma - \gamma_1 = \frac{\tau-\tau_1}{G_0}\left(1 + \left|\frac{\tau-\tau_1}{2\tau_y}\right|^{R_0-1}\right) \qquad \text{(A-2)}$$

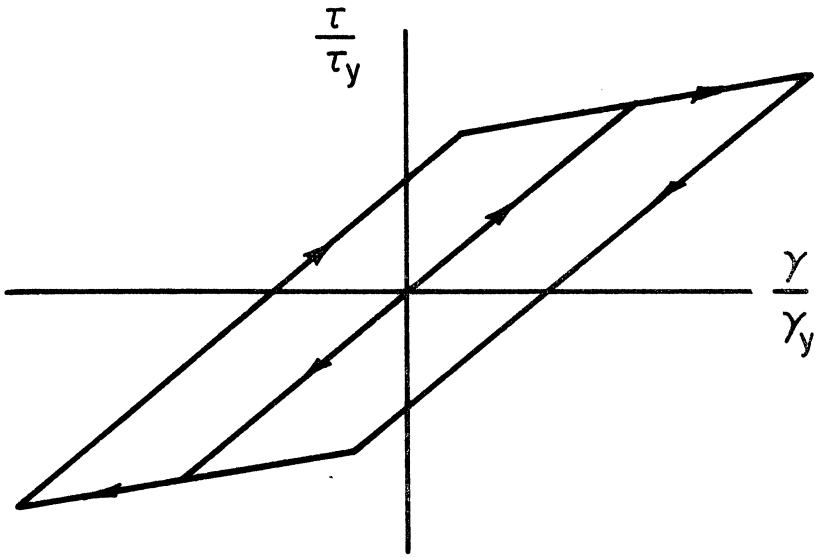

BILINEAR HYSTERETIC MODEL

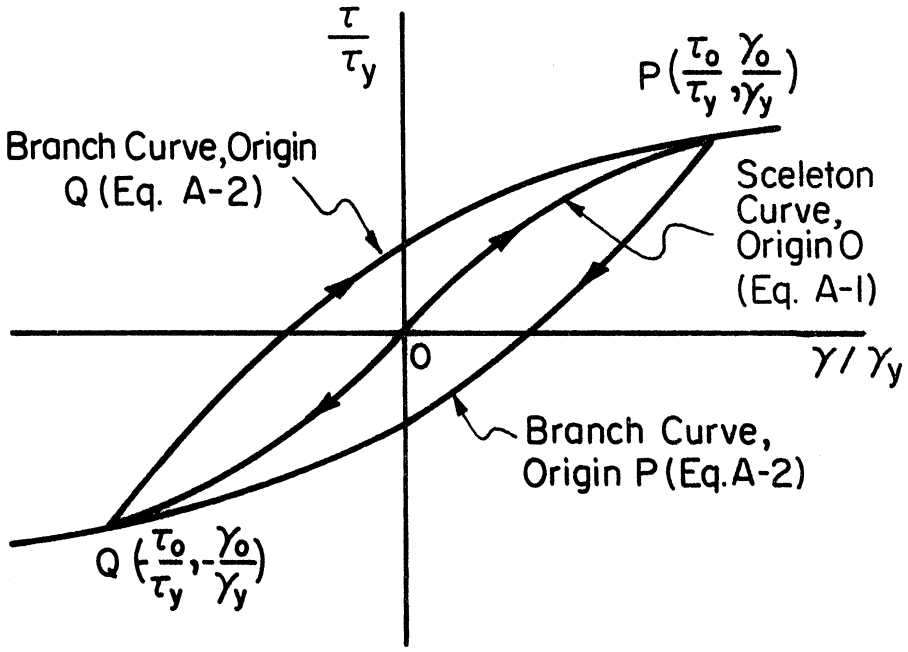

RAMBERG-OSGOOD MODEL

Figure A-1. Bilinear and Ramberg-Osgood hysteretic models.

for unloading from (τ_1, γ_1). The shearing stress is indicated by τ, γ is the shearing strain, G_0 is the shear modulus at $\gamma = 0$ and the subscript y represents values at "yield" (or reference values).

Equations (A-1) and (A-2) were used by Streeter, Wylie and Richart [71] to describe the nonlinear behavior of "strain-softening" soil layers. Constantopoulos [15] used a similar Ramberg-Osgood model without the refinement of the absolute values in equations (A-1) and (A-2) which complicates the analysis but permits the use of noninteger values of the coefficient R_0. A wide variety of physical behaviors may emanate from equations (A-1) and (A-2). For $R_0 = 1$ the linear elastic behavior of a system can be modeled. The elastoplastic case is represented by $R_0 \to \infty$.

For a cyclic loading with fixed amplitude, a unique hysteresis loop is defined. A very clear description of the hysteresis law in the case of the Ramberg-Osgood model is given by Goel [24].

APPENDIX 2

HARMONIC ANALYSIS OF TRANSIENT MOTIONS

If n equidistant displacement values u_j, j = 0,...n-1, are obtained from a digitized seismogram of ground motion, the displacement at a time t can be represented by the complex form of a finite Fourier series:

$$u(t) = \sum_{s=0}^{n-1} a_s \exp(i\omega_s t) \qquad \text{(A-3)}$$

where $\omega_s = 2\pi s/(n\Delta t)$, (s = 0,...n-1), Δt is the time step between the data points and a_s are the Fourier coefficients:

$$a_s = \frac{1}{n} \sum_{j=0}^{n-1} u_j \exp(-2\pi isj/n) \quad ; \quad s=0,....n-1 \qquad \text{(A-4)}$$

Using the Inverse Fast Fourier Transform Algorithm developed by Cooley and Tukey [16], the calculation of the Fourier coefficients is performed n/ln(n) times faster than direct computation. The use of a number of data points n equal to 2^{ℓ} where ℓ is an integer, offers important advantages for computers with binary arithmetics, both in addressing and in multiplication economy. If n is less than the closest 2^{ℓ}, the remaining 2^{ℓ}-n data locations should be filled out with zeroes to satisfy the requirement of a quiet zone after the acceleration record. The subroutine HARM of the IBM Scientific Subroutine Package [32] was used to calculate the Fourier coefficients, with the variable IFSET = -1. According to the above procedure, a transient motion represented by n equidistant values is analyzed to

n harmonics. In order to reobtain the n equidistant displacement values, the subroutine HARM can be used, this time with IFSET = 1.

The Fast Fourier Transform Algorithm was used in soil vibration problems by Schnabel, Seed and Lysmer [58] in a similar fashion to the one presented above.

The Fourier coefficients obtained from equation (A-4) are complex numbers. However, the displacement values obtained from equation (A-3) have imaginary parts zero. The Fourier analysis of the transient function u(t) is valid only at the data points originally considered. There is no guarantee that between these points values of the function u(t) will be approximated correctly by equation (A-3). This drawback can be avoided by employing a least squares criterion in conjunction with the Fourier Transform [55].

If 2N+1 equidistant displacement values are obtained from a digitized seismogram, the function u(t) can be analyzed into M harmonics ($M \leq N$) :

$$u(t) \cong \sum_{m=0}^{M} (a_m \cos\omega_m t + b_m \sin\omega_m t) \qquad \text{(A-5)}$$

where $\omega_m = 2\pi m/(2N+1)\Delta t$, $(m = 0,\ldots M)$, Δt is the time step between data points and a_m, b_m are the Fourier coefficients obtained from the least squares criterion:

$$\sum_{n=1}^{2N+1} [u(t_n) - \sum_{m=0}^{M} (a_m \cos\omega_m t_n + b_m \sin\omega_m t_n)]^2 = \min. \qquad \text{(A-6)}$$

When N = M the least squares criterion becomes equivalent to the requirement that the two members of (A-5) agree exactly at the 2N+1 points considered. The coefficients a_j and b_j (j = 0, 1,...M) of the Fourier series which approximates the given displacement function, are obtained by using the subroutine FORIT of the IBM Scientific Subroutine Package [32].

Equation (A-5) for the purposes of the present analysis may be written as:

$$u(t) \cong \text{Re} \left\{ \sum_{m=0}^{M} a_m' \exp(i\omega_m t) \right\} \tag{A-7}$$

where Re stands for "real part of" and:

$$a_m' = \sqrt{a_m^2 + b_m^2} \exp(-i\phi_m) \tag{A-8}$$

with

$$\phi_m = \tan^{-1}(b_m/a_m) \tag{A-9}$$

Equations (A-3) and (A-7) are analogous, the only difference being the number of harmonics used. However, equation (A-7) approximates closely the values of the function u(t) between the tabulated data points if a sufficient number of harmonics is employed. In case of earthquake motions, this technique is more expensive in computer time.

APPENDIX 3

BESSEL FUNCTIONS WITH COMPLEX ARGUMENTS

Bessel functions of the first kind, of order q equal to zero or one, from definition are:

$$J_q[\rho\exp(i\phi)] = \sum_{K=0}^{\infty} \frac{(-1)^K(\rho/2)^{2K+q}\exp[(2K+q)i\phi]}{K!\ (K+q)!} \qquad \text{(A-10)}$$

In complex form Bessel functions of the first kind are written as:

$$J_q[\rho\exp(i\phi)] = u_q(\rho,\phi) + iv_q(\rho,\phi) \qquad \text{(A-11)}$$

where $$u_q(\rho,\phi) = \sum_{K=0}^{\infty} \frac{(-1)^K(\rho/2)^{2K+q}}{K!(K+q)!}\cos(2K+q)\phi \qquad \text{(A-12)}$$

$$v_q(\rho,\phi) = \sum_{K=0}^{\infty} \frac{(-1)^K(\rho/2)^{2K+q}}{K!(K+q)!}\sin(2K+q)\phi \qquad \text{(A-13)}$$

When 26 terms of the above series are considered, the truncating error induced by omitting the rest of the terms and by working in single precision was found to be of the order of 10^{-4}.

Equation (A-11) holds for the first quadrant of the complex plane. For the fourth quadrant:

$$J_q[\rho\exp(-i\phi)] = u_q(\rho,\phi) - iv_q(\rho,\phi) \qquad \text{(A-14)}$$

Bessel functions of the second kind, of order zero or one may be written as:

$$Y_q[\rho\exp(i\phi)] = U_q(\rho,\phi) + iV_q(\rho,\phi) \qquad \text{(A-15)}$$

where

$$U_0(\rho,\phi) = \frac{2}{\pi}\left[u_0(\rho,\phi)\left(\gamma+\ln\frac{\rho}{2}\right) - \phi v_0(\rho,\phi) + S(\rho,\phi)\right] \quad \text{(A-16)}$$

$$V_0(\rho,\phi) = \frac{2}{\pi}\left[v_0(\rho,\phi)\left(\gamma+\ln\frac{\rho}{2}\right) + \phi u_0(\rho,\phi) + T(\rho,\phi)\right] \quad \text{(A-17)}$$

γ_E = Euler's constant = 0.5772156649 ...

$$S(\rho,\phi) = \sum_{K=1}^{\infty} \frac{(-1)^{K+1}(\rho/2)^{2K}}{K!\ K!}\left(1+\frac{1}{2}+\ldots+\frac{1}{K}\right)\cos 2K\phi \quad \text{(A-18)}$$

$$T(\rho,\phi) = \sum_{K=1}^{\infty} \frac{(-1)^{K+1}(\rho/2)^{2K}}{K!\ K!}\left(1+\frac{1}{2}+\ldots+\frac{1}{K}\right)\sin 2K\phi \quad \text{(A-19)}$$

Bessel functions of the second kind, of order one can be found from the "cross-relation" between Bessel functions of both kinds [47]:

$$J_0(z)Y_1(z) - J_1(z)Y_0(z) = -\frac{2}{\pi z} \quad \text{(A-20)}$$

where z is complex. This leads to the following relations between real and imaginary parts of the Bessel functions:

$$u_0U_1 - v_0V_1 = u_1U_0 - v_1V_0 - 2\cos\phi/\pi\rho \quad \text{(A-21)}$$

$$v_0U_1 + u_0V_1 = u_1V_0 + v_1U_0 + 2\sin\phi/\pi\rho \quad \text{(A-22)}$$

From Equations (A-21) and (A-22), V_1 and U_1 are obtained in order to calculate $Y_1[\rho\exp(i\phi)]$.

Equation (A-15) holds for the first quadrant of the complex plane. For the fourth quadrant:

$$Y_q[\rho\exp(-i\phi)] = U_q(\rho,\phi) - iV_q(\rho,\phi) \quad \text{(A-23)}$$

The use of existing tables [49,50] to evaluate Bessel functions of the first or second kind and of order zero or one, for any complex argument, was found to be excessively time consuming because of the necessity of double interpolations in the values of ρ and ϕ. Therefore, subroutine BES, included in Appendix 7, was written to calculate any Bessel function of the first or second kind and of order zero or one with complex argument. Single precision proved to give satisfactory results.

APPENDIX 4

DERIVATION OF BIOT'S EQUATIONS OF EQUILIBRIUM IN EULERIAN COORDINATES

The Lagrangian viewpoint and the concept of generalized coordinates were used by Biot [9] to derive the equations of equilibrium (116) and (117) which govern the vertical propagation of waves through a saturated elastic porous medium when dissipation is present. Biot used Lagrange's equation after expressing the kinetic energy of the system per unit volume in terms of the generalized coordinates.

An Eulerian analysis is used in the following to derive Biot's equations of equilibrium with the additional consideration of the gravity forces acting on the system. A non-deformable control volume fixed in space is employed. Fluid and solid particles move through the fixed control volume with velocities U and V respectively. The fluid particle velocity U is actually the seepage velocity. The corresponding superficial velocity is nU where n is the porosity. The fixed control volume has a cross-sectional area A_0 and height Δz. Assuming that the relative flow of fluid with respect to the solid skeleton is laminar, the equation of motion for the fluid constituent (Figure A-2) may be written as:

$$A_0\Delta z\rho_L n\frac{\partial U}{\partial t} - A_0\Delta z\rho_a\left(\frac{\partial V}{\partial t} - \frac{\partial U}{\partial t}\right) =$$

$$-A_0\Delta z\frac{\partial (np)}{\partial z} + A_0\Delta zn\rho_L g - A_0\Delta z\frac{n^2\rho_L g(U-V)}{k} \qquad \text{(A-24)}$$

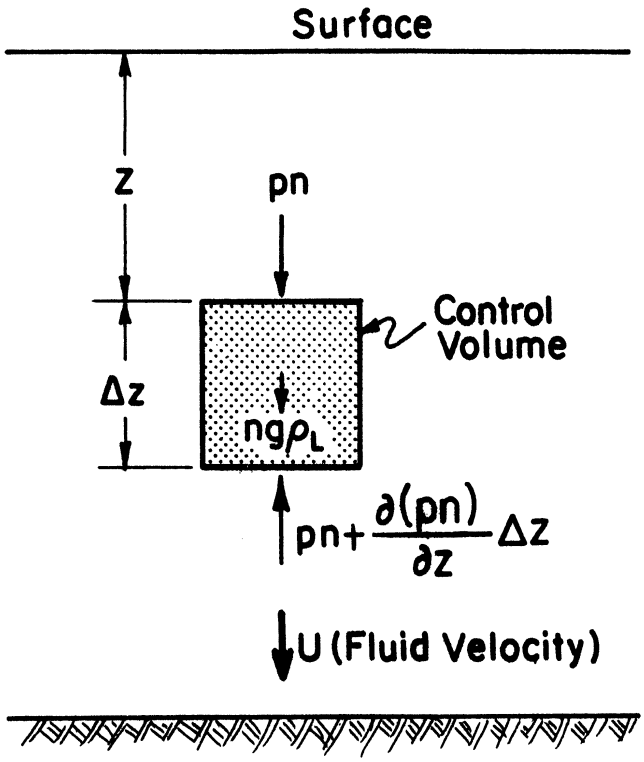

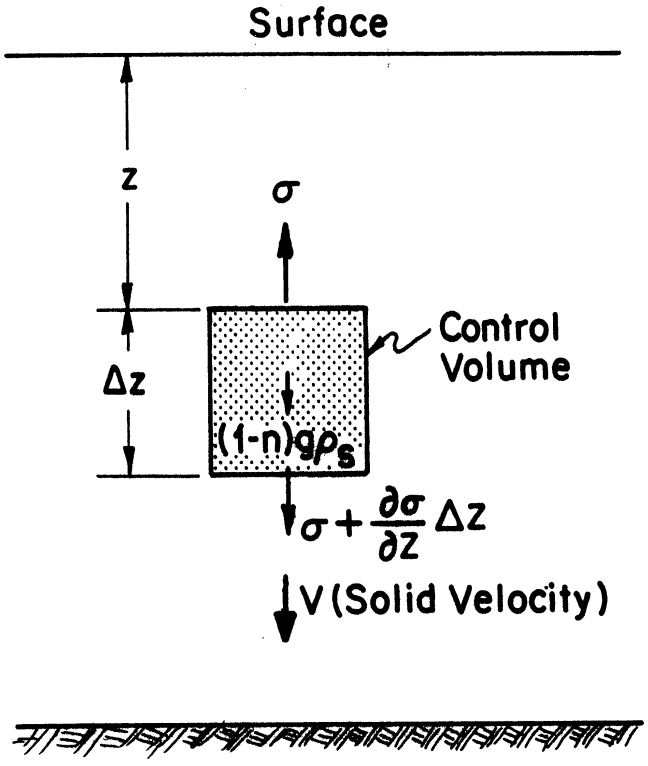

Figure A-2. Flow of fluid and solid constituents of a saturated porous medium through a fixed control volume.

where ρ_L = mass density of fluid; ρ_a = apparent mass density; p = porewater pressure; k = coefficient of permeability; and g = acceleration of gravity. Small terms, such as $V\partial V/\partial t$ and $U\partial U/\partial t$, have been omitted from Equation (A-24).

The second term of the left hand side of Equation (A-24) represents the apparent mass effect. By considering that the solid part of the porous medium is accelerating relative to the liquid part, the force pushing the solid part has to perform work to increase the kinetic energy not only of the solid but also of the fluid.

The second term of the right hand side of Equation (A-24) represents the force due to gravity. The last term of Equation (A-24) represent a viscous force resisting the flow. If $\partial U/\partial t$ and $\partial V/\partial t$ are set to zero and the gravity force is omitted, Equation (A-24) degenerates to:

$$n(U-V) = -k \frac{1}{\rho_L g} \frac{\partial p}{\partial z} \qquad \text{(A-25)}$$

which is Darcy's equation. Therefore, Darcy's friction is the dissipative mechanism represented by the last term of Equation (A-24).

Division of Equation (A-24) by the volume of the fixed control volume, yields:

$$(n\rho_L+\rho_a) \frac{\partial U}{\partial t} - \rho_a \frac{\partial V}{\partial t} = - \frac{\partial (np)}{\partial z} + n\rho_L g + \frac{n^2 \rho_L g}{k} (V-U) \qquad \text{(A-26)}$$

where p = - s/n = porewater pressure and s = stress on the fluid part per unit area, negative when pressure. The

coefficient of permeability k is connected with the intrinsic permeability K through the relation:

$$k = K \frac{\rho_L g}{\mu_L} \tag{A-27}$$

By expressing the velocities of the liquid and solid constituents in terms of the corresponding displacements, i.e, $U = \partial\bar{w}/\partial t$ and $V = \partial w/\partial t$, and by substituting Equations (119), (120), (121) and (A-27) into Equation (A-26), the latter becomes:

$$\frac{\partial^2}{\partial t^2}(\rho_{12}w+\rho_{22}\bar{w}) - (\rho_{12}+\rho_{22})g - b\frac{\partial}{\partial t}(w-\bar{w}) = \frac{\partial s}{\partial z} \tag{A-28}$$

The equation of motion of the fluid as derived above (Eq. A-28) contains the effect of gravity. Therefore, static stresses should be considered as initial conditions. If however a purely dynamic solution is sufficient, the second term of Equation (A-28) should be omitted and initial conditions should be zero throughout the saturated soil deposit. In this case, Equation (A-28) becomes identical with Biot's dynamic equation of equilibrium in the z-direction for the fluid constituent (Equation 117).

The equation of motion for the solid constituent moving vertically through the fixed control volume (Figure A-2) may be written as:

$$A_0\Delta z\rho_S(1-n)\frac{\partial V}{\partial t} + A_0\Delta z\rho_a(\frac{\partial V}{\partial t} - \frac{\partial U}{\partial t}) =$$

$$A_0\Delta z\frac{\partial \sigma}{\partial z} + A_0\Delta z(1-n)\rho_S g + A_0\Delta z\frac{n^2\rho_L g(U-V)}{k} \tag{A-29}$$

where ρ_S = mass density of solid; and σ = stress on the solid part of a unit area, positive when tension. The forces due to the apparent mass and due to Darcy's friction expressed by the second and fifth terms of Equation (A-29) are the same in magnitude with the corresponding forces in Equation (A-24) but with opposite signs owing to the law of action and reaction. The last term of Equation (A-29) may be visualized as a kind of drag force excerted on the soil skeleton due to the fluid flowing through the pores. Division of Equation (A-29) by the volume of the fixed control volume, yields:

$$[(1-n)\rho_S+\rho_a]\frac{\partial V}{\partial t} - \rho_a \frac{\partial U}{\partial t} = \frac{\partial \sigma}{\partial z} + (1-n)\rho_S g - \frac{n^2 \rho_L g}{k}(V-U) \qquad \text{(A-30)}$$

By expressing the velocities of the fluid and solid constituents in terms of the corresponding displacements and by substituting Equations (118), (120), (121) and (A-27) into Equation (A-30), the latter may be written as:

$$\frac{\partial^2}{\partial t^2}(\rho_{11}w+\rho_{12}\bar{w}) - (\rho_{11}+\rho_{12})g + b\frac{\partial}{\partial t}(w-\bar{w}) = \frac{\partial \sigma}{\partial z} \qquad \text{(A-31)}$$

Equation (A-31) becomes identical with Biot's dynamic equation of equilibrium in the z-direction for the solid constituent (Equation 116) by omitting the second term which expresses the effect of gravity.

Note: In the preceding development the porous material was assumed to be statistically isotropic. Therefore, all cross-sections have the same ratio n of fluid area to total area since the volume of fluid in a thin slab is always a fraction n of the total volume (n = porosity).

APPENDIX 5

```
C     ************************************************
C     METHOD OF CHARACTERISTICS+VALVE STROKING CONCEPT
C     FIND BEDROCK MOTION FROM A KNOWN SURFACE MOTION
C     SEMI-INFINITE SOIL LAYER. UNITS IN PSF,FT,SEC.
C     SOIL LINEARLY VISCOELASTIC.
C     IF IND=1 EARTHQUAKE MOTION.IF IND=2 STEADY OSCIL.MOTION.
C     IF IND=1 READ EQUIDISTANT VELOCITY VALUES FROM DEVICE 7
C     IF IWR=2 PRINTOUT REDUCED.
C     X=0 IS AT SURFACE.
C     ************************************************
      REAL L,MIU,MIUD
      DIMENSION TAU(20,200),V(20,200),G(20),VS(20),X(20),MIU(20),
     1L(20),RO(20),MIUD(20),GO(20),ROD(20),U(200),VPL(200),TPL(200),
     2T(200)
      NAMELIST/DIN/NL,L,GO,MIUD,DT,ROD,TMAX,TOTL,A,OM,IND,IEND,IWR
   10 READ(5,DIN,END=99)
      WRITE(6,DIN)
      X(1)=0.0
      U(1)=0.0
      N=0
      NN=0
C     SHEAR MODULUS CONSTANT FOR EACH REACH
      DO 300 J=1,NL
      GG=GO(J)/144.
      VVS=SQRT((GO(J)+MIUD(J)/DT)/ROD(J))
      DX=VVS*DT
      K=1+NN
      N=L(J)/DX+1
      DIF=L(J)-DX*N
      IF(ABS(DIF).GT.(0.95*DX))N=N-1
      NN=NN+N
      DL=L(J)-N*DX
      DO 102 I=K,NN
      G(I)=GG
      MIU(I)=MIUD(J)
      RO(I)=ROD(J)
      VS(I)=VVS
      JJ=I+1
  102 X(JJ)=X(I)+DX
      IF((J+1).GT.NL)GO TO 300
      L(J+1)=L(J+1)+DL
  300 CONTINUE
      N1=JJ
      N=N1-1
      WRITE(6,13)(X(I),I=1,N1)
   13 FORMAT(8X,'X=',(15F8.2))
      WRITE(6,14)(VS(I),I=1,N)
   14 FORMAT(7X,'VS=',4X,(14F8.2))
      WRITE(6,16)(G(I),I=1,N)
   16 FORMAT(3X,'G(PSI)=',4X,(14F8.0))
      IF(IEND.EQ.1)STOP
      DO 12 I=1,N1
      TAU(I,1)=0.0
   12 V(I,1)=0.0
      JLIM=TMAX/DT
      JM=JLIM+N
      DO 212 J=1,N
      TAU(1,J)=0.0
  212 V(1,J)=0.0
      DO 213 J=N1,JM
```

```
  213 TAU(1,J)=0.0
      IF(IND.EQ.1)READ(7,20)(V(1,J),J=N1,JM)
   20 FORMAT(7(F10.5))
      IF(IND.EQ.1)GO TO 50
      DO 214 J=N1,JM
      TT=(J-N1)*DT
  214 V(1,J)=A*SIN(OM*TT)
   50 K=JM-1
      DO 100 I=2,N1
      DO 120 J=2,K
      C1=RO(I-1)*VS(I-1)
      C2=MIU(I-1)/(X(I)-X(I-1))
      CP=TAU(I-1,J-1)-(C1-C2)*V(I-1,J-1)-C2*V(I,J-1)
      CM=TAU(I-1,J+1)+C1*V(I-1,J+1)-C2*V(I-1,J)
      V(I,J)=(CP-CM)/(C2-2.*C1)
      IF(I.EQ.N1)U(J)=U(J-1)+0.5*(V(I,J)+V(I,J-1))*DT
  120 TAU(I,J)=CP+C1*V(I,J)
      K=K-1
  100 CONTINUE
      DO 70 J=1,JLIM
   70 T(J)=(J-1)*DT
      IF(IWR.EQ.2)GO TO 55
      DO 72 J=1,JLIM
      WRITE(6,2)T(J),(V(I,J),I=1,N1),U(J)
    2 FORMAT(' T=',F5.2,'V=',(12F9.3),'U=',F8.3)
      WRITE(6,3)(TAU(I,J),I=1,N1)
    3 FORMAT(6X,'TAU=',(13F9.2))
   72 CONTINUE
   55 DO 60 J=1,JLIM
      VPL(J)=V(N1,J)
   60 TPL(J)=TAU(N1,J)
      CALL PLOT(T,VPL,JLIM,XMIN,YMIN,DX,DY)
      CALL PLOT(T,TPL,JLIM,XMIN,YMIN,DX,DY)
      CALL PLOT(T,U,JLIM,XMIN,YMIN,DX,DY)
      GO TO 10
   99 STOP
      END
C     ***************************************************
      SUBROUTINE PLOT(X,Y,K,XMIN,YMIN,DX,DY)
      DIMENSION X(800),Y(800)
      CALL PSCALE(8.,1.,XMIN,DX,X(1),K,1)
      CALL PSCALE(6.,1.,YMIN,DY,Y(1),K,1)
      CALL PLTOFS(XMIN,DX,YMIN,DY,2.,2.)
      CALL PAXIS(2.,2.,14HX ( TIME,SEC ),-14,8.,0.,XMIN,DX,1.)
      CALL PAXIS(2.,2.,14HY (           ),14,6.,90.,YMIN,DY,1.)
      CALL PLINE(X(1),Y(1),K,1,0,0,1)
      CALL PLTEND
      RETURN
      END
```

APPENDIX 6

```
C     ************************************************
C     METHOD OF CHARACTERISTICS+IMPLICIT METHOD. VALVE STROKING CONCEPT.
C     RAMBERG-OSGOOD STRESS-STRAIN NONLINEAR BEHAVIOUR.
C     VISCOELASTIC DISSIPATION NOT INCLUDED.
C     VELOCITY KNOWN AT SURFACE-FIND BEDROCK MOTION.
C     ************************************************
      COMMON R(12),TY(12),GO(12),IVC(12),G(12),L
      DIMENSION V(12,300),VV(12,300),TA(12,300),TT(12,300),X(12),
     1RO(12),U(12,300),YYY(300),XXX(300),T(300),VPL(300),DT(12),
     2GKIP(300),TKIP(300)
      NAMELIST/DIN/DT,F,R,RO,GO,TMAX,III,N,K,ISTOP,IST,NIT,ICUR,MM
     1/DV/VPL
      DATA TA/3600*0.0/
   10 READ(5,DIN,END=99)
      READ(5,DV)
      WRITE(6,DIN)
      U(1,1)=0.0
      V(1,1)=0.0
      DO 20 I=2,K
      V(1,I)=VPL(I)
      U(1,I)=U(1,I-1)+0.5*(V(1,I)+V(1,I-1))*DT
   20 T(I)=T(I-1)+DT
      P=2.*F
      CC=2.*DT
      CA=P*DT*CC
      CB=CA*P/2.
      D=1.-F
      K1=K
      N1=N+1
      V(N1,1)=0.0
      KK=K-N1
      KL=K-III-1
      NK=KL-IST
      T(1)=0.0
      X(1)=0.0
      DO 16 I=2,N1
   16 X(I)=X(I-1)+DT*SQRT(GO(I-1)/RO(I-1))
      WRITE(6,32)(X(I),I=1,N1)
      DO 100 I=2,N1
      IF(I.EQ.ISTOP)GO TO 99
      K=K-1
      L=I-1
      DX=X(I)-X(L)
      C=RO(L)*SQRT(GO(L)/RO(L))
      TY(L)=0.4616*RO(L)*32.2*(X(I)+X(L))/2.
      DT(L)=0.0
      G(L)=GO(L)
      IVC(L)=1
      JST=N1+2-I
      V(L,JST-1)=0.0
      V(L,JST)=0.0
      CP=TA(L,JST-1)-C*V(L,JST-1)
      CM=TA(L,JST+1)+C*V(L,JST+1)
      TA(I,JST)=(CM+CP)/2.
      V(I,JST)=(TA(I,JST)-CP)/C
      TTT=0.5*(TA(I,JST)+TA(L,JST))
      CALL GG(TTT,DT(L))
      DT(L)=TTT
      JSTART=JST+1
      U(I,JST)=0.0
```

```
      YYY(JST)=0.0
      XXX(JST)=0.0
      JIND=ICUR
      IF(I.GE.4)JIND=ICUR-40
      M=JST
      WRITE(6,38)M,T(M),V(I,M),TA(I,M),U(I,M),TTT,GO(L),XXX(M),YYY(M)
      DO 200 NJ=JSTART,K
      J=NJ
      JJS=1
      GOO=G(L)
      INDEX=1
      LJ=J-1
   51 CI=SQRT(G(L)/RO(L))
      C=CI*RO(L)
      CP=TA(L,LJ)-C*V(L,LJ)
      CM=TA(L,J+1)+C*V(L,J+1)
      TT(L,J)=(CM+CP)/2.
      VV(L,J)=(TT(L,J)-CP)/C
      IF(JJS.EQ.2)GO TO 59
      DX1=DT*CI
      S=DX-DX1
      IF(S.LT.0.1)GO TO 59
      A1=(V(I,LJ)-V(L,LJ))/DX
      A2=(TA(I,LJ)-TA(L,LJ))/DX
      A11=A1*S
      A22=A2*S
      SK=S*S
      IF(S.LT.DX/3.)GO TO 121
      N=S+I+NIT
      CALL IMP(A1,A2,N,D,F,S,SK,CA,CB,CC,V,TA,VV,TT,I,L,J,LJ,G,RO)
      GO TO 122
  121 VV(L,LJ)=V(I,LJ)-A11
      TT(L,LJ)=TA(I,LJ)-A22
  122 C1=VV(L,J)-VV(L,LJ)-V(I,LJ)
      C2=D*(TA(I,LJ)-TT(L,LJ))-F*TT(L,J)
      C11=D*(V(I,LJ)-VV(L,LJ))-F*VV(L,J)
      C22=TT(L,J)-TT(L,LJ)-TA(I,LJ)
      A=CC*S*(F*C22-C2)
      V(I,J)=(A-CA*G(L)*C11+RO(L)*C1*SK)/(G(L)*CB-RO(L)*SK)
      TA(I,J)=CC*G(L)*(F*V(I,J)+C11)/S-C22
      GO TO 69
   59 TA(I,J)=TT(L,J)
      V(I,J)=VV(L,J)
   69 TTT=0.5*(TA(I,J)+TA(L,J))
      U(I,J)=U(I,J-1)+0.5*(V(I,J)+V(I,J-1))*DT
      YYY(J)=(TA(I,J)+TA(L,J))/TY(L)*0.5
      XXX(J)=(U(I,J)-U(L,J))/DX*GO(L)/TY(L)
      IF(INDEX.EQ.2)GO TO 55
      CALL GG(TTT,DT(L))
      IF(J.LT.JIND+3)GO TO 50
      IF(JJS.EQ.2.OR.I.LE.2)GO TO 50
      IF(G(L).LT.GOO)GO TO 50
      JJS=2
      JIND=J
      G(L)=GO(L)
      GO TO 51
   50 DT(L)=TTT
      GKIP(J)=GOO
      TKIP(J)=TTT
      IF(I.LE.3.OR.NJ.LT.MM.OR.TA(I,J)*TA(I,J-2).LT.0.0)GO TO 56
```

```
      TB=ABS(TA(I,LJ))
      IF(TB.LT.ABS(TA(I,J)).AND.TB.LT.ABS(TA(I,J-2)))INDEX=2
      IF(INDEX.NE.2)GO TO 56
      TA(I,LJ)=(TA(I,J)+TA(I,J-2))/2.
      V(I,LJ)=(V(I,J)+V(I,J-2))/2.
      J=LJ
      GO TO 69
   55 TKIP(J)=TTT
   56 CONTINUE
  200 CONTINUE
      DO 201 J=JSTART,K
  201 WRITE(6,38)J,T(J),V(I,J),TA(I,J),U(I,J),TKIP(J),GKIP(J),
     1XXX(J),YYY(J)
   38 FORMAT(I5,F5.2,F10.3,F10.1,F10.4,2F10.1,2F10.6)
      IF(L.NE.III)GO TO 82
      DO 31 II=1,NK
      XXX(II)=XXX(II+IST)
   31 YYY(II)=YYY(II+IST)
      CALL PLOT(XXX,YYY,NK,XMIN,YMIN,DX,DY)
   82 CONTINUE
  100 CONTINUE
      CALL PLOT(T,VPL,K1,XMIN,YMIN,DX,DY)
      DO 21 I=1,KK
   21 VPL(I)=V(N1,I)
      CALL PLOT(T,VPL,KK,XMIN,YMIN,DX,DY)
   32 FORMAT((16F8.4))
      GO TO 10
   99 STOP
      END
C     ***************************************************
      SUBROUTINE GG(TT,DTT)
      COMMON R(12),TY(12),GO(12),IVC(12),G(12),I
      DIMENSION IC(12),UP(12),YM(15,12)
      GV(DY,DR)=1./(1.+(DR)*ABS(DY)**(DR-1.))
      GRO(DY,DY0,DR)=1./(1.+(DR)*ABS((DY-DY0)/2.)**(DR-1.))
      T=TT/TY(I)
      DT=DTT/TY(I)
      IF(IVC(I).EQ.0) GO TO 10
      IF(ABS(T).LT. ABS(DT)) GO TO 5
    9 G(I)=GO(I)*GV(T,R(I))
      IC(I)=0
      RETURN
    5 IVC(I)=0
      UP(I)=1.
      IF(T.LT.DT) UP(I)=-1.
      IC(I)=2
      YM(1,I)=-DT
      YM(2,I)=DT
      G(I)=GO(I)*GRO(T,DT,R(I))
      RETURN
   10 IF(ABS(T).GE.ABS(YM(1,I)))GO TO 15
      IF((T-DT)*UP(I).GT..0) GO TO 20
      UP(I)=1.
      IF(T.LT.DT) UP(I)=-1.
      IC(I)=IC(I)+1
      IF (UP(I)*(T-YM(IC(I)-1,I)).GT..0) GO TO 22
      YM(IC(I),I)=DT
   11 G(I)=GO(I)*GRO(T,YM(IC(I),I),R(I))
      RETURN
   15 IVC(I)=1
```

```
      GO TO 9
   20 IF(UP(I)*(T-YM(IC(I)-1,I)).LT..0) GO TO 11
   22 IC(I)=IC(I)-2
      IF(IC(I).EQ.1) IC(I)=2
      IF(IC(I).EQ.2) GO TO 11
      GO TO 20
      END
C     ****************************************************
      SUBROUTINE IMP(A1,A2,N,D,F,S,SK,CA,CB,CC,V,TA,VV,TT,I,L,J,LJ,G,RO)
      DIMENSION V(12,300),TA(12,300),VV(12,300),TT(12,300),G(12),RO(12)
      S=S/N
      SK=S*S
      NN=N-1
      DO 20 IA=1,NN
      VE=V(I,LJ)-A1*N*S
      TE=TA(I,LJ)-A2*N*S
      VV(L,LJ)=V(I,LJ)-A1*S*(N-1)
      TT(L,LJ)=TA(I,LJ)-A2*S*(N-1)
      C1=VV(L,J)-VE-VV(L,LJ)
      C2=D*(TT(L,LJ)-TE)-F*TT(L,J)
      C11=D*(VV(L,LJ)-VE)-F*VV(L,J)
      C22=TT(L,J)-TE-TT(L,LJ)
      A=CC*S*(F*C22-C2)
      VV(L,J)=(A-CA*G(L)*C11+RO(L)*C1*SK)/(G(L)*CB-RO(L)*SK)
      TT(L,J)=CC*G(L)*(F*VV(L,J)+C11)/S-C22
   20 N=N-1
      RETURN
      END
C     ****************************************************
      SUBROUTINE PLOT(X,Y,K,XMIN,YMIN,DX,DY)
      DIMENSION X(800),Y(800)
      CALL PSCALE(10.,1.,XMIN,DX,X(1),K,1)
      CALL PSCALE(8.,1.,YMIN,DY,Y(1),K,1)
      CALL PLTOFS(XMIN,DX,YMIN,DY,2.,2.)
      CALL PAXIS(2.,2.,14HX ( TIME,SEC ),-14,10.,0.,XMIN,DX,1.)
      CALL PAXIS(2.,2.,14HY (           ),14,8.,90.,YMIN,DY,1.)
      CALL PLINE(X(1),Y(1),K,1,0,0,1)
      CALL PLTEND
      RETURN
      END
```

APPENDIX 7

```
C     ***************************************************
C      TRIANGULAR EARTH DAM. ANALYTICAL SOLUTION. BESSEL FUNCTIONS
C     WITH COMPLEX ARGUMENTS.  VISCOUS DAMPING INCLUDED.
C     DAM CREST YH(FT) BELOW TOP. (TRUNCATED TOP ONLY)
C     FIND DISPLACEMENTS AND VELOCITIES AT CREST.
C     READ N1 EQUIDISTANT VALUES OF BASE DISPLACEMENTS U FROM
C     DEVICE 7. FIND FOURIER COEF.BY LEAST SQUARES FITTING.
C     IF INDEX=2,READ FOURIER COEF. FROM DEVICE 8.
C     ***************************************************
      IMPLICIT COMPLEX*16(Z),REAL*8(A-H,O-Y)
      DIMENSION U(512),ZU(300),A(512),OM(512),ZA(512),V(512),T(512)
     1,B(200)
      NAMELIST/DIN/YH,H,G,RO,DT,N,M,NI,NNM,AMU,INDEX
   10 READ(5,DIN,END=99)
      N1=2*N+1
      MM=M+1
      ZP=DCMPLX(0.0D0,1.0D0)
      IF(INDEX.EQ.2)READ(8,14)(ZA(I),OM(I),I=1,MM)
   14 FORMAT(4(2F10.5,F8.3))
      IF(INDEX.EQ.2)GO TO 82
      READ(7,11)(U(J),J=1,N1)
   11 FORMAT(7(F10.5))
      CALL FORIT(U,N,M,A,B,IER)
      OM(1)=0.0D0
      ZA(1)=DCMPLX(A(1),0.0D0)
      CON=6.283186/(N1*DT)
      DO 50 I=2,MM
      OM(I)=CON*(I-1)
   50 ZA(I)=DCMPLX(A(I),-B(I))
   82 DO 80 J=1,N1
   80 T(J)=(J-1)*DT
      X=G/RO
      XX=AMU/RO
      DO 40 I=2,MM
      ZC=DCMPLX(X,XX*OM(I))
      ZVEL=CDSQRT(ZC)
      ZH=OM(I)*H/ZVEL
      ZHY=OM(I)*YH/ZVEL
      RH=CDABS(ZH)
      RYH=CDABS(ZHY)
      V1=DREAL(ZVEL)
      V2=DIMAG(ZVEL)
      PH=DABS(DATAN2(V2,V1))
      CALL BES(RH,PH,ZHJ0,ZHJ1,ZHY0,ZHY1,I,NI,NNM)
      CALL BES(RYH,PH,ZHYJ0,ZHYJ1,ZHYY0,ZHYY1,I,NI,NNM)
      ZS=(ZHYJ1+ZP*ZHYY1)/(ZHYJ1-ZP*ZHYY1)
      ZS1=ZHYJ0+ZP*ZHYY0-ZS*(ZHYJ0-ZP*ZHYY0)
      ZS2=ZHJ0+ZP*ZHY0-ZS*(ZHJ0-ZP*ZHY0)
      ZSS=ZS1/ZS2
      WRITE(6,20)ZVEL,PH
      WRITE(6,75)RH,ZHJ0,ZHJ1,ZHY0,ZHY1
      WRITE(6,75)RYH,ZHYJ0,ZHYJ1,ZHYY0,ZHYY1
   75 FORMAT(F12.5,8F12.5)
      WRITE(6,77)ZS,ZS1,ZS2,ZSS,OM(I)
   77 FORMAT(8F14.5,F10.3)
   20 FORMAT(3F10.4)
   40 ZA(I)=ZA(I)*ZSS
      DO 200 I=1,N1
      ZAA=ZA(1)
      DO 205 J=2,MM
```

```
      Z1=DCMPLX(0.0D0,DM(J)*T(I))
  205 ZAA=ZAA+ZA(J)*CDEXP(Z1)
  200 ZU(I)=ZAA
      WRITE(6,15)
   15 FORMAT('     DISPLACEMENTS AT CREST')
   13 FORMAT(7(F9.5))
      DO 65 J=1,N1
   65 A(J)=DREAL(ZU(J))
      WRITE(4,13)(A(J),J=1,N1)
      V(1)=0.0
      DO 68 I=2,N1
   68 V(I)=(A(I)-A(I-1))/DT
      WRITE(6,26)
   26 FORMAT('     VELOCITIES AT CREST')
      WRITE(4,13)(V(J),J=1,N1)
   99 CALL EXIT
      END
C     ***************************************************
      SUBROUTINE BES(RO,PHI,ZBJ0,ZBJ1,ZBY0,ZBY1,M,NI,NNM)
      IMPLICIT COMPLEX*16(Z),REAL*8(A-H,O-Y)
C     ONLY FOR BESSEL FUNCTIONS WITH COMPLEX ARGUMENTS OF THE FIRST
C     AND SECOND KIND OF ORDER 0 AND 1.VALUES FOR THE 4TH QUADRANT.
      G=0.57721566
      P=2./3.14159
      R=RO/2.
      UJ0=0.0
      VJ0=0.0
      UJ1=0.0
      VJ1=0.0
      FJ=1.
      NN=26
      IF(M.GT.NI)NN=NNM
      NM=NN-1
      DO 50 I=1,NN
      K=I-1
      FJ=K*FJ
      IF(K.EQ.0)FJ=1.
      CON=(-1)**K*R**(2*K)/FJ
      CON=CON/FJ
      C=CON*R/I
      ANG=2*K*PHI
      ANG1=ANG+PHI
      UJ0=UJ0+CON*DCOS(ANG)
      VJ0=VJ0+CON*DSIN(ANG)
      UJ1=UJ1+C*DCOS(ANG1)
      VJ1=VJ1+C*DSIN(ANG1)
   50 CONTINUE
      ZBJ0=DCMPLX(UJ0,-VJ0)
      ZBJ1=DCMPLX(UJ1,-VJ1)
      FY=1.
      FF=0.0
      S0=0.0
      T0=0.0
      DO 150 K=1,NM
      AK=K
      FF=FF+1./AK
      FY=K*FY
      CON=(-1)**(K+1)*R**(2*K)*FF/FY
      CON=CON/FY
      AN=2.*K*PHI
```

```
      SO=SO+CON*DCOS(AN)
      TO=TO+CON*DSIN(AN)
  150 CONTINUE
      CC=G+DLOG(R)
      UYO=P*(UJO*CC-PHI*VJO+SO)
      VYO=P*(VJO*CC+PHI*UJO+TO)
      C1=UJ1*UYO-VJ1*VYO-P*DCOS(PHI)/RO
      C2=UJ1*VYO+VJ1*UYO+P*DSIN(PHI)/RO
      VY1=(C2*UJO-C1*VJO)/(UJO*UJO+VJO*VJO)
      UY1=(C2-UJO*VY1)/VJO
      ZBYO=DCMPLX(UYO,-VYO)
      ZBY1=DCMPLX(UY1,-VY1)
      RETURN
      END
C     ******************************************************
      SUBROUTINE FORIT(FNT,N,M,A,B,IER)
      IMPLICIT REAL*8(A-H,O-Y)
      DIMENSION A(1),B(1),FNT(1)
      IER=0
   20 IF(M) 30,40,40
   30 IER=2
      RETURN
   40 IF(M-N)60,60,50
   50 IER=1
      RETURN
   60 AN=N
      COEF=2.0D0/(2.0D0*AN+1.0D0)
      CONST=3.141593*COEF
      S1=DSIN(CONST)
      C1=DCOS(CONST)
      C=1.0D0
      S=0.0D0
      J=1
      FNTZ=FNT(1)
   70 U2=0.0D0
      U1=0.0D0
      I=2*N+1
   75 UO=FNT(I)+2.0D0*C*U1-U2
      U2=U1
      U1=UO
      I=I-1
      IF(I-1) 80,80,75
   80 A(J)=COEF*(FNTZ+C*U1-U2)
      B(J)=COEF*S*U1
      IF(J-(M+1)) 90,100,100
   90 P=C1*C-S1*S
      S=C1*S+S1*C
      C=P
      J=J+1
      GO TO 70
  100 A(1)=A(1)*0.5D0
      RETURN
      END
```

APPENDIX 8

```
C     ****************************************************
C     ONE DIMENSIONAL PROPAGATION OF SHEAR WAVES THROUGH EARTH DAMS OF
C     TRIANGULAR CROSS-SECTION.  METHOD OF CHARACTERISTICS.
C     IF IMOT=1 EARTHQUAKE VELOCITIES AT BASE READ FROM DEVICE 7,
C     IF IMOT=2 STEADY OSCILL.MOTION.
C     IF ITOP=1 CREST AT DISTANCE DY BELOW TOP OF TRIANG.
C     IF ITOP=2 THE CREST IS AT Y=0.
C     SOIL VISCOELASTIC
C     ****************************************************
      DIMENSION V(20),VP(20),TAU(20),TAUP(20),VV(600),ACS(600),ACM(600),
     1T(600),AA(20),BB(20),ACT(600),VPM(600),VPS(600),VPT(600),SH(600)
      NAMELIST/DIN/G,UM,RO,DT,TMAX,A,OM,H,NJ,IMOT,IM,ITOP,GR
   10 READ(5,DIN,END=99)
      WRITE(6,DIN)
      IF(IMOT.EQ.1)READ(7,11)(VV(J),J=1,NJ)
   11 FORMAT(7(F10.5))
      VS=SQRT((G+UM/DT)/RO)
      DY=VS*DT
      NR=H/DY
      N1=NR+1
      II=1
      ACS(1)=0.0
      ACM(1)=0.0
      ACT(1)=0.0
      VPM(1)=0.0
      VPS(1)=0.0
      VPT(1)=0.0
      SH(1)=0.0
      Q=UM/DY
      CON=Q/2.
      D=RO*VS
      CA=CON-D
      IF(ITOP.EQ.2)GO TO 35
      K=2
      ACA=0.5*ALOG(2.)+1.
      COE=0.5*ALOG(H/(H-DY))
      GO TO 36
   35 K=1
      ACA=2.
      COE=1./(2.*N1-3.)
   36 T(II)=0.0
      KK=K+1
      DO 42 I=KK,NR
      SA=I-1
      SB=I-2
      IF(ITOP.EQ.2)GO TO 25
      AA(I)=0.5*ALOG(SA/SB)
      BB(I)=0.5*ALOG(I/SA)
      GO TO 26
   25 AA(I)=1./(2.*I-3.)
      BB(I)=1./(2.*I-1.)
   26 DUM=1.
   42 CONTINUE
      DO 12 I=1,N1
      V(I)=0.0
   12 TAU(I)=0.0
      TAUP(2)=0.0
      WRITE(6,14)DY,NR,VS
   14 FORMAT(5X,'DY=',F7.3,'  NR=',I2,'  VS=',F10.2)
   20 WRITE(6,15)T(II),(V(I),I=K,N1)
```

```
   15 FORMAT(5X,F7.3,(13F8.3))
      WRITE(6,16)(TAU(I),I=K,N1)
   16 FORMAT(12X,(13F8.2))
      II=II+1
      T(II)=DT*(II-1)
      IF(T(II).GE.TMAX)GO TO 18
C     INTERIOR POINTS
      DO 22 I=KK,NR
      CP=TAU(I-1)*(1.-AA(I))-CON*V(I+1)+CA*V(I-1)
      CM=TAU(I+1)*(1.+BB(I))+CON*V(I-1)-CA*V(I+1)
      TAUP(I)=(CM+CP)/(2.+AA(I)-BB(I))
      VP(I)=(TAUP(I)*(1.+AA(I))-CP)/D
      IF(ITOP.EQ.2)ACT(II)=ACT(II-1)+(VP(2)+V(2))*DT/2.
   22 IF(I.EQ.IM)ACM(II)=(VP(IM)+V(IM))*DT/2.+ACM(II-1)
C     TOP B.C.
      VP(K)=V(KK)+(TAU(KK)*ACA-Q*(V(KK)-V(K)))/D
      ACS(II)=(VP(K)+V(K))*DT/2.+ACS(II-1)
C     BOTTOM B.C.
      IF(IMOT.EQ.2)VP(N1)=A*SIN(OM*T(II))
      IF(IMOT.EQ.1)VP(N1)=VV(II)
      AP=D*(VP(N1)-V(NR))
      TAUP(N1)=(TAU(NR)*(1.-COE)+AP-Q*(V(N1)-V(NR)))/(1.+COE)
      VPM(II)=VP(IM)
      VPS(II)=VP(K)
      IF(ITOP.EQ.2)VPT(II)=VP(2)
      SH(II)=TAUP(N1)
      DO 23 I=K,N1
      V(I)=VP(I)
   23 TAU(I)=TAUP(I)
      GO TO 20
   18 II=II-1
      WRITE(8,11)(ACM(J),J=1,II)
      WRITE(8,11)(ACS(J),J=1,II)
      IF(ITOP.EQ.2)WRITE(8,11)(ACT(J),J=1,II)
      CALL PLOT(T,ACM,II,0.0,-3.,3.,0.5,4.,12.)
      CALL PLOT(T,ACS,II,0.0,-3.,3.,0.5,4.,12.)
      CALL PLOT(T,VPM,II,0.0,-3.,3.,0.5,4.,12.)
      CALL PLOT(T,VPS,II,0.0,-3.,3.,0.5,4.,12.)
      CALL PLOT(T,SH,II,0.0,-3000.,3.,1000.,4.,6.)
      IF(ITOP.EQ.1)GO TO 10
      CALL PLOT(T,ACT,II,0.0,-3.,3.,0.5,4.,12.)
      CALL PLOT(T,VPT,II,0.0,-3.,3.,0.5,4.,12.)
      GO TO 10
   99 STOP
      END
C     ************************************************
      SUBROUTINE PLOT(X,Y,K,XMIN,YMIN,DX,DY,XL,YL)
      DIMENSION X(800),Y(800)
      CALL PLTOFS(XMIN,DX,YMIN,DY,2.,2.)
      CALL PAXIS(2.,2.,14HX ( TIME,SEC ),-14,XL,0.,XMIN,DX,1.)
      CALL PAXIS(2.,2.,14HY (           ),14,YL,90.,YMIN,DY,1.)
      CALL PLINE(X(1),Y(1),K,1,0,0,1)
      CALL PLTEND
      RETURN
      END
```

APPENDIX 9

```
C     ***************************************************
C     PRESSURE WAVE PROPAGATION THROUGH SATURATED ELASTIC SOIL.
C     BIOT'S THEORY. ONE DIMENSIONAL. DISSIPATION PRESENT.
C     UNIFORM PROPERTIES. N SUBLAYERS OF THICKNESS DX.
C     STEADY OSCILLATORY EXCITATION OF THE BEDROCK.
C     ***************************************************
      IMPLICIT COMPLEX(Z),REAL(M)
      NAMELIST/DIN/C1,C2,C3,F1,F2,F3,VC,RO,MU,H,OM,E,PER,POR,P,Q,R,DT,
     1DX,TMAX,N
   10 READ(5,DIN,END=99)
      WRITE(6,DIN)
      A=C1*F2+C2*F1-2.*C3*F3
      AA=A*A
      B=(C1*C2-C3*C3)*2.
      BB=SQRT(AA-2.*B*(F1*F2-F3*F3))
      AZ=(A+BB)/B
      BZ=(A-BB)/B
      VN1=VC/SQRT(AZ)
      VN2=VC/SQRT(BZ)
      WRITE(6,12)AZ,BZ,VN1,VN2
   12 FORMAT('    Z=',2F10.4,'    UNDAMPED VEL=',2F10.2)
      R=MU*POR*POR/(PER*OM*RO)
      RR=R/(B/2.)
      Z=CMPLX(0.0,RR)
      ZP=CMPLX(0.0,R)
      WRITE(6,13)Z
   13 FORMAT('  ZCOMP =',2F10.3)
      ZC=(AZ+BZ-Z)/2.
      ZCC=AZ*BZ-Z
      ZTE=ZC*ZC-ZCC
      ZI=ZC+CSQRT(ZTE)
      ZII=ZC-CSQRT(ZTE)
      ZVI=VC/CSQRT(ZI)
      ZVII=VC/CSQRT(ZII)
      WRITE(6,14)ZI,ZII,ZVI,ZVII
   14 FORMAT(4F10.4,'    DAMPED PROP.VEL.=',4F10.2)
      ZPI=(F1-C1*ZI-ZP)/(ZI*C3-F3-ZP)
      ZPII=(F1-C1*ZII-ZP)/(ZII*C3-F3-ZP)
      ZEI=CMPLX(0.0,OM*H)/ZVI
      ZIE=CONJG(ZEI)
      ZEII=CMPLX(0.0,OM*H)/ZVII
      ZIIE=CONJG(ZEII)
      ZEI=CEXP(ZEI)+CEXP(ZIE)
      ZEII=CEXP(ZEII)+CEXP(ZIIE)
      ZCO=ZEII*(1.-ZPI)/(ZEI*(ZPII-1.))
      ZAI=E/(ZEI+ZCO*ZEII)
      ZAII=ZAI*ZCO
      ZCI=ZPI*ZAI
      ZCII=ZPII*ZAII
      ZC=CMPLX(0.0,OM)
      ZCONI=ZC/ZVI
      ZCONII=ZC/ZVII
      ZCOI=P*ZAI+Q*ZCI
      ZCOII=P*ZAII+Q*ZCII
      ZOI=Q*ZAI+R*ZCI
      ZOII=Q*ZAII+R*ZCII
      WRITE(6,18)ZAI,ZAII,ZCI,ZCII
   18 FORMAT('  COMP.DISPL.AMPL,SOL.  ',4F10.6/18X,'LIQ.',4F10.6)
      N1=N+1
      X=0.0
```

```
      DO 20 I=1,N1
      WRITE(6,19)X
   19 FORMAT('  DISTANCE FROM SURFACE IS ',F7.2, '  FEET')
      ZEI=CMPLX(0.0,OM*X)/ZVI
      ZIE=CONJG(ZEI)
      ZEII=CMPLX(0.0,OM*X)/ZVII
      ZIIE=CONJG(ZEII)
      Z1=CEXP(ZEI)
      Z2=CEXP(ZIE)
      Z3=CEXP(ZEII)
      Z4=CEXP(ZIIE)
      ZPSI=Z1-Z2
      ZPSII=Z3-Z4
      ZTHI=Z1+Z2
      ZTHII=Z3+Z4
      T=0.0
   15 IF(T.GT.TMAX)GO TO 8
      ZE=CMPLX(0.0,OM*T)
      ZEE=CEXP(ZE)
      ZUS=ZEE*(ZAI*ZTHI+ZAII*ZTHII)
      ZUF=ZEE*(ZCI*ZTHI+ZCII*ZTHII)
      ZVS=ZUS*ZC
      ZVF=ZUF*ZC
      Z5=ZCONI*ZEE*ZPSI
      Z6=ZCONII*ZEE*ZPSII
      ZSIG=Z5*ZCOI+Z6*ZCOII
      ZS=Z5*ZOI+Z6*ZOII
      ZP=-ZS/POR
      WRITE(6,22)T,ZUS,ZUF,ZSIG,ZP,ZVS,ZVF
   22 FORMAT(F6.3,4F10.5,4F10.2,4F10.4)
      T=T+DT
      GO TO 15
    8 X=X+DX
   20 CONTINUE
      GO TO 10
   99 STOP
      END
```

APPENDIX 10

```
C     ************************************************
C     TRANSIENT SOLUTION OF BIOT'S EQUATIONS BY METHOD OF CHARACTER.
C     SPECIFIED TIME INTERVALS. LINEAR INTERPOLATION.
C     *** ONE DIMENSIONAL PROPAGATION OF PRESSURE
C     WAVES THROUGH SATURATED ELASTIC POROUS MEDIA***
C     IND=1 STEADY OSCILL.MOTION,IND=2 QUAKE MOTION
C     IF IND=2 READ VELOCITIES OF BEDROCK FROM DEVICE 4.
C     W VEL OF SOLIS PHASE.V VEL. OF LIQUID PHASE.
C     SI=PRESSURE ON SOIL SCELETON,SIG=PRES.ON FLUID PART
C     ************************************************
      REAL MU
      DIMENSION SIP(25),SP(25),VP(25),WP(25),S(25),VEL(2000),R1(2000)
     1,R2(2000),R3(2000),R4(2000),TT(2000)
      COMMON SI(25),V(25),W(25),SIT(25),VT(25),WT(25),TV,N,DX,DXL
      NAMELIST/DIN/MU,POR,PER,DT,TMAX,RO1,RO2,G,CL,R,Q,H,A,OM
     1,IND,NV,IPRINT,II
   10 READ(5,DIN,END=99)
      WRITE(6,DIN)
      IF(IND.EQ.2)READ(4,16)(VEL(I),I=1,NV)
   16 FORMAT(7(F10.5))
      V1=SQRT(R/RO2)
      V2=SQRT((2.*G+CL)/RO1)
      DX=DT*V1
      J1=0
      DXL=DT*V2
      AN=H/DX
      K=H/DX
      IF(AN.GT.(K+0.5))GO TO 11
      N=K
      GO TO 12
   11 N=K+1
   12 N1=N+1
      B=MU*POR*POR/PER
      B1=B*V1*DT/2.
      B2=B*V2*DT/2.
      A1=V1*RO2+B1
      A2=V2*RO1+B2
      TV=V2/V1
      E1=V1*RO2
      E2=V2*RO1
      D1=Q*DT/(DX*2.)
      D2=Q*DT/(DXL*2.)
      CON=B1*B2-A1*A2
      T=0.0
C     INITIAL CONDITIONS(S,SI ZERO ONLY IF VIBRATION STEADY OSCIL.)
      DO 13 I=1,N1
      SI(I)=0.0
      S(I)=0.0
      V(I)=0.0
   13 W(I)=0.0
C     AT SURFACE
      SP(1)=0.0
      SIP(1)=0.0
      WRITE(6,14)DX,V1,V2
   14 FORMAT(3E10.2)
   20 IF(IPRINT.EQ.2)GO TO 29
      WRITE(6,21)T
   21 FORMAT(10X,'TIME=',F10.5)
      WRITE(6,22)(SI(I),S(I),W(I),V(I),I=1,N1)
   22 FORMAT(5X,2F15.2,2F15.4)
```

```
   29 T=T+DT
      IF(T.GT.TMAX)GO TO 40
      J1=J1+1
C     INTERIOR POINTS
      DO 25 I=2,N
      EN=D1*(W(I+1)-W(I-1))
      C3=S(I-1)-E1*V(I-1)-B1*(W(I-1)-V(I-1))+EN
      C4=S(I+1)+E1*V(I+1)+B1*(W(I+1)-V(I+1))+EN
      SP(I)=(C3+C4)/2.
      CALL INTER(I)
      ENN=D2*(VT(I+1)-VT(I-1))
      C1=SIT(I-1)-E2*WT(I-1)+B2*(WT(I-1)-VT(I-1))+ENN
      C2=SIT(I+1)+E2*WT(I+1)-B2*(WT(I+1)-VT(I+1))+ENN
      SIP(I)=(C1+C2)/2.
      VP(I)=(B1*(C1-C2)+A2*(C3-C4))/(2.*CON)
   25 WP(I)=(A1*(C1-C2)+B2*(C3-C4))/(2.*CON)
      I=N1
C     BEDROCK BOUNDARY
      IF(IND.EQ.1)VP(N1)=A*SIN(OM*T)*(1.-EXP(-8.*T))
      IF(IND.EQ.2)VP(N1)=VEL(J1)
      WP(N1)=VP(N1)
      SP(N1)=(A1-B1)*WP(N1)+S(N)-RO2*V1*V(N)-B1*(W(N)-V(N))+2.*D1*
     1(W(N1)-W(N))
      CALL INTER(I)
      SIP(N1)=(A2-B2)*VP(N1)+SIT(N)-RO1*V2*WT(N)+B2*(WT(N)-VT(N))+
     12.*D2*(V(N1)-VT(N))
C     SURFACE BOUNDARY
      I=1
      C6=S(2)+RO2*V1*V(2)+B1*(W(2)-V(2))+2.*D1*(W(2)-W(1))
      CALL INTER(I)
      C5=SIT(2)+RO1*V2*WT(2)-B2*(WT(2)-VT(2))+2.*D2*(VT(2)-V(1))
      VP(1)=-(B1*C5+A2*C6)/CON
      WP(1)=(C5+B2*VP(1))/A2
      DO 30 I=1,N1
      V(I)=VP(I)
      W(I)=WP(I)
      S(I)=SP(I)
   30 SI(I)=SIP(I)
      R1(J1)=SI(II)
      R2(J1)=S(II)/(-POR)
      R3(J1)=V(II)
      R4(J1)=W(II)
      TT(J1)=T
      GO TO 20
   40 CALL PLOT(TT,R1,J1,0.0,-5000.,3.,2500.,5.,4.)
      CALL PLOT(TT,R2,J1,0.0,-5000.,3.,2500.,5.,4.)
      CALL PLOT(TT,R3,J1,0.0,-2.,3.,0.5,5.,8.)
      CALL PLOT(TT,R4,J1,0.0,-2.,3.,0.5,5.,8.)
      GO TO 10
   99 CALL EXIT
      STOP
      END
C     ************************************************
      SUBROUTINE INTER(I)
      COMMON SI(25),V(25),W(25),SIT(25),VT(25),WT(25),TV,N,DX,DXL
      IF(I.EQ.1)GO TO 10
      SIT(I-1)=SI(I)-TV*(SI(I)-SI(I-1))
      VT(I-1)=V(I)-TV*(V(I)-V(I-1))
      WT(I-1)=W(I)-TV*(W(I)-W(I-1))
      IF(I.EQ.(N+1))GO TO 20
```

```
   10 SIT(I+1)=SI(I)-TV*(SI(I)-SI(I+1))
      VT(I+1)=V(I)-TV*(V(I)-V(I+1))
      WT(I+1)=W(I)-TV*(W(I)-W(I+1))
   20 RETURN
      END
C     ***************************************************
      SUBROUTINE PLOT(X,Y,K,XMIN,YMIN,DX,DY,XL,YL)
      DIMENSION X(3000),Y(3000)
      CALL PLTOFS(XMIN,DX,YMIN,DY,2.,2.)
      CALL PAXIS(2.,2.,14HX ( TIME,SEC ),-14,XL,0.,XMIN,DX,1.)
      CALL PAXIS(2.,2.,14HY (           ),14,YL,90.,YMIN,DY,1.)
      CALL PLINE(X(1),Y(1),K,1,0,0,1)
      CALL PLTEND
      RETURN
      END
```

APPENDIX 11

```
C     ***************************************************
C     TWO DIMENSIONAL PROPAGATION OF COMPRESSION AND SHEAR WAVES
C     THROUGH HOMOGENEOUS SOIL. STEPWISE LATERAL BOUNDARIES.
C     APLICABLE TO EARTH DAMS AND TO VALLEYS
C     ONE LAYER. CONSTANT MODULI. POR=POISSON RATIO
C     AT EACH NODE 16 EQUATIONS AND 16 UNKNOWNS.
C     ANY RATIO OF VPR/VSH (INTERPOLATIONS).
C     ISUP=1 OR 2 REDUCES PRINTOUT(2 PRINTS ABSOL.MAX.HORIZ.
C     ACCELERATIONS AT SURFACE ONLY).
C     IF IH=1 ONLY HORIZONTAL MOTION INPUT.
C     IF IDYNAM=1,ONLY DYNAMIC STRESSES COMPUTED, STATIC STRESSES
C     IF KNOWN CAN BE SUPERIMPOSED.
C     ***************************************************
      DIMENSION PU(700),PD(700),PL(700),PR(700),PUP(700),PDP(700),
     1PLP(700),PRP(700),TU(700),TD(700),TR(700),TL(700),TUP(700),
     2TDP(700),TRP(700),TLP(700),VU(700),VD(700),VL(700),VR(700)
     3,VUP(700),VDP(700),VLP(700),VRP(700),VVU(700),VVD(700),VVL(700),
     4VVR(700),VVUP(700),VVDP(700),VVLP(700),VVRP(700),VHO(700),VVE(700)
     5,TH(700),VH(700),VV(700),TV(700),INDEX(30),VER(700),HOR(700),
     6IBOUND(50),ISUR(30),INR(10),INL(10),ILB(50),INTH(30),INTV(30),
     7INSR(10),INSL(10),IPRINT(30),AV(100),AH(100),AST(100)
      INTEGER PERIND(150)
      DATA VV,VH,VHO,VVE,VU,VD,VL,VR,VVU,VVD,VVL,VVR,TD,TU,TL,TR,
     1TV,TH,VUP,VDP,VLP,VRP,VVUP,VVDP,VVLP,VVRP,TDP,TUP,TLP,TRP,
     2PUP,PDP,PLP,PRP,VER,HOR,AST,PU,PD,PL,PR/28100*0.0/
      NAMELIST/DIN/POR,E,INDEX,AMU,RO,GR,DT,TMAX,NR,NJ,LL,MM,IBOUND,
     1ISUR,ILB,INTH,INTV,INSR,INSL,IPRINT,NSTEP,INL,INR,OK,PERIND,ISUP,
     2TSTART,NSURF,NPER,IH,IDYNAM
C     FOR EARTHQUAKE MOTION READ HORIZONTAL VELOCITIES FROM
C     DEVICE 4 AND VERTICAL VELOCITIES FROM DEVICE 3.
   10 READ(5,DIN,END=99)
      READ(4,7)(HOR(I),I=1,NSTEP)
    7 FORMAT(7(F10.5))
      IF(IH.GT.1)READ(3,7)(VER(I),I=1,NSTEP)
      G=E/(2.*(1.+POR))
      AL=POR*E/((1.+POR)*(1.-2.*POR))
      TM=AL+2.*G
      VPR=SQRT((TM*DT+AMU)/(RO*DT))
      VSH=SQRT((G*DT+AMU)/(RO*DT))
      DX=2.*VSH*DT
      T2=VPR/(2.*VSH)
      T1=1.-T2
      RATI=VPR/VSH
      WRITE(6,20)DX,VPR,VSH,RATI,G,TM,OK
   20 FORMAT('  DX(FT)=',F6.2,'  VPR(FT/SEC)=',F7.2,'  VSH=',F7.2,
     1'  RATIO=',F5.2,'  G=',F9.1,'  T=',F11.1,'KO=',F5.2/)
      IN=(NJ-2)*2
      ISTEP=1
      T=TSTART
      IF(IDYNAM.EQ.1)GO TO 18
C     STATIC PRESSURES
      DO 15 J=1,NPER,3
      I1=PERIND(J)
      I2=PERIND(J+1)
      I3=PERIND(J+2)
      DO 17 IO=I1,I2
      DO 16 II=1,I3
      I=IO-(II-1)*NJ
      PD(I)=DX*RO*GR*(II-1)
      PU(I)=PD(I)
```

```
      PL(I)=OK*PD(I)
   16 PR(I)=PL(I)
   17 CONTINUE
   15 CONTINUE
   18 C1=AMU/DX
      C=RO*VSH
      CC=RO*VPR
      COC=C+CC
      C2=CC*GR*DT
      IF(IDYNAM.EQ.1)C2=0.0
      C3=2.*C2
      C4=2.*C1
      CM=C-C4
      CD=2.*C
      CCM=CC-AMU/(VPR*DT)
      CE=1./(E*DT)
      G1=-2.-CE*CC
      G2=POR*CE*CC
      A5=G2*G2-G1*G1
      C11=4.*C1
      IIN=IN-2
      N1N=IBOUND(1)
      N2N=INDEX(1)
      N3N=ISUR(1)
      N4N=ILB(1)
      N5N=INL(1)
      N6N=INR(1)
      N7N=INTH(1)
      N8N=INTV(1)
      N9N=INSR(1)
      N10N=INSL(1)
      N11N=IPRINT(1)
   30 IF(ISUP.EQ.2)GO TO 508
      WRITE(6,31)T
   31 FORMAT('  TIME=',F7.3,' SEC'/' NODE')
      IF(ISUP.EQ.1)GO TO 507
      DO 32 IO=2,N11N,2
      I1=IPRINT(IO)
      I2=IPRINT(IO+1)
      DO 33 I=I1,I2
   33 WRITE(6,34)I,VU(I),VD(I),VL(I),VR(I),TU(I),TD(I),TL(I),TR(I),PU(I)
     1,PD(I),PL(I),PR(I),VHO(I),VVF(I)
   34 FORMAT(2X,I3,12F9.2,2F6.2)
   32 CONTINUE
      GO TO 508
  507 J=0
      DO 333 IO=2,N3N,2
      I1=ISUR(IO)
      I2=ISUR(IO+1)
      DO 336 I=I1,I2
      J=J+1
  336 WRITE(6,335)I,VD(I),VVD(I),VHO(I),VVF(I),AV(J),AH(J)
  335 FORMAT(2X,I3,6F6.2)
  333 CONTINUE
  508 T=T+DT
      ISTEP=ISTEP+1
      IF(T.GT.TMAX)GO TO 441
      DO 50 IO=2,N1N,2
      I1=IBOUND(IO)
      I2=IBOUND(IO+1)
```

```
      DO 53 I=I1,I2
      VUP(I)=VER(ISTEP)
      VDP(I)=VER(ISTEP)
      VVLP(I)=VER(ISTEP)
      VVRP(I)=VER(ISTEP)
      VLP(I)=HOR(ISTEP)
      VRP(I)=HOR(ISTEP)
      VVUP(I)=HOR(ISTEP)
   53 VVDP(I)=HOR(ISTEP)
   50 CONTINUE
      VHO(LL)=HOR(ISTEP)
      VVE(LL)=VER(ISTEP)
      VHO(MM)=HOR(ISTEP)
      VVE(MM)=VER(ISTEP)
C     INTERIOR POINTS
      DO 101 IO=2,N2N,2
      I1=INDEX(IO)
      I2=INDEX(IO+1)
      DO 102 I=I1,I2
      J=I+1
      K=I+NJ
      L=I-1
      M=I-NJ
      E11=T1*PR(I)+T2*PL(J)
      E12=T1*VR(I)+T2*VL(J)
      E21=T1*PL(I)+T2*PR(L)
      E22=T1*VL(I)+T2*VR(L)
      E31=T1*PD(I)+T2*PU(M)
      E32=T1*VD(I)+T2*VU(M)
      E41=T1*PU(I)+T2*PD(K)
      E42=T1*VU(I)+T2*VD(K)
      F1=E11-E12*CCM-C1*VR(I)
      F2=E21+E22*CCM+C1*VL(I)
      F3=E31+E32*CCM+C1*VD(I)-C2
      F4=E41-E42*CCM-C1*VU(I)+C2
      F5=TH(L)-VH(L)*CM-C4*VVL(I)
      F6=TH(I)+VH(I)*CM+C4*VVR(I)
      F7=TV(M)-VV(M)*CM-C4*VVD(I)
      F8=TV(I)+VV(I)*CM+C4*VVU(I)
      F9=(PU(I)+PD(I))*CE
      F10=(PR(I)+PL(I))*CE
      Q1=CE*(F1+F2)
      Q2=CE*(F4+F3)
      G10=POR*Q1-Q2-POR*F10+F9
      G20=POR*Q2-Q1-POR*F9+F10
      B10=(F2+F8-F1-F7)/COC
      B20=(F3-F4+F6-F5)/COC
      A10=(G2*G10-G1*G20)/A5
      A20=(G2*G20-G1*G10)/A5
      VLP(I)=(A10+B10)/2.
      VDP(I)=(A20+B20)/2.
      VRP(I)=(B10-A10)/2.
      VUP(I)=(B20-A20)/2.
      VHO(I)=(VLP(I)+VRP(I))/2.
      VVE(I)=(VUP(I)+VDP(I))/2.
      VVDP(I)=VHO(I)
      VVUP(I)=VVDP(I)
      VVLP(I)=VVE(I)
      VVRP(I)=VVLP(I)
      PRP(I)=F1+CC*VRP(I)
```

```
      PLP(I)=F2-CC*VLP(I)
      PDP(I)=F3-CC*VDP(I)
      PUP(I)=F4+CC*VUP(I)
      TLP(I)=F5+C*VVLP(I)
      TRP(I)=F6-C*VVRP(I)
      TDP(I)=F7+C*VVDP(I)
      TUP(I)=F8-C*VVUP(I)
  102 CONTINUE
  101 CONTINUE
C     SURFACE POINTS
      J=0
      DO 51 IO=2,N3N,2
      I1=ISUR(IO)
      I2=ISUR(IO+1)
      DO 40 I=I1,I2
      J=J+1
      M=I-NJ
      F31=T1*PD(I)+T2*PU(M)
      F32=T1*VD(I)+T2*VU(M)
      F3=F31+F32*CCM+C1*VD(I)-C2
      F7=TV(M)-VV(M)*CM-C4*VVD(I)
      VDP(I)=F3/CC
      VVDP(I)=-F7/C
      VHO(I)=VVDP(I)
      VVE(I)=VDP(I)
      AH(J)=(VVDP(I)-VVD(I))/DT
      AV(J)=(VDP(I)-VD(I))/DT
   40 IF(ABS(AST(J)).LT.ABS(AH(J)))AST(J)=ABS(AH(J))
   51 CONTINUE
C     BEDROCK
      DO 205 IO=2,N4N,2
      I1=ILB(IO)
      I2=ILB(IO+1)
      DO 206 I=I1,I2
      K=I+NJ
      F41=T1*PU(I)+T2*PD(K)
      F42=T1*VU(I)+T2*VD(K)
      F4=F41-F42*CCM-C1*VU(I)+C2
      F8=TV(I)+VV(I)*CM+C4*VVU(I)
      TUP(I)=F8-C*VVUP(I)
      PUP(I)=F4+CC*VUP(I)
      TDP(I)=0.0
      PDP(I)=0.0
      VHO(I)=VVUP(I)
  206 VVE(I)=VUP(I)
  205 CONTINUE
C     SIDES
      IF(N6N.EQ.0)GO TO 151
      DO 90 IO=2,N6N
      I=INR(IO)
      JI=I+1
      F6=TH(I)+VH(I)*CM+C4*VVR(I)
      TRP(I)=F6-C*VVRP(I)
      TLP(I)=0.0
      F11=T1*PR(I)+T2*PL(JI)
      F12=T1*VR(I)+T2*VL(JI)
      F1=F11-F12*CCM-C1*VR(I)
      PRP(I)=F1+CC*VRP(I)
      PLP(I)=0.0
      VHO(I)=VRP(I)
```

```
   90 VVE(I)=VVRP(I)
  151 IF(N5N.EQ.0)GO TO 152
      DO 95 IO=2,N5N
      I=INL(IO)
      L=I-1
      F5=TH(L)-VH(L)*CM-C4*VVL(I)
      TLP(I)=F5+C*VVLP(I)
      TRP(I)=0.0
      F21=T1*PL(I)+T2*PR(L)
      F22=T1*VL(I)+T2*VR(L)
      F2=F21+F22*CCM+C1*VL(I)
      PLP(I)=F2-CC*VLP(I)
      VHO(I)=VLP(I)
      VVE(I)=VVLP(I)
   95 PRP(I)=0.0
C     CORNER SURFACE POINTS
  152 IF(N9N.EQ.0)GO TO 153
      DO 96 IO=2,N9N
      I=INSR(IO)
      L=I-1
      F5=TH(L)-VH(L)*CM-C4*VVL(I)
      F21=T1*PL(I)+T2*PR(L)
      F22=T1*VL(I)+T2*VR(L)
      F2=F21+F22*CCM+C1*VL(I)
      VVLP(I)=-F5/C
      VLP(I)=F2/CC
   96 VVE(I)=VVLP(I)
  153 IF(N10N.EQ.0)GO TO 154
      DO 97 IO=2,N10N
      I=INSL(IO)
      JI=I+1
      F6=TH(I)+VH(I)*CM+C4*VVR(I)
      F11=T1*PR(I)+T2*PL(JI)
      F12=T1*VR(I)+T2*VL(JI)
      F1=F11-F12*CCM-C1*VR(I)
      VVRP(I)=F6/C
      VRP(I)=-F1/CC
   97 VVE(I)=VVRP(I)
C     MIDDLE POINTS
  154 DO 190 IO=2,N8N,2
      I1=INTV(IO)
      I2=INTV(IO+1)
      DO 191 I=I1,I2
      K=I+NJ
      CON=VV(I)
      VV(I)=(TD(K)-TU(I)+(VVU(I)+VVD(K))*CM+C11*VV(I))/CD
  191 TV(I)=TU(I)+VV(I)*C-CON*C4-VVU(I)*CM
  190 CONTINUE
      DO 180 IO=2,N7N,2
      I1=INTH(IO)
      I2=INTH(IO+1)
      DO 181 I=I1,I2
      J=I+1
      CON=VH(I)
      VH(I)=(TL(J)-TR(I)+(VVR(I)+VVL(J))*CM+C11*VH(I))/CD
  181 TH(I)=TR(I)+VH(I)*C-CON*C4-VVR(I)*CM
  180 CONTINUE
      DO 98 IO=2,N11N,2
      I1=IPRINT(IO)
      I2=IPRINT(IO+1)
```

```
      DO 94 I=I1,I2
      TU(I)=TUP(I)
      TD(I)=TDP(I)
      TR(I)=TRP(I)
      TL(I)=TLP(I)
      PU(I)=PUP(I)
      PD(I)=PDP(I)
      PR(I)=PRP(I)
      PL(I)=PLP(I)
      VU(I)=VUP(I)
      VD(I)=VDP(I)
      VL(I)=VLP(I)
      VR(I)=VRP(I)
      VVU(I)=VVUP(I)
      VVD(I)=VVDP(I)
      VVL(I)=VVLP(I)
   94 VVR(I)=VVRP(I)
   98 CONTINUE
      GO TO 30
  441 DO 442 I=1,NSURF
  442 AST(I)=AST(I)/AC1
      WRITE(6,340)(AST(I),I=1,NSURF)
  340 FORMAT(8(F10.3))
      GO TO 10
   99 STOP
      END
```

REFERENCES

1. Ambraseys, N. N., "A Note on the Response of an Elastic Overburden of Varying Rigidity to an Arbitrary Ground Motion," Bull. Seism. Soc. of Am., Vol. 49, No. 3, July 1959, pp. 211-220.

2. Ambraseys, N. N., "On the Shear Response of a two-dimensional Truncated Wedge Subjected to an Arbitrary Disturbance," Bull. Seism. Soc. of Am., Vol. 50, No. 1, January 1960, pp. 45-56.

3. Ambraseys, N. N., "The Seismic Stability of Earth Dams," Proc. 2nd World Conf. Earthquake Eng., Tokyo, Japan, Vol. II, 1960.

4. Ambraseys, N. N., "On the Seismic Behavior of Earth Dams," Proc. 2nd World Conf. Earthquake Eng., Tokyo, Japan, 1960.

5. Ambraseys, N. N., and Sarma, S. K., "The Response of Earth Dams to Strong Earthquakes," Geotechnique, Vol. 17, No. 3, September 1967, pp. 181-213.

6. Baltzer, R. A., Lai C., "Computer Simulation of Unsteady Flows in Waterways," Journal of the Hydraulics Division, ASCE, Vol. 94, No. HY4, 1968, pp. 1083-1117.

7. Berg, G. V., "A Study of the Earthquake Response of Inelastic Systems," Proceedings, Structural Engineers Assoc. of California, Oct. 1965.

8. Berg, G. V., and Housner, G. W., "Integrated Velocity and Displacement of Strong Earthquake Ground Motion," Bulletin of the Seismological Society of America, Vol. 51, No. 2, pp. 175-189, April 1961.

9. Biot, M. A., "Theory of Propagation of Elastic Waves in a Fluid Saturated Porous Solid. I. Low-Frequency Range," Journal of the Acoustical Soc. of Amer., Vol. 28, No. 2, March 1956, pp. 168-178.

10. Biot, M. A., "Theory of Deformation of a Porous Viscoelastic Anisotropic Solid," Journal of Applied Physics, Vol. 27, No. 5, May 1956, pp. 459-467.

11. Biot, M. A., "Mechanics of Deformation and Acoustic Propagation in Porous Media," Journal of Applied Physics, Vol. 33, No. 4, April 1962, pp. 1482-1498.

12. Bogdanoff, J. L., Goldberg, J. E., and Bernard, M. C., "Response of a Simple Structure to a Random Earthquake Disturbance," Bulletin Seismological Society of America, Vol. 51, No. 2, 1961, pp. 293-310.

13. Chopra, A. K., "Earthquake Response of Earth Dams," Journal of the Soil Mechanics and Foundation Division, ASCE, Vol. 93, No. SM2, Proc. Paper 5137, March 1967, pp. 65-81.

14. Clough, R. W., and Chopra, A. K., "Earthquake Stress Analysis in Earth Dams," Journal of the Engineering Mechanics Division, ASCE, Vol. 92, No. EM2, Proc. Paper 4793, April 1966, pp. 197-212.

15. Constantopoulos, I. V., "Amplification Studies for a Nonlinear Hysteretic Soil Model," Sc.D. thesis, Department of Civil Engineering, Massachusetts Institute of Technology, 1973.

16. Cooley, J. W. and Tukey, J. W., "An Algorithm for the Machine Calculation of Complex Fourier Series," Mathematics of Computation, Vol. 19, No. 90, 1965, pp. 297-301.

17. Deresiewicz, H., "The Effect of Boundaries on Wave Propagation in a Liquid-filled Porous Solid; Reflection of Plane Waves at a Free Plane Boundary (Non-Dissipative Case)", Bulletin of the Seismological Society of America, Vol. 50, No. 4, Oct. 1960, pp. 599-607.

18. Dezfulian, H., and Seed, H. B., "Seismic Response of Soil Deposits Underlain by Sloping Rock Boundaries," Earthquake Eng. Res. Center, Univ. of California, Rep. No. EERC 69-9, August 1969.

19. Dezfulian, H., and Seed, H. B., "Response of Non-Uniform Soil Deposits to Travelling Seismic Waves," Report No. EERC 69-13, College of Engineering, University of California, Berkeley, Sept. 1969.

20. Dibaj, M., and Penzien, J., "Nonlinear Seismic Response on Earth Structures," Report No. EERC 69-2, College of Engineering, University of California, Berkeley, January 1969.

21. Duffy, J., and Midlin, R. D., "Stress-Strain Relation and Vibrations of a Granular Medium," Journal of Applied Mechanics, ASME, Vol. 24, 1957, p. 585.

22. Ghaboussi, J., "Dynamic Stress Analysis of Porous Elastic Solids Saturated with Compressible Fluids," Report No. EERC 71-6, College of Engineering, University of California, Berkeley, August 1971.

23. Ghaboussi, J., and Wilson, E. L., "Variational Formulation of Dynamics of Fluid Saturated Porous Elastic Solids," Journal of the Engineering Mechanics Division, Vol. 98, No. EM4, Proc. Paper 9152, August 1972, pp. 947-963.

24. Goel, S. C., "Inelastic Behavior of Multistory Building Frames Subjected to Earthquake Motion," Ph.D. Thesis, Department of Civil Engineering, University of Michigan, Ann Arbor, December 1967.

25. Hardin, B. O., and Drnevich, V. P., "Shear Modulus and Damping in Soils: Design Equations and Curves," Journal of Soil Mechanics and Foundations Division, ASCE, Vol. 98, No. SM7, July 1972, pp. 667-692.

26. Hardin, B. O., and Richart, F. E., Jr., "Elastic Wave Velocities in Granular Soils," Journal of the Soil Mechanics and Foundations Division, ASCE, Vol. 89, No. SM1, Proc. Paper 3407, Feb. 1963, pp. 33-66.

27. Hatanaka, M., "Fundamental Considerations on the Earthquake Resistant Properties of the Earth Dam," Bull. No. 11, Disaster Prevention Research Institute, Kyoto University, December 1955.

28. Heierli, W., "Inelastic Wave Propagation in Soil Columns," Journal of the Soil Mechanics and Foundations Division, ASCE, No. SM6, December 1962, pp. 33-63.

29. Herrera, I., and Rosenblueth, E., "Response Spectra on Stratified Soil," Proceedings, 3rd World Conference on Earthquake Engineering, New Zealand, 1965.

30. Hildebrand, F. B., Advanced Calculus for Applications, Prentice Hall, Inc., Englewood Cliffs, N. J., 1962, p. 646.

31. Housner, G. W., "Strong Ground Motion," Chapter 4, Earthquake Engineering, edited by Wiegel, Prentice-Hall, Inc., 1970, pp. 75-91.

32. IBM, "System/360 Scientific Subroutine Package, Version III, Programmer's Manual", Publication GH20-0205-4, 5th Edition, August 1970, pp. 276-278.

33. Idriss, I. M., and Seed, H. B., "The Response of Earth Banks During Earthquakes," Report, Soil Mechanics and Bituminous Materials Laboratory, University of California, Berkeley, 1966.

34. Idriss, I. M., and Seed, H. B., "Response of Earth Banks During Earthquakes," Journal of the Soil Mechanics and Foundations Division, ASCE, Vol. 93, No. SM3, Proc. Paper 5232, May 1967, pp. 61-82.

35. Idriss, I. M., and Seed, H. B., "Response of Horizontal Soil Layers During Earthquakes," Research Report, Soil Mechanics and Bituminous Materials Research Laboratory, University of California, Berkeley, August 1967.

36. Idriss, I. M., and Seed, H. B., "Seismic Response of Horizontal Soil Layers," Journal of the Soil Mechanics and Foundations Division, ASCE, Vol. 94, No. SM4, Proc. Paper 6043, July 1968, pp. 1003-1031.

37. Isenberg, J., and Adham, S. A., "Interaction of Soil and Power Plants in Earthquakes," Journal of the Power Division, ASCE, Vol. 98, No. PO2, Proc. Paper 9242, October 1972, pp. 273-291.

38. Ishihara, K., "Propagation of Compressional Waves in a Saturated Soil," Proc. of the International Symposium of Wave Propagation and Dynamic Properties of Earth Materials, Univ. of New Mexico Press, 1968, pp. 195-206.

39. Ishihara, K., "Approximate Forms of Wave Equations for Water-Saturated Porous Materials and Related Dynamic Modulus," Journal of Soils and Foundations, Vol. 10, No. 4, 1970, pp. 10-38.

40. Jacobsen, L., "Motion of a Soil Subjected to a Simple Harmonic Ground Vibration," Bull. Seism. Soc. Am., Vol. 20, 1930, pp. 160-196.

41. Jennings, P. C., "Periodic Response of a General Yielding Structure," Journal of the Engineering Mechanics Division, Proc. ASCE, Vol. 40, EM2, April 1964, pp. 131-166.

42. Kanai, K., "The Effect of Solid Viscosity of Surface Layer on the Earthquake Movements," Bull. Earthquake Research Institute, University of Tokyo, Vol. 28, 1950, pp. 31-35.

43. Kanai, K., "Relations Between the Nature of Surface Layer and the Amplitude of Earthquake Motions," Bulletin, Earthquake Research Institute, Tokyo University, Vol. 30, 1952, pp. 31-37.

44. Kanai, K., "An Empirical Formula for the Spectrum of Strong Earthquake Motions," Bulletin Earthquake Research Institute, Tokyo University, Vol. 39, 1961.

45. Kuhlemeyer, R. L., and Lysmer, J., "Finite Element Method Accuracy for Wave Propagation Problems," Journal of the Soil Mechanics and Foundations Division, ASCE, Technical Note, Vol. 99, SM5, May 1973, pp. 421-427.

46. Liggett, J. A., and Woolhiser, D. A., "Difference Solution of the Shallow-Water Equations," Journal of the Engineering Mechanics Division, ASCE, Vol. 95, No. EM2, 1967, pp. 39-71.

47. McLachlan, N. W., Bessel Functions for Engineers, Oxford Clarendon Press, 2nd Edition, 1955, p. 240.

48. Monomobe, N., Takata, A., and Matumura, M., "Seismic Stability of the Earth Dam," Proceedings, 2nd Congress on Large Dams, Washington, D. C., 1936, Vol. IV, pp. 435-442.

49. National Bureau of Standards, Mathematical Tables Project, Table of the Bessel Functions $J_0(z)$ and $J_1(z)$ for Complex Arguments, Columbia University Press, New York, 1943, p. 403.

50. National Bureau of Standards, Computation Laboratory Table of the Bessel Function $Y_0(z)$ and $Y_1(z)$ for Complex Arguments, Columbia University Press, New York, 1950, p. 427.

51. Okamoto, S., Motohiko, K., Katsuyuki, K., and Fusayoshi, K., "On the Dynamical Behavior of an Earth Dam During Earthquake," Proceedings, 3rd World Conference on Earthquake Engineering, New Zealand, 1965.

52. Parmelee, R. A., Penzien, J., Scheffey, C. F., Seed, H. B., and Thiers, G. R., "Seismic Effects on Structures Supported on Piles Extending Through Deep Sensitive Clay," Report No. 64-2, Inst. of Engrg. Research, University of California, Berkeley, August 1964.

53. Parmelee, R. A., Perelman, D. S., Lee, S. L., and Keer, L. M., "Seismic Response of Structure Foundation Systems," Journal of the Engineering Mechanics Division, ASCE, Vol. 94, No. EM6, Dec. 1968, pp. 1295-1315.

54. Penzien, J., Scheffey, C. F., and Parmelee, R. A., "Seismic Analysis of Bridges on Long Piles," Journal of the Engineering Mechanics Division, ASCE, Vol. 90, No. EM3, Proc. Paper 3953, June 1964, pp. 223-254.

55. Ralston, A., and Wilf, H. S., Mathematical Methods for Digital Computers, John Wiley & Sons, New York, 1960, Vol. I, pp. 258-262.

56. Ramberg, W., and Osgood, W. T., "Description of Stress-Strain Curves by Three Parameters," Technical Note 902, NACA, 1943.

57. Richart, F. E., Jr., Hall, J. R., Jr., and Woods, R. D., Vibrations of Soils and Foundations, Prentice-Hall, Inc., Englewood Cliffs, New Jersey, 1970, p. 414.

58. Schnabel, P. B., Lysmer, J., and Seed, H. B., "SHAKE, A Computer Program for Earthquake Response Analysis of Horizontally Layered Sites," Report No. 72-12, Earthquake Engineering Research Center, Univ. of California, Berkeley, December 1972.

59. Schnabel, P. B., Seed, H. B., and Lysmer, J., "Modification of Seismograph Records for Effects of Local Soil Conditions," Earthquake Eng. Res. Center, University of California, Berkeley, Rep. No. EERC 71-8, December 1971.

60. Seed, H. B., "Earth Slope Stability During Earthquakes," Chapter 15, Earthquake Engineering, Edited by Wiegel, Prentice-Hall, Inc. 1970, pp. 383-401.

61. Seed, H. B., and Idriss, I. M., "Influence of Soil Conditions on Ground Motions During Earthquakes," Journal of the Soil Mechanics and Foundations Division, ASCE, Vol. 95, No. SM1, Proc. Paper 6347, January 1969, pp. 99-137.

62. Seed, H. B., Idriss, I. M., and Dezfulian, H., "Relationships Between Soil Conditions and Building Damage in the Caracas Earthquake of July 29, 1967," Earthquake Eng. Res. Center, Univ. of California, Rep. No. EERC 70-2, February 1970.

63. Seed, H. B., and Martin, G. R., "Seismic Coefficient in Earth Dam Design," Journal of the Soil Mechanics and Foundation Division, ASCE, Vol. 92, No. SM3, Proc. Paper 4824, May 1966, pp. 25-58.

64. Seed, H. B., Whitman, R. V., Dezfulian, H., Dobry, R., and Idriss, I. M., "Soil Conditions and Building Damage in 1967 Caracas Earthquake," Journal of the Soil Mechanics and Foundations Division, ASCE, Vol. 98, No. SM8, Proc. Paper 9108, August 1972, pp. 787-806.

65. Sezawa, K., "On the Decay of Waves in Viscoelastic Soil Bodies," Bull. Earthquake Research Institute, University of Tokyo, Vol. 3, 1927, pp. 43-54.

66. Streeter, V. L., "Valve Stroking for Complex Piping Systems," Journal of the Hydraulics Division, ASCE, Vol. 93, No. HY3, Proc. Paper 5238, May 1967, pp. 81-98.

67. Streeter, V. L., "Unsteady Flow Calculations by Numerical Methods," ASME, Winter Annual Meeting, Washington, D. C., Paper No. 71-WA/F3-13, November 1971.

68. Streeter, V. L., "Numerical Methods for Calculation of Transient Flow," International Conference on Pressure Surges, University of Kent, England, Sept. 1972.

69. Streeter, V. L., and Wylie, E. B., Hydraulic Transients, McGraw-Hill Book Co., New York, 1967, p. 329.

70. Streeter, V. L., and Wylie, E. B., "Two and Three-Dimensional Transients," Journal of Basic Engineering, Trans. ASME, Vol. 90, Ser. D, No. 4, December 1968, pp. 501-510.

71. Streeter, V. L., Wylie, E. B., and Richart, F. E., Jr., "Soil Motion Computations by Characteristics Method," ASCE National Structural Eng. Meeting, San Francisco, Meeting Reprint 1952, April 1973.

72. Westergaard, H. M., "Earthquake Shock Transmission in Tall Buildings," Engrg. Newsrecord, Vol. III, pp. 654-656, November 1933.

73. Whitman, R. V., "Effect of Soil Conditions Upon Damage to Structures, Caracas Earthquake of 29 July 1967," Study conducted for the Presidential Commission for Study of the Earthquake, November 1969.

74. Wilson, E. L., and Clough, R. W., "Dynamic Response by Step-by-Step Matrix Analysis," Proceedings, Symposium on the Use of Computers in Civil Engineering, Lisbon, Portugal, October 1962.

75. Zwikker, C., and Kosten, C. W., Sound Absorbing Materials, Elsevier Publich. Co., Inc., New York, 1949.